Structure, Bonding and Catalytic Activity of Modified Mesoporous Silicates

Jacqueline Mary Dixon

A thesis submitted in partial fulfilment of the requirements of The Nottingham Trent University for the degree of Doctor of Philosophy

June 2004

Abstract

The family of mesoporous silicates designated M41S are a relatively new development in the field of catalysis, having been introduced to the scientific community by scientists from Mobil in 1992. They possess the novel physical property of a uniform pore size, which can be tailored over a wide range of diameters with narrow size distributions.

The scope for the use of mesoporous materials in catalysis is great, since it opens up areas such as pharmaceutical and fine chemical production; where traditional molecular sieves have a limited application because of their small pore size compared to reactant molecules.

However these materials are chemically rather inactive; so have little scope for catalytic applications in the absence of chemical modification. Strategies for modifying these materials range from the inclusion of metal ions; to bestow acid, base or redox properties, to the production of inorganic/organic hybrid materials, which can be functionalised through the organic species.

The focus of this work is MCM-41, a member of the M41S family with hexagonally arranged, unidirectional, non-intersecting, cylindrical, pores. Modification strategies here include the incorporation of aluminium, one of the earliest attempted methods to instil acidity in the materials, and a study of the effects of inclusion on physical and chemical properties. Aluminium-containing materials have been tested in the acylation of anisole with acetic anhydride, and the structural effects of aluminium investigated. Although the materials are, to some extent, active in this reaction, significant effects on pore structure have been observed.

Incorporation of iron, both synthetically and by post-synthetic modification, has been explored. In addition to the possibility of creating a redox active material this has allowed for examination of the similarities and differences between iron incorporated by the different routes. The redox behaviour of samples has been investigated and their catalytic activity in carbon monoxide oxidation established. Samples with iron incorporated synthetically and post-synthetically, somewhat surprisingly, display very similar redox behaviour, despite some evidence that the location of the iron species is different.

Additionally a number of inorganic/organic hybrid materials have been produced, by a very simple method, and investigated. The nature of the organic attachment appears to affect the stability of the resultant material and the effects on the pore void of the MCM-41. Functionalisation of hybrid material has been attempted, with little initial success, but the remarkable stability of one of the resultant materials is, in itself, interesting because MCM-41 is known to have little hydrothermal or long-term stability.

An integral part of this project was to design and build a piece of apparatus for temperature-programmed desorption, and the development of this is also reported here; although few results of the use of this equipment are included in the project.

Acknowledgments

I would like to thank my supervisors, Dr. Michael Stockenhuber and Professor Richard Joyner for their help, support and supervision.

I would also like to acknowledge the help of, and thank, the following:

Dr. Gerd Grubert

Dr. Fran Karpowicz

Isabel Salla Caball

Dr. Gary Paine

Ing. M. W. E. Van Den Berg

Karina Mathisen

John Spray

Larry Wilson

Dr. Olga P. Tkachenko

Simon Meir

Garry Burgess

Michael Duggan

Kevin, Liam and Joe

Contents

Chapter 5. Iron-Modified MCM-41

Chapter.6 Modification of Siliceous MCM-41 by Attachment of Organic Species

1. Introduction

1.1 Catalysis and Waste Management

Over the last few decades there has been a considerable change in attitude to environmental issues, not only on the individual level but also at Governmental levels. There is an increasing awareness of issues such as non-renewable fuels/feedstocks and the need to reduce pollution because of damage to the environment such as global warming. Alongside this there has also been an increasing amount of Health and Safety legislation aimed at reducing the exposure of workers to potentially damaging chemicals (for example halogenated solvents). Given this background it could be tempting to view the eradication of waste as purely altruistic but there is also a compelling economic case; waste is not only costly to dispose of, it is costly to produce. In the pharmaceutical industry it is not uncommon to produce over 100 lb of waste per pound of product, in contrast to the petroleum and petrochemical industries where waste is minimised to less than 0.1 lb/lb. The main reason for this higher efficiency is the use of heterogeneous catalysis[1]. Within the petrochemical industry the use of zeolites as acid catalysts has been well established over a number of years. These microporous crystalline aluminosilicates possess high internal surface areas and can display strong acidity. Because of their well-defined pore structures they exhibit size and shape selectivity. However, their application is limited by their pore size, ca. 3-10 Å.

The driving force for this greater efficiency, and therefore for the use of catalysis, in these industries, has been an economic one, arising from a relatively free market. This has led the industry itself to drive down its own costs. By contrast the market in both the fine chemical and pharmaceutical industries is far less of a free market and this, alongside zealous patent laws in the latter case, leads to inelastic economic conditions, making the economic case for lowering production costs a lesser consideration.

The application of solid catalysis in the search for cleaner and safer technological processes is the greatest challenge for the future. Catalysts reduce the activation energy of chemical reactions, thus increasing the rate of reaction.

This rate increase results in better time efficiency, larger throughput and better volume efficiency, which in turn results in a significant overall reduction in energy costs.

Additionally a well-chosen catalyst can reduce unwanted by-products of reaction. These can occur in a number of ways. The waste product may merely be an unwanted side product of the reaction; but, particularly in fields such as fine chemicals and pharmaceuticals, a particular isomer or even enantiomer of an organic molecule may be required; thus with an unselective reagent large quantities of waste may be generated. In the latter case this is even more inconvenient as racemic mixtures are troublesome to separate; usually involving reaction with, or selective adsorption on, a further optically active material. The elimination of unwanted by-products produces further cost benefits; since a greater proportion of the reactants result in the desired product there are savings on raw materials, and the disposal of unwanted by-products can be very expensive.

Solid reagents and catalysts have certain other advantages over liquid phase reagents; they are easier to separate from the reaction, which not only makes the products easier to purify but also facilitates the possible regeneration of the catalyst. From a health and safety aspect solids are also easier to handle and therefore safer for the worker.

With a solid catalyst or reagent there is the possibility of a high dispersion of active sites giving the benefits of enhanced activity and for this reason the higher the surface area the better, which favours porous materials that can possess surface areas from ~ 500 m^2/g to 1100 m^2/g. For larger reactant molecules, which may be involved in fine chemical and pharmaceutical production, microporous molecular sieves are sometimes inappropriate merely on the grounds of their pore sizes; therefore mesoporous materials are of increasing interest.

The development of mesoporous catalysts suitable for use in these fields is a relatively unexploited area and therefore one which offers great potential; especially as an increasing weight of legislative pressure is brought to bear on all of industry.

1.2 M41S

In 1992 scientists at Mobil introduced a new class of mesoporous silicate/aluminosilicate molecular sieves to the scientific community[2, 3]. Formed by a liquid crystal templating mechanism, using a surfactant in the presence of a silica source, subsequent calcination removes the surfactant leaving the silicate material porous, This family of materials, designated M41S, contain regular arrays of uniform channels and a pore size which can be tailored within the range 15-100 Å[2, 3]; at the lower end of this size range (<40 Å) this is achieved by varying the alkyl chain length of the surfactant used; while for larger pore sizes an auxiliary hydrocarbon (mesitylene) was added to the synthesis mixture in various proportions. In addition to the hexagonal material, designated MCM-41, they also produced a cubic material by varying the surfactant to silica ratios. There were great hopes for the potential of these new materials.

Although a pre-existing patent for low density silica [4] described a preparation that, Ciesla and co-workers claimed, results in a material identical to MCM-41[5], it was the scientists at Mobil who first realised the unusual properties of this type of material fully, certainly the original patent made no mention of unusual properties or applications of the material other than to suggest that it could be used in the manufacture of Zn_2SiO_4 phosphors.

It was hoped that a mesoporous analogue to zeolites had been found, with a consequential catalytic scope for larger reactant molecules and the opportunity to tailor the pore size to the target molecule by design.

However these materials are essentially amorphous, and lack high acid strength, with even the aluminosilicate materials appearing to show inferior activity to comparable zeolites in acid-catalysed reactions[6]. However it has been reported that all silica MCM-41 can show catalytic activity in reactions which are normally acid catalysed. Seddegi et al. reported increased activity for the cracking of high density polyethylene over pure silica MCM-41 compared to thermal cracking[7]. They reported higher activity in their smaller pore samples than those with larger pores, but that all the materials gave an increase in activity. Product distributions led them to conclude that the reaction over MCM-41 proceeds via a carbocation intermediate, and that suggested some acidity in the all silica MCM-41. This

acidity can only arise from the silanol groups, and it led these workers to conclude that the presence of these groups within the pores of the material confers extra activity over amorphous silica. Koch and Reschetilowski compared the hydrocarbon cracking behaviour of aluminium containing MCM-41 with that of zeolite Y[8]. They found that with n-hexadecane as the feed the steady state activity of the MCM-41 materials was lower than that of zeolite Y, also that higher aluminium content in the MCM-41 samples led to a lower stable activity. However using a bulky feed (1,3,5-triisopropylbenzene) the activity of the MCM-41 was higher, demonstrating that MCM-41 can have an advantage over more acidic, and active, materials in circumstances where there are geometrical restrictions associated with the use of microporous materials.
Also because of their pore size and shape uniformity M41S materials have no shape or pore size selectivity. Zhao and co-workers have developed a method of partial template removal from the uncalcined material followed by chemical vapour deposition of tetraethylorthosilicate to reduce the pore opening size, but not the pore diameter, thus creating ink bottle shaped pores[9].

1.3 MCM-41

MCM-41 is the most well-known and widely explored member of the M41S family of molecular sieves. It is formed by the liquid crystal templating mechanism common to this group and exhibits a hexagonally arranged array of unidirectional cylindrical pores. The diameter of these pores can be tailored within the range 15-100 Å[2, 3] by varying the alkyl chain length of the surfactant and the addition of auxiliary hydrocarbons, for example alkylated benzenes, to the reaction mixture[2, 3] as discussed previously. It was, however, observed by the Mobil group that the ordering of the pores decreased with increasing pore size. Later Wang and Kabe developed a further method of tailoring the pore size of MCM-41 by controlling the initial pH of the reaction mixture within the range of 10-11.5[10]. They produced MCM-41 materials with narrow pore size distributions with the pore size rising from 38.3 Å.to 52.7 Å as pH was reduced

from 11.5 to 10; accompanied by a thickening of the pore walls. They concluded that since varying OH^- concentration affected the pore size their synthesis was via a mediated pathway with OH^- acting as the counter-ion.

Beck et al originally proposed two possible mechanisms for the liquid crystal template formation: mechanism one, in which the surfactant spontaneously formed the ordered hexagonal liquid crystal phase and mechanism two, where the addition of the silicate mediates in the subsequent ordering of the resultant silica encased micelles, but that silicate condensation was not a dominant factor in the materials' formation[3] (see figure 1.3.1).

Figure 1.3.1

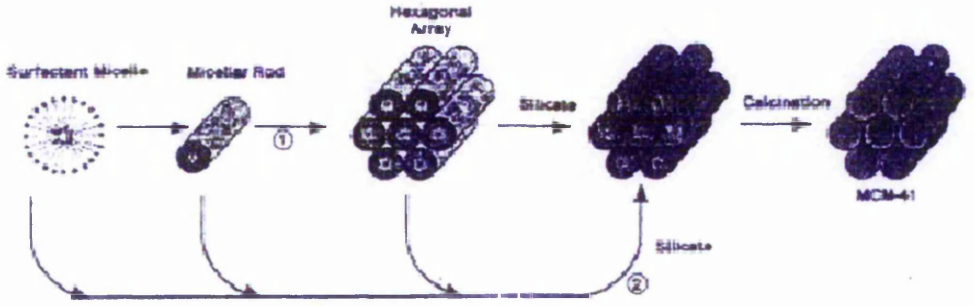

(Reproduced from Reference 3)

The original preparation of these materials devised at Mobil used high surfactant concentrations at which hexadecyltrimethylammonium bromide (cetyltrimethylammonium bromide, CTAB), for example, may form a hexagonal liquid crystal phase in the absence of other components. Further work by Monnier et al.[11] and later by Pang et al[12] showed that the MCM-41 morphology can be produced with very low surfactant concentrations; even below the critical micelle concentration for CTAB in the latter case. Pang's group produced an MCM-41 material at a surfactant concentration of ~ 0.1 wt% CTAB; the critical micelle concentration of which is 0.30 wt%.for spherical micelles. At ca 11 wt% - 20.5 wt% the surfactant alone forms flexible rods and it is not until the region of ~ 26 wt%– 65 wt% that the hexagonal liquid crystal phase is achieved in the absence of other additives (at 298 K, in aqueous solution)[12]. It

is, however, documented in surfactant literature that critical micelle concentrations are affected (lowered) by the presence of electrolytes and organic molecules (and the silica source here, TEOS, is essentially such an organic additive)[13].

Monnier and co-workers felt that the originally proposed mechanisms were insufficient; they conducted a series of experiments using a wide range of reactant compositions and temperatures and found that they could synthesise the material under conditions of pH and concentration where neither the silicate would condense alone, nor would the surfactant form a liquid crystal phase. By varying the temperature they found that they could slow the synthesis at temperatures between ca 300 K - 375 K and under these conditions observed first the formation of a lamellar mesophase. The variation of the d-spacing of this phase with alkyl chain length of the surfactant indicated a monolayer assembly. With time the lamellar phase disappeared and the hexagonal phase was simultaneously formed. They concluded that during the reaction silica condensation increases firstly to form silica oligomers with a high charge density, which act as multidentate ligands to the cationic surfactant, and the arrangement optimises charge balancing between the two (the lamellar arrangement). During transformation polymerisation takes hold and this is accompanied by a lowering of charge density of the silicate species; the surfactant consequently rearranges to optimise the charge density balancing, forming the hexagonal phase.

They further tested their model by using an oligomeric silica source (Cab-O-Sil) and found a greater favouring of the hexagonal phase, supporting their hypothesis.

Overall they concluded that the formation of the hexagonal structure was, in fact, driven by co-operative forces at the silicate/micelle interface, and that, contrary to the assertion of Beck et al. the polymerisation of the silica did play a significant part in the formation of the hexagonal phase.

1.4 Hydrolysis of Alkoxides

In the work presented here the silica source used for the preparation of MCM-41 is Tetraethyl orthosilicate (TEOS), an alkoxide of silicon. Silicon alkoxides are commonly referred to as esters of silicic acid ($Si(OH)_4$)[14, 15] although structurally they are analogous to ethers since the bonding comprises 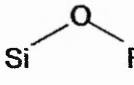 , where R is a hydrocarbon group, cf an ether; 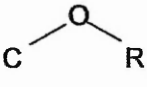 . Organic esters, however, contain the functional group 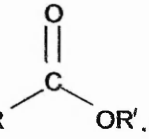 .

Metal alkoxides can be prepared by reacting a halide of the metal with an alcohol[14, 16]. For example:

$$SiCl_4 + 4\ C_2H_5OH \rightleftharpoons Si(O\ C_2H_5)_4 + HCl$$

Or, alternatively, by the reaction of metal oxides or hydroxides with alcohol:

$$SiO_2 + 4C_2H_5OH \rightleftharpoons Si(O\ C_2H_5)_4 + 2H_2O$$

or,

$$Si(OH)_4 + 4C_2H_5OH \rightleftharpoons Si(O\ C_2H_5)_4 + 4H_2O$$

However, when prepared by the latter two methods, the reversibility of the reaction coupled with the extreme susceptibility of the product to hydrolysis necessitates constant removal of the water formed as a by-product[17]. This susceptibility to hydrolysis is a feature of metal alkoxides although the extent of it varies. For a homologous series of monomeric alkoxides, $M(OR)_n$, stability increases with increasing molecular weight of the R group[14, 17].
Hydrolysis occurs under mild conditions and can be catalysed by both acids and bases, yielding primarily silicic acid and the alcohol:

$$Si(O\ C_2H_5)_4 + 4H_2O \longrightarrow Si(OH)_4 + 4C_2H_5OH$$

However, silicic acid is unstable and polymerisation followed by condensation rapidly occurs forming high molecular weight SiO_2 species:

$$nSi(OH)_4 \longrightarrow Si(O_2)_n + 2nH_2O$$

It has been postulated that the process involves the formation of dimeric, trimeric and ultimately polymeric species (shown in figures 1.4.1 and 1.4.2)[17]. These then condense, with water loss, to form the SiO_2 polymer (a section of which is shown in figure 1.4.3).

Figure 1.4.1

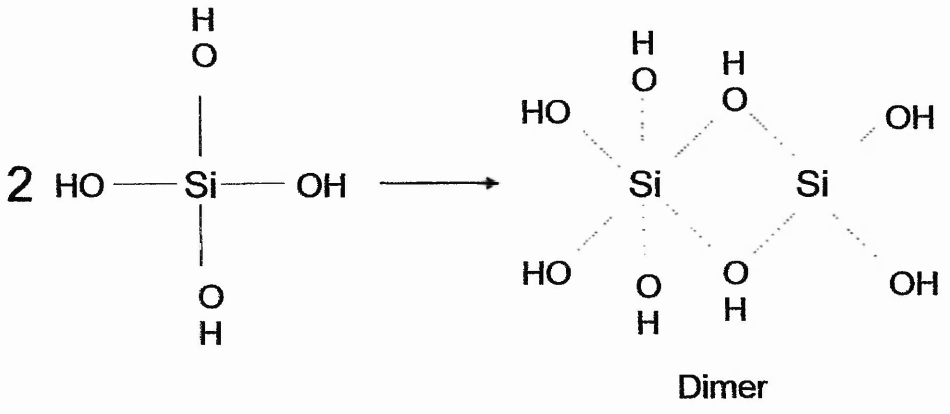

Figure 1.4.2

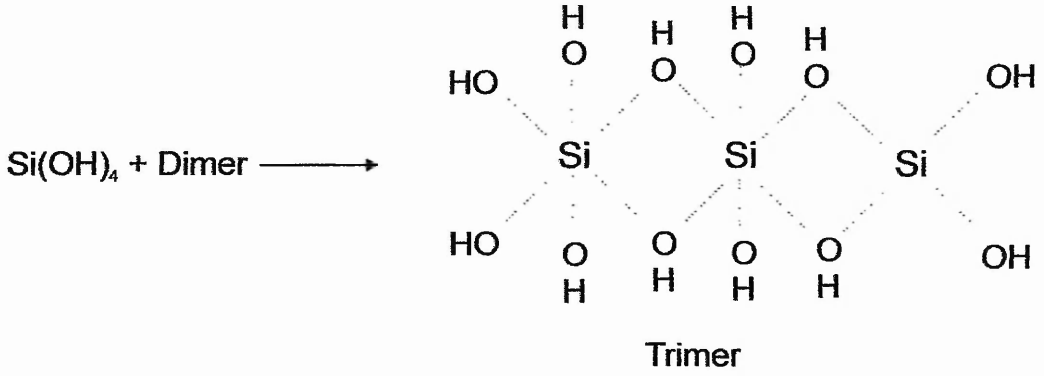

As suggested this mechanism involves a six co-ordinate silica intermediate. While this is rare it is not unknown for silica, occurring, for example, in $[SiF_6]^{2-}$, and OH^- behaves similarly as a ligand to F^-[15, 18, 19].

Figure 1.4.3 Section of condensation reaction.

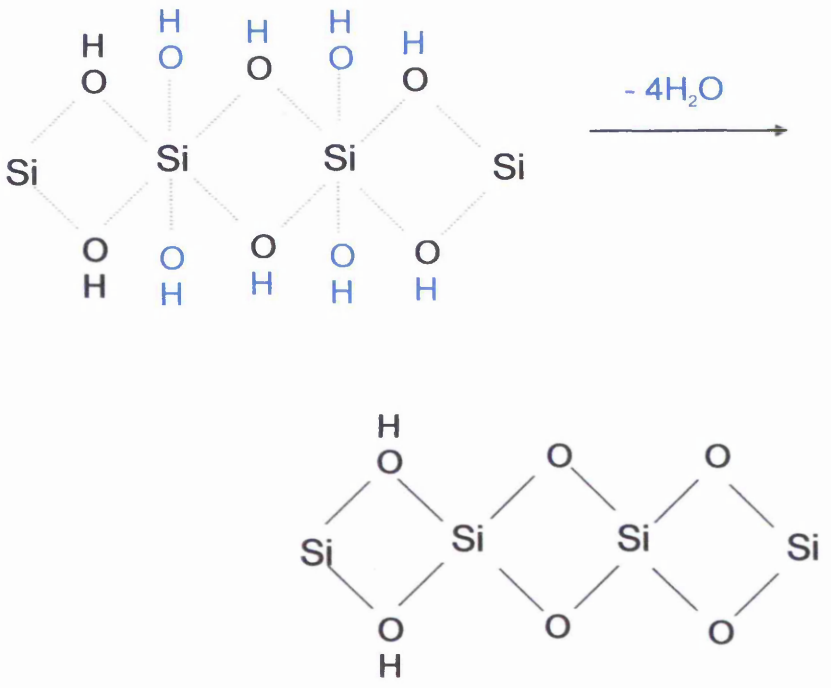

Iler reports that condensation occurs in 3 dimensions regardless of the nature or size of the R group in the alkoxide, with an absence of linear polymers. Also that polysiloxanes are isolable only in highly acidic solutions with insufficient water present[14]. This suggests that acidic conditions stabilise the hydroxyl groups in the intermediate.

1.5 Adsorption Characteristics and Physical Properties of MCM-41

Adsorption

Although MCM-41 has been proposed as a model mesopore adsorbent for studying properties such as pore size and hysteresis[20-22], it has been observed to exhibit anomalous adsorption behaviour for a mesoporous material. Its characteristics were mainly investigated by the Mobil scientists using benzene and argon adsorption[3], they obtained type IV isotherms, with the steep step arising from capillary condensation in the mesopores.

Type IV isotherms are usually associated with the presence of reproducible hysteresis loops. That is, in the area of the isotherm resulting from capillary condensation the amount adsorbed at a given value of P/P^{o} is greater during desorption than during adsorption (see chapter 2, figure 2.1.1).

Various theories have been proposed to explain the observed phenomenon of hysteresis.

Zsigmondy suggested, in 1911, that hysteresis was the result of a different contact angle existing during adsorption and desorption; and that the contact angle was effectively zero during desorption; as the pore walls are totally wetted[22].

This means that if the Kelvin equation is applied:

$$Ln\frac{P}{P^{0}} = \frac{-2\gamma v}{r_{K} R T} Cos\theta$$

And $\theta_{(Ads)}$ is between 0 and 90°, then Ln P_{Ads}/P^{o} will have a smaller negative value than Ln P_{Des}/P^{o}. That is, P_{Des}/P^{o}.will be smaller than P_{Ads}/P^{o}. There have been several further suggestions that hysteresis occurs as the result of differing contact angles during adsorption and desorption[22].

McBain proposed that the presence of pores with smaller diameters at their entrances than in the body of the pore ("ink bottle pores") would lead to hysteresis. During adsorption the channel radius would satisfy the Kelvin equation. However during desorption the main body of the pore could not empty while the smaller neck of the pore was still full of liquid. In this case it is the

radius of the pore neck which fulfills the Kelvin equation; and hysteresis occurs[22].

More recently Saam and Cole (1975) developed a theory for hysteresis considering the differing states of stability, metastability and instability in cylindrical pores[22, 23]. According to this approach there are opposing effects governing the metastability of a multilayer film in such a pore. Long range adsorption forces stabilise the film, while capillary forces drive condensation. This theory also proposes a change in meniscus between adsorption and desorption; from cylindrical during adsorption to hemispherical during desorption. The free energy of an adsorbate molecule is given by:

$$\frac{\Delta G_s}{\Delta n} = -\frac{\alpha}{(R-\alpha)^3} - \frac{\gamma_\infty v_m}{\alpha}$$

for adsorption.

And:

$$\frac{\Delta G_a}{\Delta n} = -\frac{\alpha}{(R-\alpha)^3} - \frac{2\gamma_\infty v_m}{\alpha}$$

for desorption.

Where:

$\Delta G/\Delta n$ = Molar free energy

n = Molar amount adsorbed

α = Fluid-solid interaction parameter

R = Pore radius

$R - \alpha$ = Thickness of adsorbate film (t)

γ_∞ = Surface tension of saturated fluid with infinite curvature

v_m = Molar volume of saturated adsorbate

The subscripts s and a refer to adsorption (symmetrical state) and desorption (asymmetrical state), respectively.

The point of instability of the film fits the condition $\delta\Delta G/\Delta t$.

The difference between the instability point for adsorption and desorption, Δt' is related to the pore radius by:

$$\Delta t' = \sqrt{\frac{3\alpha}{8\gamma_\infty v_m}} \times \left[1 - \sqrt{1 + \frac{4R}{\sqrt{\frac{3\alpha}{2\gamma_\infty v_m}}}} - \sqrt{2} + \sqrt{2 + \frac{8R}{\sqrt{\frac{3\alpha}{\gamma_\infty v_m}}}} \right]$$

Nitrogen adsorption on MCM-41, however, revealed type IV isotherms often lacking the hysteresis loop usually associated with this class of isotherm[2, 24-28].

This, rare, reversible type IV isotherm has been designated a type IVc. It has been observed that in MCM-41 this reversibility depends on a number of factors, such as adsorbate, pore size and temperature. Ravikovitch et al observed hysteresis in the argon isotherm for samples for which it was absent using nitrogen as the adsorbate[27]. Branton et al studied the adsorption of alcohols and found hysteresis in all isotherms, the size of the loop increasing with alkyl chain length[21]. It has been seen that hysteresis is generally present in materials with pore diameters larger than a critical size, usually ca 40 Å[24, 26, 28].

This lack of hysteresis has been attributed to a number of reasons, but it has been experimentally observed that hysteresis is dependent on pore size and temperature as well as the adsorbate.

According to Ravikovitch et al these experimental findings are consistent with thermodynamic theory that the size of the loop will decrease with an increase in temperature or decrease in pore size[29]. This group conducted an experimental study alongside a theoretical one using nonlocal density functional theory (NLDFT) and found that experimentally results regarding the temperature dependence of hysteresis agreed with theoretical models. For a sample of 45 Å pore diameter, hysteresis was absent from the nitrogen isotherm at 82 K and 77.4 K but present at 70.6 K. The same theory predicts that, at a given

temperature, there is a critical pore size below which irreversible filling always changes to reversible pore filling. However, according to their calculations, this size is ca 18 Å for MCM-41 at 77.4 K. The results of their theoretical calculations predicted substantial hysteresis for the previously mentioned sample at 77.4 K, but experimentally none was observed. They concluded that lack of hysteresis in samples with pores smaller than 40 Å cannot be ascribed to 77.4 K being a critical temperature for nitrogen in these pores.

Sonwane and Bhatia, however, used a theoretical approach to calculate the critical pore size for nitrogen adsorption on MCM-41 at 77.4 K and arrived at a value of 38 Å, which is close to the experimentally observed value[23].

Kruk et al, who observed hysteresis for pore diameters of 47 Å and 51 Å but not 42 Å, attribute the presence or absence of hysteresis primarily to a variation of pore diameter along the length of channels creating pore blocking[30]. This is similar to the arguements of Tanev and Vlaev on hysteresis. In a study of hysteresis type in mesoporous aluminium hydroxide, aluminium oxide and silica gel they concluded that as the degree of pore blocking increased the hysteresis type changes in the manner $H_1 < H_3 \leq H_4 \ll H_2$[31].

Luan et al, who did observe hysteresis in the nitrogen isotherm of MCM-41 of only 30 Å diameter, suggest that particle size, and therefore pore length is the decisive factor for the presence of hysteresis. They argue that long mesopores limit the emptying of pore volume, whereas in materials with smaller particles, and therefore shorter pores, this limitation is removed[32].

Conner et al studied a number of samples, some with the characteristic hexagonal pore arrangement and others having an amorphous pore void[33]. They found hysteresis present in the isotherms of some samples but absent in most. More importantly they found no correlation between the presence of hysteresis and the ordering of the pore structure, as measured by x-ray diffraction[33].

Stability of MCM-41

Although the thermal stability of MCM-41 is high, up to 1000 K in dry air[34, 35], it has long been observed that the hydrothermal stability is low. MCM-41 has

even been observed to deteriorate at room temperature. Zhao et al. reported the irreversible collapse of MCM-41 rehydrated at room temperature overnight[36] while Edler and White studied the long-term stability of several samples of MCM-41, prepared under different synthesis conditions. They observed the breakdown of the materials under ambient conditions over a period of 22 months[37]. They reported materials resulting from heated preparations to be more stable than those prepared at room temperature, but improved still further by controlling pH to 11 during synthesis. This is in agreement with the findings of Landau et al[38] who studied wetting stability in neutral, acidic and basic aqueous solution and found that the room temperature-prepared material lost its hexagonal structure and most of its surface area on wetting with neutral water and recalcination. They proposed a mechanism involving the collapse of several pores to form a single, larger, one; although this is in contrast to the findings of Edler and White who reported no evidence of this from their small x-ray scattering measurements. The hydrothermally prepared sample, by contrast, retained both the hexagonal pore structure and over 70% of its surface area with neutral wetting and recalcination. This sample lost only ca. 15% of its surface area under these conditions while maintaining the integrity of the pore structure. Under basic conditions the sample started to deteriorate due to silica leaching from the pore walls. These groups attributed the breakdown to the hydrolysis of strained siloxane units in the pore walls[36, 37].

Because of this lack of stability there have been a number of attempts at improvement.

Both Ryoo and Jun and Landau et al found salt addition and repeated pH adjustment during hydrothermal crystallisation improved the hydrothermal stability[38, 39]. Das et al, however, found that salt addition without repeated pH adjustment led to increased hydrothermal stability[40]. None of these groups reported pore wall thickening and the increase in stability was attributed to increased silica condensation due to a modification of the electrostatic interactions between micelle and silicate during polymerisation.

Mokaya improved the thermal stability of MCM-41 by two methods; using calcined MCM-41 as the silica source for a secondary crystallisation, and increasing the hydrothermal crystallisation time[41]. Both these methods led to pore wall thickening; the probable cause of the greater stability, which is in

agreement with the findings of Cheng et al[42]. Combination of the two methods provided even greater improvement[43]. Chen et al reported a method of increasing stability, alongside pore wall thinning, by post-synthetic hydrothermal treatment[35].

The Mobil scientists first reported the silylation of MCM-41 and the consequent decrease in pore diameter[3] More recently Koyano et al. and Zhao and Lu have utilised silylation to effectively improve the hydrothermal stability of MCM-41[44, 45]. Both these groups observed that this was not due to a thickening of the pore walls but to an increase in the hydrophobicity of the material. Since silanol groups are the only available sites for silylation, the silylating agent effectively caps them, and decreases the available sites for water adsorption. From this it was suggested that water molecules adsorbed on the silanol groups causes the hydrolysis of nearby siloxane bonds[44, 45].

1.6 Modification of Mesoporous Materials

Because of the lack of intrinsic acidity of MCM-41 there is little scope for catalytic activity without modification. Research into creating activity in MCM-41 has included attempts to improve or bestow acidity and the production of redox active catalysts by the incorporation of transition metals.

Attempts at improving the acidic properties of MCM-41 have often involved creating new methods of aluminium incorporation. The inclusion of aluminium in tetrahedrally co-ordinated framework positions is important in any efforts to create Brönsted activity in the materials[46, 47]. Luan et al[32] studied the inclusion of aluminium during synthesis using several different aluminium sources, including reproducing the preparation of the Mobil scientists. They found that the original method, using Catapal alumina, resulted only in octahedrally co-ordinated aluminium, as was also the case using a sodium aluminate source. The use of aluminium sulphate, however, led to a material in which almost all the aluminium was tetrahedrally co-ordinated. The other sources used: aluminium acetylacetonate, aluminium isopropylate and

aluminium hydroxide hydrate produced both co-ordination environments to differing extents. Matsumoto et al also found that using the isopropoxide as aluminium source led to tetrahedrally co-ordinated aluminium species[48]. Cesteros and Haller studied the effects of several factors, including aluminium source, on the properties of aluminosilicate MCM-41. Although they found the levels of tetrahedral aluminium to be generally low, they found that the use of δ alumina increased the amount of tetrahedral co-ordination over PHF alumina and aluminium sulphate. They concluded that the choice of aluminium source is critical in determining the location and co-ordination of the aluminium in the final product.

There have also been a number of methods developed for the post-synthetic introduction of aluminium. These have included the use of trimethylaluminium[49], aluminium chloride[50], and aluminium isopropoxide[50-53].

Oumi et al found high levels of tetrahedral aluminium for the post-synthetic grafting of trimethylaluminium onto MCM-41. They also observed Brönsted acidity, as well as strong and weak Lewis acidity, by pyridine adsorption. As aluminium content increased the amount of Brönsted acidity increased to a maximum, leading them to conclude that beyond this level of incorporation non-framework and 3 co-ordinate aluminium was being produced. However the acid site strength was low compared to that of mordenite, as was the activity in cumene cracking; a reaction which requires medium to high acid strength.

Studies have been made comparing the acidity, or activity, of materials prepared by different routes. Mokaya and Jones found a higher acidity in their samples prepared by post-synthetic grafting of aluminium isopropoxide compared to hydrothermally prepared samples[51]. However Chen et al found direct synthesis led to higher acidity, but they did find a sample post-synthetically modified with aluminium chloride comparable[50].

Chuah et al also compared isopropoxide grafted and directly synthesised samples[52]. They found that for post-synthetically modified materials increasing aluminium content led to an increase in acidic sites; but that this was not the case for directly synthesised materials. They tested the materials as catalysts for the synthesis of α-n-amylcinnamylaldehyde from 1-heptanol and benzaldehyde.

They found that at low to moderate levels of metal incorporation both materials showed similar activity, however the grafted materials with very high metal loadings performed rather badly.

Kugita et al compared sol-gel prepared, hydrothermally synthesised, template cation exchanged and isopropoxide-grafted samples in the Diels-Alder reaction of cyclopentadiene with α,β-unsaturated aldehydes. They found activity increasing in the order: template exchanged < sol-gel < hydrothermally synthesised < grafted. This reaction is normally catalysed by Lewis acids, and interestingly their best performing material showed higher activity than all other catalysts tested in the reaction: including ZSM-5, HY and SBA as well as the homogeneous catalysts p-toluenesulfonic acid and aluminium chloride.

Selvaraj et al have prepared mixed aluminium/zinc MCM-41 via a synthetic route and found framework species and Brönsted acid sites[54]. The acid strength was moderate but the number of acid sites increased with the inclusion of zinc. Samples with very low Si : (Al + Zn) ratios had more sites than those with much higher Si : Al (by a factor ca 3).

Activity of MCM-41 has also been enhanced by the incorporation of organic groups, followed by their functionalisation. Davis et al had already prepared a composite sulfonic acid based on zeolite beta morphology[55, 56] by the inclusion of phenylethyl groups during synthesis, followed by post-synthetic gas phase sulfonation. They have extended this to the production of a mesoporous analogue, but found that, while active, it lacks the advantage of shape selectivity possessed by the beta derived material[57].

A composite material produced by synthetic incorporation of the commercially available ion-exchange resin, Nafion, into MCM-41 has also shown promise as an acid catalyst[58]. It was found to be a selective catalyst for α-methylstyrene dimerization, although its activity was low in Friedel-Crafts reactions.

Wilson et al also produced a solid porous silica/sulfonic acid, although with large micropores (16 Å) rather than mesopores[59]. This was achieved by the synthetic co-condensation of mercaptopropyl-trimethoxysilane followed by oxidation to the acid. It was found to be active in the liquid phase esterifications of butan-1-ol and dodecanol and the Claisen-Shcmidt condensation of acetophenone with benzaldehyde.

The same group have also reported the production of basic composite materials by the incorporation, during synthesis, of aminopropyl trimethoxysilane, with or without further reaction. The aminopropylated MCMs initially produced proved to be effective base catalysts compared to aminopropylsilica[60]. Secondary amine derivatives, prepared by the reduction of an imine intermediate, showed lower activity than the corresponding imines, but enhanced stability[61].

A number of groups have reported the successful incorporation of transition metals such as titanium[62, 63], vanadium[64-67], chromium[66, 68, 69], manganese[70] iron[71-75], cobalt[75], copper[76, 77] and zinc[76, 77] by addition of metal salts to the synthesis mixture. Post-synthetic incorporation methods for various metals have included impregnation, chemical vapour deposition and processes analogous to exchange in zeolites.

Many of these materials have been shown to have catalytic applications, most notably in oxidation reactions.

Titanium-containing aluminosilicate MCM-41 has been reported to be more active in the oxidation of linalool to tert-butylhydroperoxide than zeolite beta[63]. Since titanium-containing beta is intrinsically more active with linear oleofins this must be the result of more effective diffusion. The aluminosilicate MCM-41 material shows no activity in the absence of titanium.

Siliceous vanadium-MCM-41 shows activity in the oxidation of large organic molecules such as 1-napthol and cyclododecane[65], as well as for the oxidative dehydrogenation of isobutane[64].

Parvulescu and Su also reported hydrocarbon oxidation activity for MCM-41 with iron cobalt or nickel incorporated, with the best performing catalysts being those containing cobalt[75].

Copper-MCM-41 has been used for the wet oxidation of phenol[78] while mixed metal copper/zinc materials have been shown to be active for the partial oxidation of alcohols to aldehydes[77]. Fujiyama et al reported the liquid-phase oxidation of 2,6-Di-*tert*-butylphenol over copper-impregnated materials with the addition of potassium[79].

Additionally iron-containing materials have been reported to be catalytically active in the oxidation of carbon monoxide[74].

More recently attention has also been given to the production of other classes of mesoporous oxides exploiting the techniques involved in the development of the

M41S class of materials. Although the original synthesis proposed by the scientists at Mobil centred on the use of a cationic surfactant in the presence of an anionic silica species Huo and co-workers developed a generalised synthesis. This can be applied to the preparation of a number of different mesophase structures. In addition to the original route of cationic surfactant and anionic silica ($S^+ I^-$) they used an anionic surfactant and a cationic oxide species ($S^- I^+$) and two further routes using surfactant and oxide species of the same charge in the presence of a mediating ion of the opposite charge($S^- M^+ I^-$) and ($S^+ X^- I^+$) [80].

By exploiting these methods Ciesla et al. have produced mesoporous tungsten oxide ($S^+ I^-$) with a hexagonal structure similar to that of MCM-41 and iron and lead oxide materials ($S^- I^+$), however less successfully in the latter two cases; the lead material resulting in a two phase material and in the case of iron surfactant extraction proved a problem[81].

Further developments have been the production of mesoporous materials using a non-ionic templating route ($N^\circ I^\circ$), Deng and co-workers have produced mesoporous aluminas, with pore sizes from 87-110 Å, using a block co-polymer as template, while Thieme and Schüth have produced a titanium oxo phosphate via this route. It has been observed, however, that while the non-ionic route produces mesoporous materials these are, typically disordered in their structures[82, 83]

1.7 The Scope of this Project

The focus of the research in this project is the modification in different ways of siliceous MCM-41 material. This was to be achieved by both synthetic and post synthetic routes and to encapsulate a number of different approaches.

A study of aluminium containing samples, all with aluminium incorporated during MCM-41 synthesis, aims to explore their possible activity in acid catalysed reactions, but also to investigate effects of aluminium incorporation on characteristics such as pore structure and surface area.

Iron incorporation is performed both through a synthetic route and via post synthetic modification of MCM-41. This enables a comparison between the properties of the materials obtained by the differing routes. The aim is to investigate the possible use of these materials as redox catalysts. This is a field where iron containing zeolites have been shown to have applications; for example in the selective reduction of NOx[84-87]. However in this project the focus for MCM-41 catalysis would be on oxidation.

A further strategy for modification would be to attempt the attachment of organic material to the MCM-41 surface. This aims to capitalise on a previous discovery within this research group. It has been previously observed that samples which had been in contact with methanol formed stable methoxy groups, bonded to the silica surface[72]. The interest here is whether this could be extended to other alcohols producing a class of hybrid inorganic-organic materials. Obvious effects to be investigated are the stability of such materials, if produced, and the effects on the porosity of the material. The eventual aim, however is to use the method to attach a chemically significant group, for example an organic ring which would be susceptible to electrophilic attack and therefore could perhaps be used to produce a sulfonic acid. This is a further strategy in the search for acidification of MCM-41.

1.8 References

1. Cusumano, J.A., *Environmentally Sustainable Growth in the 21st Century.* Journal of Chemical Education, 1995. **72**(11): p. 959-964.
2. Kresge, C.T., et al., *Ordered Mesoporous Molecular-Sieves Synthesized by a Liquid- Crystal Template Mechanism.* Nature, 1992. **359**(6397): p. 710-712.
3. Beck, J.S., et al., *A New Family of Mesoporous Molecular-Sieves Prepared with Liquid-Crystal Templates.* Journal of the American Chemical Society, 1992. **114**(27): p. 10834-10843.
4. Chiola, V., J.E. Ritsko, and C.D. Vanderpool. 1971: U.S. Patent No. 3556725.
5. Ciesla, U. and F. Schuth, *Ordered mesoporous materials.* Microporous and Mesoporous Materials, 1999. **27**(2-3): p. 131-149.
6. Corma, A. and D. Kumar, Studies in Surface Science and Catalysis, 1998. **117**: p. 201.
7. Seddegi, Z.S., et al., *Catalytic cracking of polyethylene over all-silica MCM-41 molecular sieve.* Applied Catalysis a-General, 2002. **225**(1-2): p. 167-176.
8. Koch, H. and W. Reschetilowski, *Is the catalytic activity of Al-MCM-41 sufficient for hydrocarbon cracking?* Microporous and Mesoporous Materials, 1998. **25**(1-3): p. 127-129.
9. Zhao, X.S., G.Q. Lu, and X. Hu, *A novel method for tailoring the pore-opening size of MCM-41 materials.* Chemical Communications, 1999: p. 1391-1392.
10. Wang, A.J. and T. Kabe, *Fine-tuning of pore size of MCM-41 by adjusting the initial pH of the synthesis mixture.* Chemical Communications, 1999(20): p. 2067-2068.
11. Monnier, A., et al., *Cooperative Formation of Inorganic-Organic Interfaces in the Synthesis of Silicate Mesostructures.* Science, 1993. **261**(5126): p. 1299-1303.

12. Chai, Q., et al., *The Preparation of Highly Ordered MCM-41 with Extremely Low Surfactant Concentration.* Microporous and Mesoporous Materials, 1999. **32**: p. 1-15.

13. Shaw, D.J., *Introduction to Colloid and Surface Chemistry*. 1992: Butterworth-Heinemann.

14. Iler, R., *The Colloid Chemistry of Silica and Silicates*. 1989, Ann Arbor: UMI.

15. Sneed, M.C. and R.C. Brasted, *Comprehensive Inorganic Chemistry*. Vol. 7. 1958, Princeton: Van Nostrand.

16. Cotton, F.A. and G. Wilkinson, *Advanced Inorganic Chemistry*. 5th ed. 1988, New York: Wiley-Interscience.

17. Bradley, D.C., R.C. Mehrotra, and D.P. Gaur, *Metal Alkoxides*. 1978, London: Academic Press.

18. Shriver, D.F., P.W. Atkins, and C.H. Langford, *Inorganic Chemistry*. 2nd ed. 1994, Oxford: Oxford University Press.

19. Nicholls, D., *Complexes and First Row Transition Elements*. 1974: Macmillan.

20. Branton, P.J., et al., *Physisorption of Argon, Nitrogen and Oxygen by Mcm-41, a Model Mesoporous Adsorbent.* Journal of the Chemical Society-Faraday Transactions, 1994. **90**(19): p. 2965-2967.

21. Branton, P.J., P.G. Hall, and K.S.W. Sing, *Physisorption of Alcohols and Water Vapour by MCM-41, a Model Mesoporous Adsorbent.* Adsorption, 1995. **1**: p. 77-82.

22. Rouquerol, F., J. Rouquerol, and K. Sing, *Adsorption by Powders and Porous Solids*. 1999: Academic Press.

23. Sonwane, C.G. and S.K. Bhatia, *Analysis of criticality and isotherm reversibility in regular mesoporous materials.* Langmuir, 1999. **15**(16): p. 5347-5354.

24. Kruk, M., et al., *Characterization of highly ordered MCM-41 silicas using X-ray diffraction and nitrogen adsorption.* Langmuir, 1999. **15**(16): p. 5279-5284.

25. Conner, W.C., et al., *Hysteresis in physical sorption for MCM.* Mesoporous Molecular Sieves 1998, 1998. **117**: p. 575-581.

26. Fenelonov, V.B., V.N. Romannikov, and A.L. Derevyankin, *Mesopore size and surface area calculations for hexagonal mesophases (types MCM41, FSM-16, etc.) using low-angle XRD and adsorption data.* Microporous and Mesoporous Materials, 1999. **28**(1): p. 57-72.

27. Ravikovitch, P.I., et al., *Evaluation of Pore Structure Parameters of MCM-41 Catalyst Supports and Catalysts by Means of Nitrogen and Argon Adsorption.* Journal of Physical Chemistry B, 1997. **101**: p. 3671-3679.

28. Sayari, A. and Y. Yong, *Highly Ordered MCM-41 Silica Prepared in the Presence of Decyltrimethylammonium Bromide.* Journal of Physical Chemistry B, 2000. **104**: p. 4835-4839.

29. Ravikovitch, P.I., et al., *Capillary hysteresis in nanopores: Theoretical and experimental studies of nitrogen adsorption on MCM-41.* Langmuir, 1995. **11**(12): p. 4765-4772.

30. Kruk, M. and M. Jaroniec, *Characterization of modified mesoporous silicas using argon and nitrogen adsorption.* Microporous and Mesoporous Materials, 2001. **44**: p. 725-732.

31. Tanev, P.T. and L.T. Vlaev, *An Attempt at a More Precise Evaluation of the Approach to Mesopore Size Distribution Calculations Depending on the Degrre of Pore Blocking.* Journal of Colloid and Interface Science, 1993. **160**: p. 110-116.

32. Luan, Z.H., et al., *Effect of Structural Aluminum on the Mesoporous Structure of Mcm-41.* Journal of the Chemical Society-Faraday Transactions, 1995. **91**(17): p. 2955-2959.

33. Conner, W.C., et al., *Hysteresis in physical sorption for MCM.* Studies in Surface Science and Catalysis, 1998. **117**(Mesoporous Molecular Sieves): p. 575-581.

34. Kim, J.M., et al., *Ion Exchange and Thermal Stability of MCM-41.* Journal of Physical Chemistry, 1995. **99**: p. 16742-16747.

35. Chen, L., et al., *Postsynthesis Hydrothermal Restructuring of M41S Mesoporous Molecular Sieves in Water.* Journal of Physical Chemistry B, 1999. **103**: p. 1216-1222.

36. Zhao, X.S., F. Audsley, and G.Q. Lu, *Irrevesible Change of Pore Structure of MCM-41 upon Hydration at Room Temperature.* Journal of Physical Chemistry B, 1998. **102**: p. 4143-4146.

37. Edler, K.J. and J.W. White, *Preparation dependent stability of pure silica MCM-41.* Journal of Materials Chemistry, 1999. **9**: p. 2611-2615.

38. Landau, M.V., et al., *Wetting stability of Si-MCM-41 mesoporous material in neutral and basic aqueous solutions.* Microporous and Mesoporous Materials, 1999. **33**: p. 149-163.

39. Ryoo, R. and S. Jun, *Improvement of Hydrothermal Stability of MCM-41 Using Salt Effects during the Crystallization Process.* Journal of Physical Chemistry B, 1997. **101**: p. 317-320.

40. Das, D., C.-M. Tsai, and S. Cheng, *Improvement of hydrothermal stability of MCM-41 mesoporous molecular sieve.* Journal of the Chemical Society-Chemical Communications, 1999: p. 473-474.

41. Mokaya, R., *Improving the Stability of Mesoporous MCM-41 Silica via Thicker More Highly Condensed Pore Walls.* Journal of Physical Chemistry B, 1999. **103**: p. 10204-10208.

42. Cheng, C.-F., et al., *Controlling the channel diameter of the mesoporous molecular sieve MCM-41.* Journal of the Chemical Society Faraday Transactions, 1997. **92**(2): p. 359-363.

43. Mokaya, R., *Hydrothermally stable restructured mesoporous silica.* Chemical Communications, 2001: p. 933-934.

44. Koyano, K.A. and T. Tatsumi, *Stabilization of Mesoporous Molecular Sieves by Trimethylsilylation.* Journal of Physical Chemistry B, 1997. **101**: p. 9436-9440.

45. Zhao, X.S. and G.Q. Lu, *Modification of MCM-41 by Surface Silylation with Trimethylchlorosilane and Adsorption Study.* Journal of Physical Chemistry B, 1998. **102**: p. 1556-1561.

46. Luan, Z.H., et al., *Mesopore Molecular-Sieve Mcm-41 Containing Framework Aluminum.* Journal of Physical Chemistry, 1995. **99**(3): p. 1018-1024.

47. Kosslick, H., H. Landmesser, and R. Fricke, *Acidity of substituted MCM-41-type mesoporous silicates probed by ammonia.* Journal of the Chemical Society-Faraday Transactions, 1997. **93**(9): p. 1849-1854.

48. Matsumoto, A., et al., *Novel route in the synthesis of MCM-41 containing framework aluminum and its characterization.* Microporous and Mesoporous Materials, 1999. **32**(1-2): p. 55-62.

49. Oumi, Y., et al., *Novel post-synthesis alumination method for MCM-41 using trimethylaluminum.* Microporous and Mesoporous Materials, 2001. **44-45**: p. 267-274.

50. Chen, L.Y., et al., *A comparison of post-synthesis alumination and sol-gel synthesis of MCM-41 with high framework aluminum content.* Microporous and Mesoporous Materials, 1999. **27**(2-3): p. 231-242.

51. Mokaya, R. and W. Jones, *Post-synthesis grafting of Al onto MCM-41.* Chemical Communications, 1997: p. 2186.

52. Chuah, G.K., et al., *Surface properties of mesoporous catalytic supports.* Applied Surface Science, 2001. **169**: p. 253-258.

53. Kugita, T., et al., *MCM-41 as a highly active catalyst for Diels-Alder reaction of anthracene with p-benzoquinone.* Microporous and Mesoporous Materials, 2001. **44-45**: p. 531-536.

54. Selvaraj, M., et al., *Synthesis, characterization and catalytic application of MCM-41 mesoporous molecular sieves containing Zn and Al.* Applied Catalysis, A: General, 2003. **242**(2): p. 347-364.

55. Jones, C.W., K. Tsuji, and M.E. Davis, *Organic-functionalized molecular sieves as shape-selective catalysts.* Nature, 1998. **393**(6680): p. 52-54.

56. Jones, C.W., K. Tsuji, and M.E. Davis, *Organic-functionalized molecular sieves (OFMSs). II. Synthesis, characterization and the transformation of OFMSs containing non-polar functional groups into solid acids.* Microporous and Mesoporous Materials, 1999. **33**(1-3): p. 223-240.

57. Jones, C.W., et al., *Organic-functionalized molecular sieves. III. Shape selective catalysis.* Microporous and Mesoporous Materials, 2001. **42**: p. 21-35.

58. Fujiwara, M., et al., *Preparation of an MCM-41/Nafion composite material; a selective catalyst for α-methylstyrene dimerization.* Journal of the Chemical Society-Chemical Communications, 2000: p. 1523-1524.

59. Wilson, K., et al., *Structure and reactivity of sol-gel sulphonic acid silicas.* Applied Catalysis a-General, 2002. **228**(1-2): p. 127-133.

60. Macquarrie, D.J. and D.B. Jackson, *Aminopropylated MCMs as base catalysts: a comparison with aminopropylated silica.* Chemical Communications, 1997(18): p. 1781-1782.

61. Utting, K.A. and D.J. Macquarrie, *Formation and evaluation of novel silica supported secondary amines via an effective 'in-situ' reduction of silica supported imines.* Applied Catalysis a-General, 2002. **232**(1-2): p. 7-12.

62. Tanev, P.T., M. Chibwe, and T.J. Pinnavala, *Titanium-containing mesoporous molecular sieves for catalytic oxidation of aromatic compounds.* Nature, 1994. **368**: p. 321-322.

63. Corma, A., M. Iglesias, and F. Sanchez, *Large Pore Bifunctional Titanium-Aluminosilicates: the Inorganic Non-enzymatic Version of the Epoxidase Conversion of Linalool to Cyclic Ethers.* Journal of the Chemical Society-Chemical Communications, 1995: p. 1635-1636.

64. Sulikowski, B., et al., *Oxidative dehydrogenation of isobutane on MCM-41 mesoporous molecular sieves.* Applied Catalysis, A: General, 2002. **232**(1-2): p. 189-202.

65. Reddy, J.S., P. Liu, and A. Sayari, *Vanadium containing crystalline mesoporous molecular sieves - Leaching of vanadium in liquid phase reactions.* Applied Catalysis a-General, 1996. **148**(1): p. 7-21.

66. Yuan, Z.Y., et al., *Vanadium and chromium-containing mesoporous MCM-41 molecular sieves with hierarchical structure.* Microporous and Mesoporous Materials, 2001. **43**: p. 227-236.

67. Grubert, G., et al., *Reducibility of Vanadium oxide species in MCM-41.* Microporous and Mesoporous Materials, 1998. **22**: p. 225-236.

68. Pak, C. and G.L. Haller, *Reversible coordination change of chromium in Cr-MCM-41 and Cr- MCM-48 studied by X-ray absorption near edge structure.* Microporous and Mesoporous Materials, 2001. **48**(1-3): p. 165-170.

69. Ulagappan, N. and C.N.R. Rao, *Synthesis and characterisation of the mesoporous chromium silicates, Cr-MCM-41.* Journal of the Chemical Society-Chemical Communications, 1996: p. 1047-1048.

70. Zhao, D. and D. Goldfarb, *Synthesis of Mesoporous Manganosilicates: Mn-MCM-41, Mn-MCM-48 and Mn-MCM-L.* Journal of the Chemical Society-Chemical Communications, 1995: p. 875-876.

71. Yuan, Z.Y., et al., *Synthesis of Iron-containing MCM-41.* Journal of the Chemical Society-Chemical Communications, 1995: p. 973-974.

72. Stockenhuber, M., M.J. Hudson, and R.W. Joyner, *Preparation, characterization, and unusual reactivity of Fe- MCM-41.* Journal of Physical Chemistry B, 2000. **104**(14): p. 3370-3374.

73. Grubert, G., et al., *The room temperature, stoichiometric conversion of N2O to adsorbed NO by Fe-MCM-41 and Fe-ZSM-5.* Journal of Catalysis, 2000. **196**(1): p. 126-133.

74. Szegedi, A., G. Pal-Borbely, and K. Lazar, *Comparison of the redox properties of iron incorporated in different amounts into MCM-41.* Reaction Kinetics and Catalysis Letters, 2001. **74**(2): p. 277-287.

75. Parvulescu, V. and B.L. Su, *Iron, cobalt or nickel substituted MCM-41 molecular sieves for oxidation of hydrocarbons.* Catalysis Today, 2001. **69**(1-4): p. 315-322.

76. Hartmann, M., S. Racouchot, and C. Bishof, *Characterisation of copper and zinc containing MCM-41 and MCM-48 molecular sieves by temperature programmed reduction and carbon monoxide adsorption.* Microporous and Mesoporous Materials, 1999. **27**: p. 309-320.

77. Velu, S., et al., *Characterization of MCM-41 mesoporous molecular sieves containing copper and zinc and their catalytic performance in the selective oxidation of alcohols to aldehydes.* Microporous and Mesoporous Materials, 2002. **54**: p. 113-126.

78. Wu, Q., et al., *Copper/MCM-41 as catalyst for the wet oxidation of phenol.* Applied Catalysis B-Environmental, 2001. **32**(3): p. 151-156.

79. Fujiyama, H., et al., *Liquid-Phase Oxidation of 2,6-Di-tert-butylphenol with Cu-Impregnated MCM-41 in the Presence of Alkali Metals.* Journal of Catalysis, 1999. **188**: p. 417-425.

80. Huo, Q.S., et al., *Generalized Synthesis of Periodic Surfactant Inorganic Composite-Materials.* Nature, 1994. **368**(6469): p. 317-321.

81. Ciesla, U., et al., *Surfactant Controlled Preparation of Mesostructured Transition- Metal Oxide Compounds.* Journal of the Chemical Society-Chemical Communications, 1994(11): p. 1387-1388.

82. Deng, W., et al., *Characterization of mesoporous alumina molecular sieves synthesized by nonionic templating.* Microporous and Mesoporous Materials, 2002. **52**(3): p. 169-177.

83. Thieme, M. and F. Schuth, *Preparation of a mesoporous high surface area titanium oxo phosphate via a non-ionic templating route.* Microporous and Mesoporous Materials, 1999. **27**: p. 193-200.

84. Chen, H.-Y., T. Voskoboinikov, and W.M.H. Sachtler, *Reduction of NOx over Fe/ZSM-5 Catalysts: Adsorrption Complexes and Their Reactivity toward Hydrocarbon.* Journal of Catalysis, 1998. **180**: p. 171-183.

85. Feng, X. and W.K. Hall, *On the Unusual stability of overexchanged FeZSM-5.* Catalysis Letters, 1996. **41**: p. 45-46.

86. Feng, X. and W.K. Hall, *FeZSM-5: A Durable SCR Catalyst for NOx Removal from Combustion Streams.* Journal of Catalysis, 1997. **166**: p. 368-376.

87. Long, R.Q. and R.T. Yang, *Catalytic Performance of Fe-ZSM-5 Catalysts for Selective Catalytic Reduction of Nitric Oxide by Ammonia.* Journal of Catalysis, 1999. **188**.

2. Experimental Procedures

2.1 Surface Area and Pore Volume Measurements

The B.D.D.T. (Brunauer, Deming, Deming and Teller) classification groups adsorption isotherms into five classes according to adsorbent-adsorbate interactions[1]. Types I, II and IV, shown in figure 2.1.1, are produced by microporous, non-porous and mesoporous adsorbents respectively. Types III and V are characteristic of weak adsorbent-adsorbate interactions and are, therefore, of less practical interest; for this reason they are not reproduced here. Although the type IV isotherm illustrated here shows the hysteresis loop which is so often characteristic of this type, it is not usually to be expected for nitrogen adsorption on MCM-41 materials with a pore diameter of ca 40 Å[2, 3]. A more in depth discussion of this matter can be found in chapter three.

Figure 2.1.1 Adsorption Isotherms From The B.D.D.T. Classification

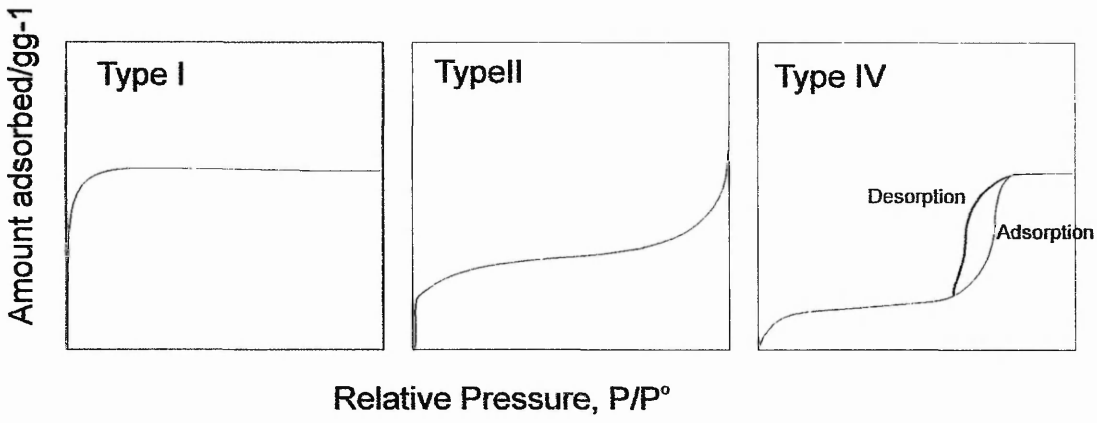

The monolayer capacity of solids giving rise to a Type II or Type IV isotherm in the B.D.D.T. classification can be determined by application of the BET equation (Brunauer, Emmett and Teller).

The BET Equation:

$$\frac{P}{(P^o - P)x} = \frac{1}{x_m c} + \frac{c-1}{x_m c} P/P^o$$

Where:

P = Pressure

P^o = Saturation vapour pressure

x_m = Monolayer capacity

C = Constant

x = Amount adsorbed at pressure P

A plot of $P/(P^o - P)x$ against P/P^o should be linear with a slope of $(C-1)/x_mC$ and intercept of $1/x_mC$. It is expected that the BET equation will fit data in the range $P/P^o = 0.05 - 0.3$.

The specific surface area is then calculated by use of the connecting equation:

$$S = \frac{x_m . N_A . A_m}{M}$$

Where:

N_A is Avagadro's number

A_m is the average area occupied by a molecule of the adsorbate in a completed monolayer (16.2 $Å^2$ for nitrogen)

M is the molar mass of the adsorbate (or molar volume for volumetric calculations)

BET surface areas were determined using a computer controlled automated volumetric apparatus. Samples (~ 100 mg, accurately weighed) were first outgassed at around 525 K overnight to a pressure of 0.06 mbar, then the sample volumes were calibrated with helium at room temperature and 77 K. The surface area was then determined using six points within the linear BET range with nitrogen as the adsorbate. Linearity across this range was checked with the

linear portion alone being used for calculation where this did not extend to $P/P^o = 0.3$.

Additionally, full nitrogen adsorption/desorption isotherms were obtained using a traditional vacuum frame apparatus (shown in figure 2.1.2), this being necessary to confirm the expected isotherm type for these materials. Additionally, in order to justify the application of the BET equation for surface area determination, it is necessary to establish an isotherm of type II or IV in the B.D.D.T. classification.

Figure 2.1.2 Vacuum Frame Apparatus for Measuring Adsorption Isotherms

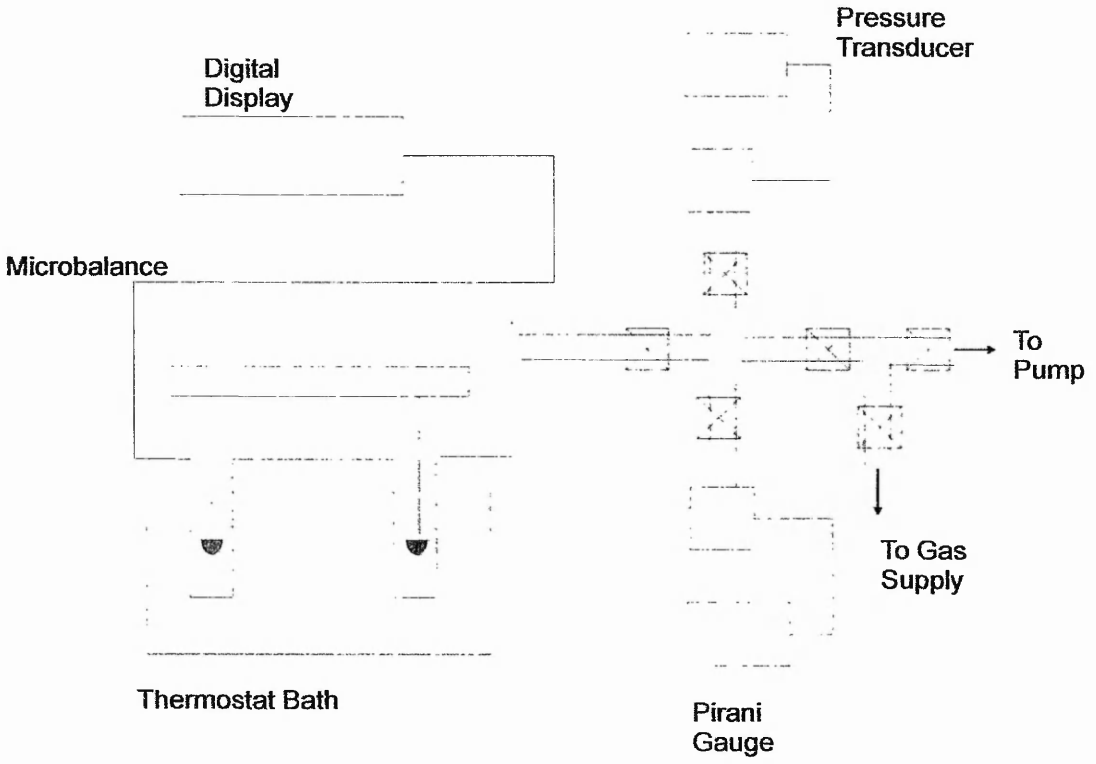

Isotherms were measured in vacuum microbalance equipped with an oil diffusion pump backed by a rotary pump. The sample (~ 40 mg) was placed in the chamber of the microbalance and evacuated to a pressure of ~ 5×10^{-3} mbar; the sample was outgassed overnight, at approximately 525 K.

The sample was then dosed with nitrogen at 77 K, using a series of valves, over the pressure range $P/P^o = 0 - 1$. Equilibrium pressures were recorded using the pressure transducer.

The desorption isotherm was recorded the following day by reducing the pressure to similar pressures used for the adsorption isotherm (at 77 K) by opening the valve to the rotary pump only. Total pore volumes were calculated from the full isotherms: either by single point analysis at $P/P^o = 0.95$ or, if the isotherm showed an upward swing at high values of P/P^o indicating multilayer surface coverage, extrapolation of the final plateau to $P/P^o = 0.95$[1].
Examples of adsorption and desorption isotherms for the MCM-41 materials can be found in the following chapter.

2.2 Powder X-Ray Diffraction

Powder x-ray diffraction (XRD) can be used to determine the unit cell of a solid, that is, the smallest repeating unit to describe the symmetry of that solid. When a solid is irradiated by x-rays they are diffracted by the electrons surrounding the atoms.
For two planes with Miller indices h, k, l, and spacing, d (see figure 2.2.1), there is an extra distance travelled by the x-ray beam for the lower plane.

Figure 2.2.1 X-ray Diffraction

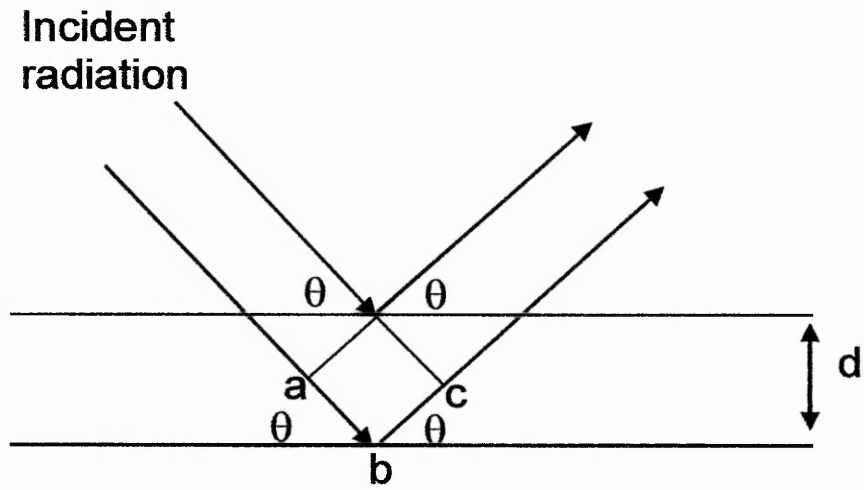

That distance, represented as abc above, is equal to 2 d sin θ. In order for diffraction to occur the diffracted x-rays must be in phase, in which case the Bragg equation applies:

$$n\lambda = 2d_{hkl}\sin\theta_{hkl}$$

Where;

λ = X-ray wavelength

d = d spacing between planes with Miller indices hkl

θ = Angle of diffraction from plane hkl and

n = any whole number

Figure 2.2.2 Schematic diagram of a Powder Diffractometer

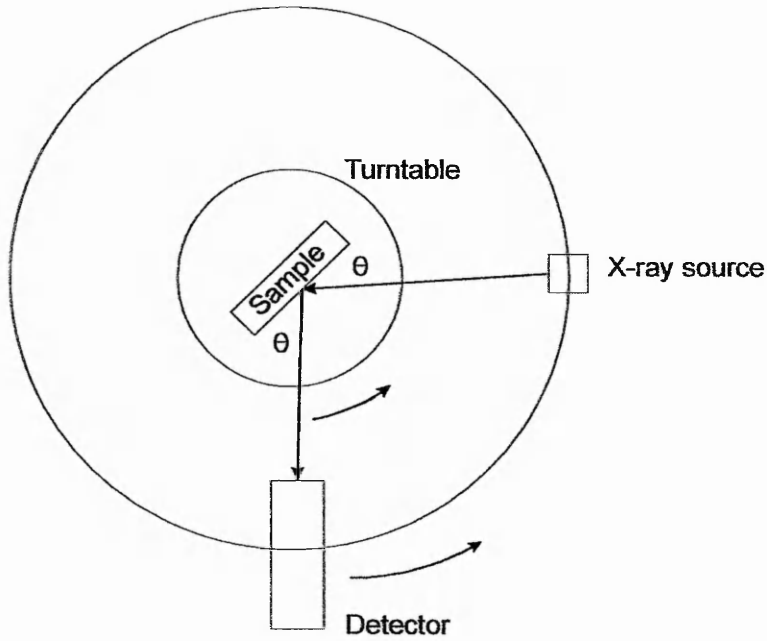

The powdered sample is placed on a turntable, which rotates at a uniform, preset, speed. The detector rotates at double the speed of the turntable in order to be correctly positioned for detection of the diffracted rays.

Diffraction patterns were recorded using a Hiltonbrooks modified Phillips powder diffractometer fitted with a Cu K α radiation source (λ = 1.542 Å) and a nickel

filter. The range used was 3.20 – 12 °2θ with a 0.02 ° step size and a dwell of 6 s/step. Because the most intense diffraction peak for these materials (hkl 100), occurs ca. 2 °2θ, and this was beyond the capabilities of the available equipment, all x-ray diffraction has been examined comparative to MCM-41 samples prepared and characterised elsewhere using the full angular range. However a lowering in the intensity and/or a loss of definition of the peaks at higher 2θ angles (hkl 110, 200) can indicate a loss of the ordering within the channels of the unidirectional pores[4, 5], therefore this method can still be a valid measure of the quality of the material's pore structure.

Although MCM-41 itself is amorphous the pore arrangement is sufficiently ordered to result in some structure in the x-ray diffraction pattern. Typically between three to five peaks are observed in the range 2 – 5 °2θ which can be indexed to the hexagonal pore structure[2, 6]. The angles are, therefore pore size dependant, but for a material with a pore size of 30 Å the angle of the first diffraction peak (hkl 100) would be approximately 2.5 °2θ. The absence of any peaks in the pattern at higher angles of 2θ (lower d spacing) shows the amorphous nature of the pore walls. Examples of x-ray diffraction patterns of MCM-41 will be shown in chapter 3.

2.3 Temperature Programmed Desorption

It was an integral part of this project to design, develop and build an apparatus for the performance of temperature programmed desorption (TPD) from catalyst samples. TPD is a powerful and versatile, yet relatively simple and inexpensive, tool for catalyst characterisation.

When applied to acid catalysts, with a simple probe molecule such as ammonia integration of the desorption peak combined with a suitable calibration method can be used for quantitative determination of the number of acid sites, while the temperature of maximum desorption (t_{max}) will give information about the relative

strengths of acid sites and the activation energy for desorption ($Ea_{desorption}$) may be estimated.
With different probe molecules the method can give an indication of the processes actually occurring in a catalytic reaction. This is particularly true if mass spectrometry is the detection method; under carefully controlled conditions reactant molecules can be adsorbed and products and intermediates identified from the mass spectrum.

Design and Development of the Temperature Programmed Desorption Apparatus

Design

It is possible to consider an apparatus for TPD as essentially consisting of three components separated from each other by various valves: the main **adsorption chamber** containing the sample, this is preceded by a **dosing section** containing the adsorbate and followed by a **detection system**. It is useful for the purposes of this report to consider these components separately.

It was decided at a very early stage that the detection method of choice is mass spectrometry. Although other methods of detection, such as gas chromatography or thermal conductivity detectors, are used in TPD, mass spectrometry has the advantage of enabling a positive identification (in most cases) of the products of desorption and bestows a versatility when using a number of different adsorbates; that is the same detection system can be used with no adjustment other than a quantitative calibration.
For this reason the design of the detection chamber was a matter of relative simplicity; high vacuum is required necessitating the use of a turbomolecular pump, as is a pressure gauge. The detection system must be isolatable from the reaction chamber but in such a way as to allow a controlled and reproducible flow of products to the detector. The design of the detection chamber is shown in figure 2.3.1.

Figure 2.3.1 TPD Detection Chamber

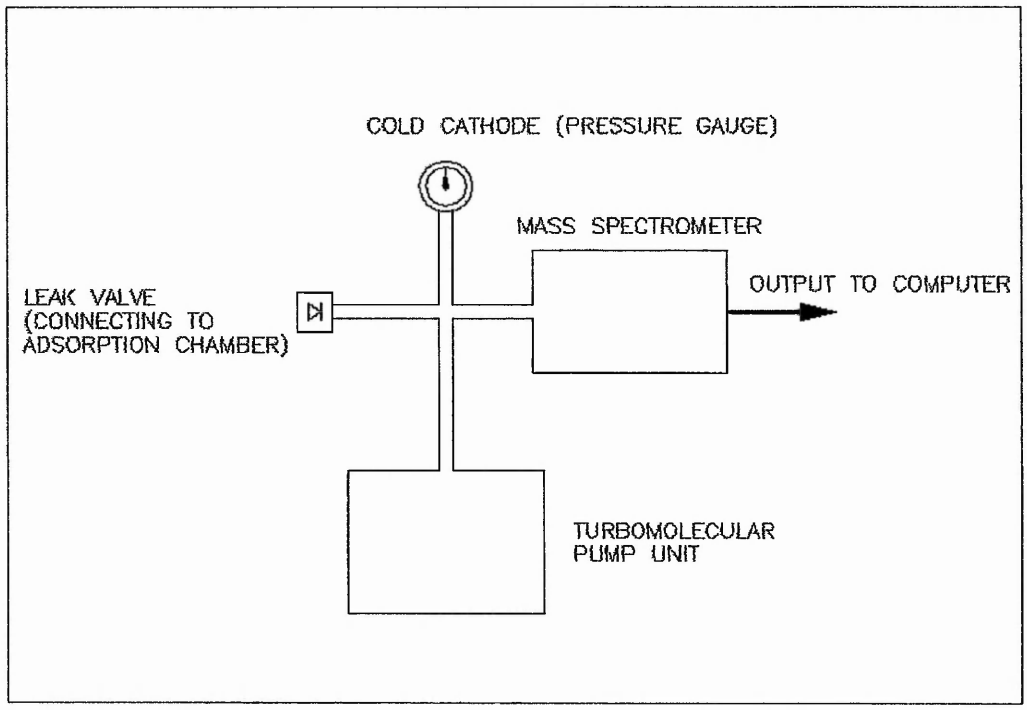

Although TPD is sometimes performed in a flow system with the adsorbate diluted in an inert carrier gas such as nitrogen the temperature of maximum desorption is flow rate dependant. Farneth and Gorte have described how, in their experiments, performing TPD in a flow system rather than a vacuum led to an error of 40 kJ/mol in the calculated desorption activation energy for ammonia from H-ZSM-5. This type of calculation, in a flow system, requires simultaneous consideration of desorption, re-adsorption and diffusion, all occurring in the presence of a carrier gas. Performing in a vacuum, with a pumping system which will remove desorption products swiftly, minimises the problems associated with re-adsorption and diffusion[7]. The first design of the adsorption chamber and the dosing system is shown in figure 2.3.2. Although the adsorption chamber and the dosing system are referred to separately it should be noted that at this first design stage the adsorption chamber was to be evacuated from the dosing

side of the apparatus; a three way valve enabling isolated pumping of the reaction chamber the dosing lines or the dosing volume.

Figure 2.3.2 Original Design of the Adsorption Chamber and Dosing System

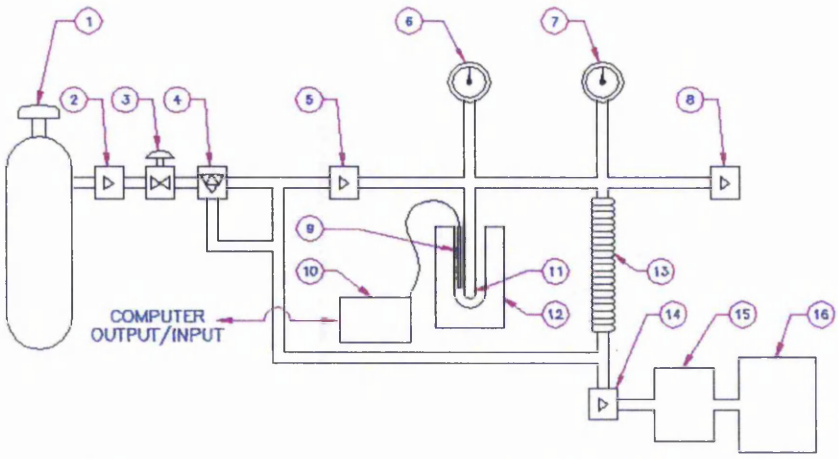

ITEM	DESCRIPTION	ITEM	DESCRIPTION
1	LECTURE BOTTLE (GAS)	9	THERMOCOUPLE
2	NEEDLE VALVE	10	TEMPERATURE PROGRAMMER & CONTROLLER
3	ON/OFF VALVE	11	SAMPLE HOLDER
4	3 WAY VALVE	12	FURNACE
5	VALVE	13	FLEXIBLE S/S TUBING
6	CAPACITANCE DIAPHRAGM (PRESSURE GAUGE)	14	VALVE
7	PIRANI GAUGE (PRESSURE GAUGE)	15	MOLECULAR SIEVE TRAP
8	LEAK VALVE TO DETECTION CHAMBER	16	ROTARY PUMP

Selection of Components

For the high vacuum detection chamber a Pfeiffer TSU 071E turbomolecular pump unit controlled via a DCU control unit was chosen. The detector selected was a Pfeiffer Prisma QMS 200 quadrupole mass spectrometer with an iridium source and a Channeltron (electron multiplier) detector, the mass range being 1-200 amu. This was protected from damage by pressure increase by a Pfeiffer IKR 261 compact cold cathode pressure gauge with a working range of $2 \times 10^{-9} - 1 \times 10^{-2}$ mbar. The valve connecting the reaction chamber and the detection chamber was a Pfeiffer UDV 040 gas dosing valve (leak valve). Vacuum in the reaction chamber was achieved using a Pfeiffer Duo 5 rotary pump; some consideration was given as to whether a turbomolecular pump was necessary here but since Pfeiffer quoted an achievable pressure $< 5 \times 10^{-3}$ mbar

it was felt that evacuation by rotary pump would be sufficient. The rotary pump was protected by a molecular sieve foreline trap (Edwards).
Pressure above the sample was to be measured by a Pfeiffer.CMR 263 compact capacitance diaphragm gauge with a range of 1 x 10^{-3} – 11 mbar and the ambient pressure measured by a Pfeiffer.TPR 265 compact pirani gauge (range, 5 x 10^{-4} – 1000 mbar); pressures from both these gauges to be monitored via a Pfeiffer TPG 252 A DualGauge.
Although each component was independently assessed, the selection of so many components from one company did provide certain advantages both in terms of system design and economic considerations.
Vacuum connections and valves were supplied by Caburn, as was the sample holder, a purpose-built metal to silica adapter fitted with a DN16 CF flange.
Furnaces were built in the science workshop at Nottingham Trent University using components from Goodfellow (ceramic tube) and Thermocoax (heating cable). These were controlled via a Eurotherm 903P temperature controller/programmer.
Also constructed in the workshop here were a brass insert for the furnaces; to ensure a good fit for the sample holder and correct positioning of the thermocouple.
The dosing system was originally constructed from Swagelok fittings as shown. Dosing was from a lecture bottle of ammonia (Argo, 99.96%).

Early Modification

The detection chamber has essentially remained unchanged from the initial design, the only change being the addition of a magnetic shield on the cold cathode because of concerns about the proximity to the turbo pump.
The dosing system was modified almost immediately because of difficulties in controlling the dosing pressure. The volume of the tube between the gas bottle and the needle valve was minimised, but as this was not effective the section was removed completely and replaced with a septum. This modified design of the whole of the temperature programmed desorption apparatus is shown in figure (2.3.3).

Figure 2.3.3 Modified TPD Apparatus (Complete)

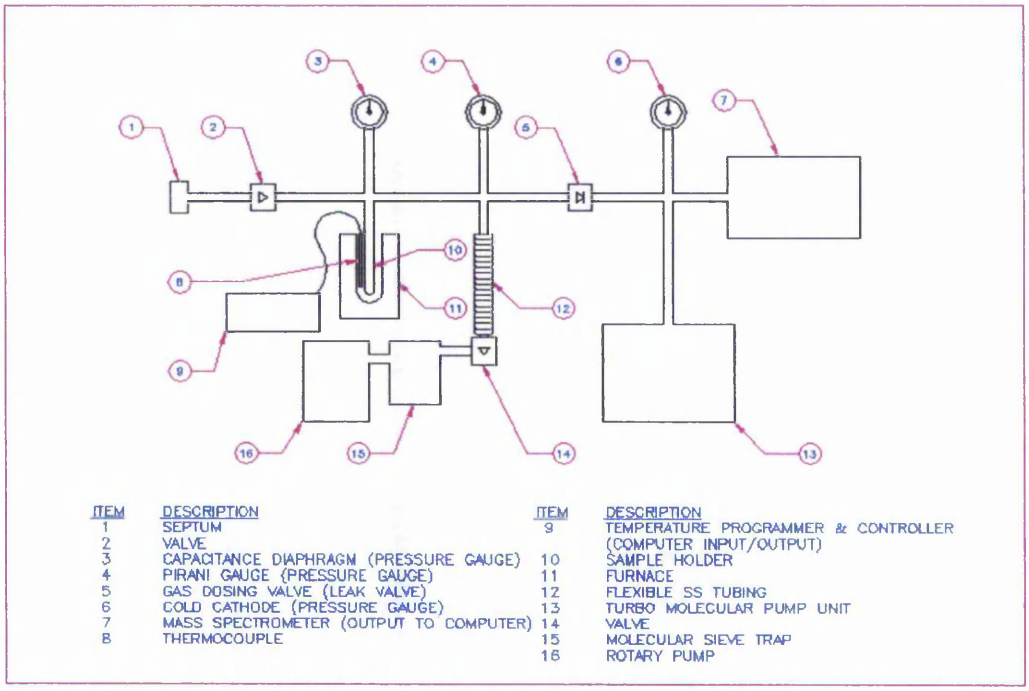

Dosing was by the injection of ~ 2 ml of ammonia (withdrawn from a gas line in the laboratory) with a gas syringe, providing a significant improvement. This entailed the movement of the rotary pump in the system, in order not to compromise pumping of the sample, this, in turn, meant that the dosing system and the adsorption chamber could no longer be pumped independently and therefore the valve between the septum and the adsorption chamber had to be left open during pre-treatment.

Operating Procedure

Samples (50 –100 mg) were placed in the sample holder, secured by a loose plug of silica glass wool and pre-treated at 823 K for one hour with a programmed ramp of 5 K/minute with the right angle valve between the septum and the adsorption chamber open and the gas dosing valve to the detector closed. The vacuum was < 10^{-4} mbar ie. below the measurable pressure on the pirani gauge.

After pre-treatment samples were cooled to 423 K (for ammonia adsorption) and the isolating valve on the rotary pump closed. Approximately 2 ml of ammonia was injected, to give a dosing pressure of ~ 5 – 10 mbar. The ammonia was adsorbed on the sample for a period of approximately 1 hour before the removal of excess and loosely bound ammonia by opening the isolating valve on the rotary pump and pumping off for 45 – 50 minutes (all at 423 K), after which time the sample was then cooled to below 303 K.

The mass spectrometer was then turned on and the leak valve to the detection chamber was opened exactly five and a half turns using its graduated scale. The precision of this opening, and of the valve itself, is vital to ensure reproducible quantitative results. The level of opening was, in this case, determined beforehand by opening the valve with a sample loaded, at room temperature prior to pre-treatment, until a change in the spectrum recorded by the mass spectrometer showed significant contribution from the adsorption chamber, rather than background from the detection chamber. Results of desorption of ammonia from a standard ZSM-5 (PQ Corp., Si/Al = 50) were monitored for reproducibility.

Desorption was then carried out over the range 303 – 873 K with a programmed ramp of 5 K/ minute. The desorption profile was recorded using a combination of the Pfeiffer Quadstar software and a computer programme written by Dr. M. Stockenhuber.

However, over a period of time the base pressure on the apparatus, as read on the pirani gauge when not in operation, gradually rose.

Routine maintenance had some effect but failed to correct the problem.

Leak testing using the mass spectrometer and an external helium supply proved that the system was relatively leak-free. There is a possibility of residual adsorption/desorption from stainless steel so the system was heated to ~ 393 K Also the distance from the system to the pump was shortened to improve pumping efficiency. Again these measures provided only temporary improvement.

Further Modification

It was decided to replace the rotary pump with a turbo pump. This would have the added benefit of enabling considerable improvements to be made to the design of the apparatus, freeing the rotary pump for use on the dosing system. This would allow the dosing area to be evacuated independently of the adsorption chamber, and if kept under vacuum would improve the controllability of adsorption pressure.

Therefore both the adsorption chamber and the dosing system were redesigned. These modifications produced a significant improvement in the base pressure readings. Again this was temporary and the reading could no longer be adjusted via the calibration scale on the gauge. During this period of apparent pressure rise the current on the turbo pump had not increased. This led to doubts that the pressure reading was correct, so the gauge was replaced.

With the new gauge head in place the pressure reading was, once again, below the measurement range of the gauge and there were no further problems with the base pressure

The dosing system was subsequently redesigned, it was again feasible to dose directly from a lecture bottle now the dosing side of the apparatus was separate, producing an entirely enclosed system; a significant improvement over injecting through the septum, and with confidence about the pressure in this part of the apparatus it was considered that the dosing pressure could be controlled sufficiently with this arrangement. It was also possible to improve the dosing system somewhat to improve vacuum and eliminate leaks merely by replacing the tube to the pump with a vacuum fitting having a wider bore.

With this new arrangement ultimate pressure $< 10^{-4}$ mbar was achievable by pumping with the rotary pump alone.

The final design of the whole of the temperature programmed desorption apparatus is shown in figure 2.3.4.

Figure 2.3.4 Complete TPD Apparatus (Final Design)

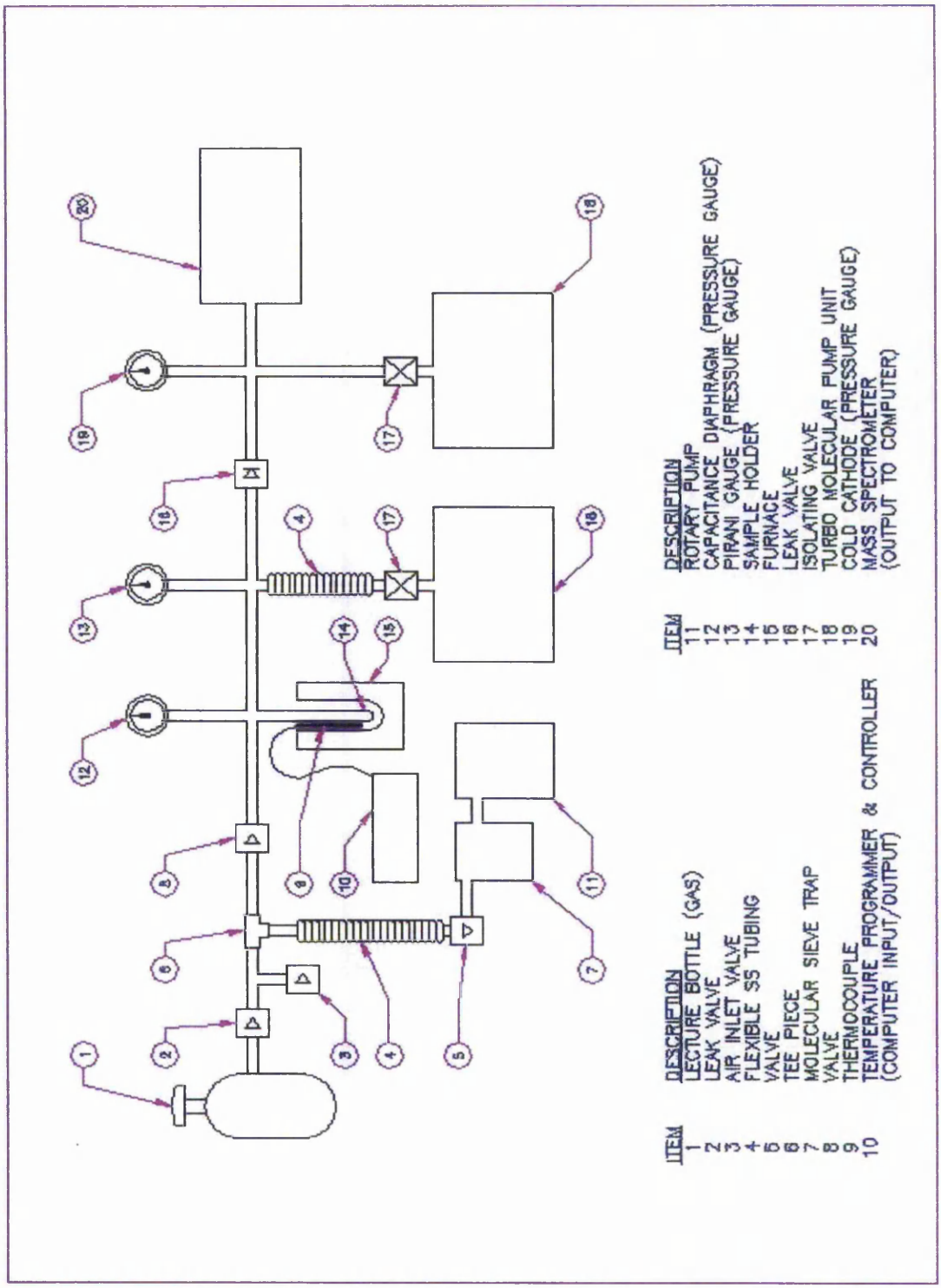

Revised Operating Procedure

Samples were pre-treated as previously but under pumping from the turbo pump attached to the adsorption chamber. The dosing system was kept under vacuum by the rotary pump.

After pre-treatment samples were cooled, as previously, to 423 K and adsorption was carried out as follows.

The isolating valves on the turbo and rotary pumps were closed and the lecture bottle opened very briefly, followed by a slight opening of the leak valve (2). The right-angled valve to the adsorption chamber (8) was then carefully opened to give a dosing pressure of ~ 5 – 10 mbar. The ammonia was adsorbed on the sample as previously before the removal of excess ammonia. During adsorption the dosing lines were pumped free of ammonia with the rotary pump. The sample was pumped down, first with the rotary pump for ~ 20 minutes, then the dosing section was isolated using the right-angled valve and the sample was further pumped with the turbo pump for ~ ½ hour (all at 423 K).

Desorption was carried out as before but with the lower base pressure and improved pumping system the gas dosing valve was now opened six and a half turns, again initial results were monitored for reproducibility, as described previously.

Calibration

Absolute calibration is preferable and therefore the method of calibration of choice was the thermal decomposition of ammonium sulphamate. According to Duval[8] this salt decomposes to give the imidosulphate and ammonia at 443 K:

$$2\ NH_3SO_3\text{-}NH_2 \rightarrow NH(SO_3NH_4)_2 + NH_3$$

and then gives the sulphate around 575 K:

$$3\ NH(SO_3NH_4)_2 \rightarrow 3\ (NH_4)_2SO_4 + 3\ SO_2 + NH_3 + N_2$$

But with the second decomposition not yielding a horizontal as the sulphate, in turn, decomposes.

Therefore ammonium sulphamate (Aldrich, 0.0078 g, 5.9 x 10^{-5} moles) was heated to 625 K (ramp 5 K/minute) in the apparatus. However, decomposition was sudden and caused a surge in pressure resulting in the cut out of the mass spectrometer by the cold cathode.

An alternative method of calibration was sought. Ammonia adsorption on a sample of high quality ZSM-5 of known Si/Al ratio was chosen. Assuming total adsorption (one molecule of ammonia per aluminium) integration of the desorption peak will allow for calibration. ZSM-5 (ammonium form, ca. 0.1 g, accurately weighed, PQ Corp., Si/Al = 50) was pre-treated and subjected to ammonia adsorption as described previously (see operating procedure). Response was calculated using the fragment m/z = 16, which is the preferred fragment for quantifying ammonia, since the m/z = 17 fragment can include a significant contribution from any water present[9]. This was repeated several times to establish reproducibility.

Figure 2.3.5 Temperature-Programmed Desorption of Ammonia (m/z = 16) from ZSM-5

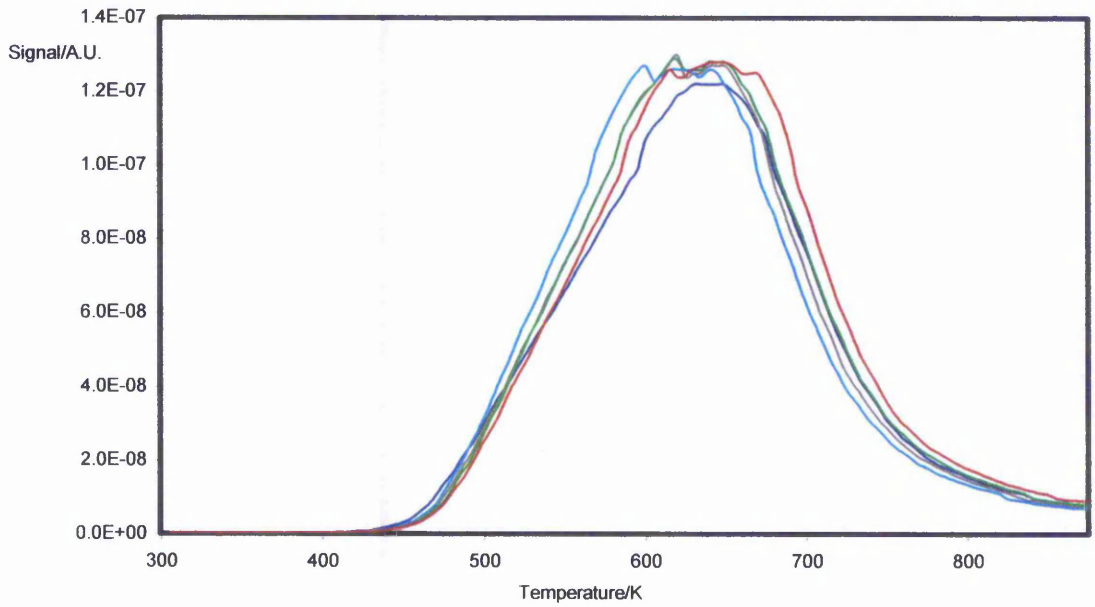

From figure 2.3.5, which shows a selection of calibration traces for ammonia desorption from ZSM-5.(Si/Al = 50, formula weight 6144.45), the calculated peak area is 0.71 ± ~ 5%/mole NH_3 (≡ Al).

2.4 in-situ Infra-red Spectroscopy

Infra-red spectroscopy is an established and widely used method for exploring the acidity of molecular sieves[7]. It can be used for direct characterisation, with the identification of different O-H stretching modes, which may have different activities. Additionally, using in-situ FTIR, changes on adsorption of molecules such as ammonia or pyridine can be observed. Quantification of acid sites can be achieved and for this purpose ammonia is an ideal and widely used probe molecule since its size means that it can penetrate almost all sites in porous materials[10].

For this work an ATI Research Series FTIR (figure 2.4.1) equipped with a specially designed vacuum cell was used.

Figure 2.4.1 The in-situ vacuum FTIR instrument

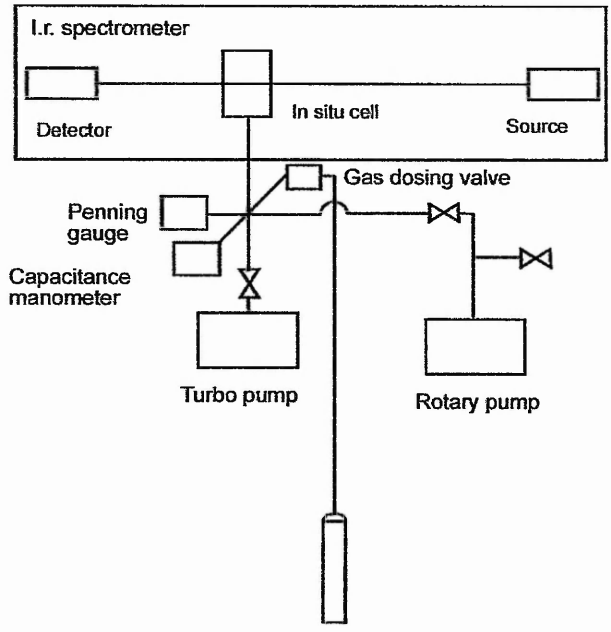

The specially designed cell is shown in figure 2.4.2, the heater coil is controlled by a Eurotherm 903P temperature controller/programmer and is capable of heating to 925 K.

Figure 2.4.2 The in-situ vacuum FTIR Cell

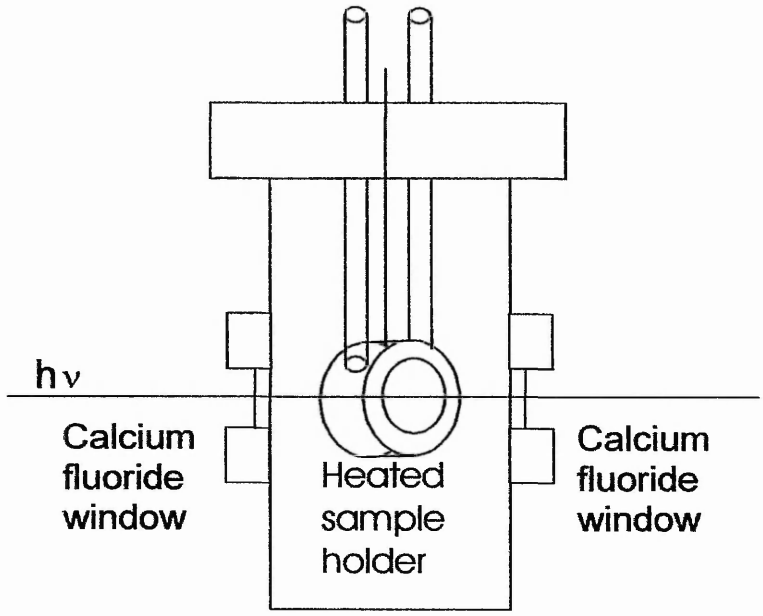

Samples were pressed into self-supporting wafers of approximate mass 25 mg and spectra were recorded in transmission mode.

2.5 References

1. Rouquerol, F., J. Rouquerol, and K. Sing, *Adsorption by Powders and Porous Solids*. 1999: Academic Press.
2. Ciesla, U. and F. Schuth, *Ordered mesoporous materials.* Microporous and Mesoporous Materials, 1999. **27**(2-3): p. 131-149.
3. Ravikovitch, P.I., et al., *Capillary hysteresis in nanopores: Theoretical and experimental studies of nitrogen adsorption on MCM-41.* Langmuir, 1995. **11**(12): p. 4765-4772.
4. Kruk, M., et al., *Characterization of highly ordered MCM-41 silicas using X-ray diffraction and nitrogen adsorption.* Langmuir, 1999. **15**(16): p. 5279-5284.
5. Kloetstra, K.R., H.W. Zandbergen, and H. Vanbekkum, *Mcm-41 Type Materials with Low Si/Al Ratios.* Catalysis Letters, 1995. **33**(1-2): p. 157-163.
6. Fenelonov, V.B., V.N. Romannikov, and A.L. Derevyankin, *Mesopore size and surface area calculations for hexagonal mesophases (types MCM41, FSM-16, etc.) using low-angle XRD and adsorption data.* Microporous and Mesoporous Materials, 1999. **28**(1): p. 57-72.
7. Farneth, W.E. and R.J. Gorte, *Methods for Characterizing Zeolite Acidity.* Chemical Reviews, 1995. **95**(3): p. 615-635.
8. Duval, C., *Inorganic Thermogravimetric Analysis.* 2nd ed. 1963: Elsevier.
9. Quadstar^{TM}., Pfeiffer Vacuum.
10. Lercher, J.A., C. Grundling, and G. Eder-Mirth, *Infrared Studies of the Surface Acidity of Oxides and Zeolites Using Adsorbed Probe Molecules.* Catalysis Today, 1996(27): p. 353-376.

3. Preparation and Characterisation of Siliceous MCM-41

1. Experimental

Preparation

Pure silica MCM-41 was prepared following the heterogeneous procedure described by Grün et al. [1]. n-Hexadecyltrimethylammonium bromide (cetyltrimethylammonium bromide CTAB, Lancaster, 98%, 2.4067 g) was dissolved, or suspended, in water, (120 ml) at 298K, using a Stuart Scientific Magnetic stirrer and stirring speed 400 rpm.

After allowing time for complete dispersion aqueous ammonia solution was added (8 ml, Fisher, 35%) and stirring continued for ca. ½ hour after which time 10 ml Tetraethylorthosilicate (TEOS, Aldrich, 98%) was added, and stirred for a further hour. The procedure was carried out at room temperature and away from direct sunlight.

For this scale of preparation, a 250 ml beaker and a medium (6 mm) magnetic follower were used.

The sample was filtered over a number 2 sinter, washed with large quantities of distilled water (typically 1-2 litres), and dried overnight at 383 K, a temperature ramp was used to achieve this (1 K/min).

The dried material was heated, in a silica tray, at 773 K for 6 hours in static air (ramp, 1 K/minute). The material was then cooled and calcined in air at 793 – 813 K for 8 - 10 hours (ramp, 1 K/minute).

Later samples were initially heated at 793 K for 6 hours under a flow of nitrogen (5 L/hour, ramp 1 K/min) to remove the majority of the surfactant without exposing the product to the heat generated by calcination. They were then cooled and calcined in an air flow (5 L/hour, 793 – 823 K for 8 - 10 hours, ramp 1 K/min).

Samples were ground only after final calcination and cooling. The ground calcined products were pure white with a distinctive, dry, chalky texture.

Since the yield from this preparation was barely more than 2 grammes it was found necessary to increase the scale. The main reasons that this was desirable were twofold; firstly because it is an uneconomic use of time to prepare a base material for modification in small batches and secondly, and more importantly, comparisons between modified materials are less ambiguous if the host, or parent, material is the same.

Therefore, the procedure was gradually scaled up by increasing the amounts of constituents used; and adaptation of the equipment. The stirring speed was reduced with increasing length of magnetic follower. Later preparations were stirred by means of an overhead stirrer (Scientific Laboratory Supplies Yellowline), fitted with a glass stirring paddle of approximately 50 x 20 mm blade size and a stirring speed of 50 – 100 rpm and carried out in a 3 litre beaker (diameter 15 cm.). Longer drying and calcination times were used for the larger batches. The largest scale-up has been ten times the original quantities, and, after initial calcination in nitrogen for ~ 12 hours, required calcination in air for ca 24 - 36 hours and resulted in a yield of 23.3 g.

From the results of characterisation (described below) the scale-up was not detrimental to the final product.

Characterisation

All MCM-41 materials were characterised by BET surface measurement, powder x-ray diffraction and full nitrogen adsorption isotherms as described in chapter two. X-ray diffraction was by comparison, as described in that chapter, with a standard material prepared by Dr. Gerd Grubert at Reading University and more thoroughly characterised (sample designated GG).

3.2. Results and Discussion

Various characteristics of the different batches of MCM-41 are summarised overleaf in table 3.2.1. Total pore volumes have been calculated at a single point, $P/P^0 = 0.95$[2], except where the isotherm showed evidence of multilayer surface coverage in this region (an upward turn in the isotherm at high values of P/P^0). In these cases, in order to avoid overestimation of the pore volume, the flat section of the isotherm was extrapolated to $P/P^0 = 0.95$, and this value used. Pore diameters have been estimated by two methods. Firstly the Kelvin equation was applied with comparison to a material of a known pore diameter [3] (MCM-41 Fe5, see chapter 5). This material had previously been characterised by nitrogen adsorption using a Micrometrics ASAP 2000 which gave a value for the pore diameter of 27 Å using the Barrett, Joyner and Halenda (BJH) method[4].

If a liquid is present in a capillary of radius, r, then the equilibrium vapour pressure of the liquid will be less than the saturated pressure if the contact angle is less than 90°. The vapour pressure is related to the pore radius by the Kelvin equation:

$$Ln\frac{P}{P^0} = \frac{-2\gamma v}{r_K RT} Cos\theta$$

Where:

P = Pressure

P^o = Saturation vapour pressure

γ = Surface tension of the liquid adsorbate

v = Molar volume of the liquid

r_K = Radius of the capillary

θ = Contact angle

Pores fill at a value of P that satisfies the equation. Therefore, if pore size is not uniform, all pores with a radius less than r_K will be filled at the corresponding pressure. Effectively this makes the capillary condensation step of the isotherm analogous to a cumulative frequency curve of pore radius.

Assuming the given pore diameter of the comparison material to be accurate enables calculation of a value for $-2\gamma\nu\text{Cos}\theta$, which can then be substituted in the equation for the other materials.

Secondly a geometrical method was used [1]. This method assumes a regular array of cylindrical non-connecting pores; mathematically the mean pore diameter is then equal to 4Vp/a, where 4Vp is the pore volume and a is the BET surface area.

From table 3.2.1 it can be seen that all the parent MCM-41 materials exhibited surface areas in the region of 900 –1100 m^2/g and total pore volumes of ca. 0.7 – 0.8 ml/g, as expected of this type of material[2], and gave linear BET plots in the region P/P^o = 0.05 – ca. 0.25 (used for calculation if not linear in the range P/P^o = 0.05 – 0.3).

Estimated using the Kelvin equation, samples had pore sizes centred in the region of 26 to 31 Å, however the values obtained by calculation assuming the cylindrical model were consistently higher; ca. 28 to 32 Å. Applying this method to the comparison material (BJH pore diameter 27 Å) gave a value of just over 32 Å. These systematic differences may result from the fact that the former method provides a median pore diameter, while the latter gives a mean value, if so this suggests an asymmetrical pore size distribution.

Table 3.2.1 Properties of Siliceous MCM-41

Designation	Scale	Yield	% yield	Estimated Pore Diameter (Kelvin)/Å	BET Surface Area/ m^2g^{-1}	Total Pore Volume/ ml g^{-1}	Pore Diameter/ Å $(4Vp/a)^A$	Position of 110 x-ray diffraction peak/ $^o2\theta$	Relative Intensity of 110 x-ray diffraction peak[B]	Subsequent Use
Batch 1	1	2.01	76				Not known	4.29	0.79	Organic modification: butanol, pentanol, dilute cyclohexanol
Batch 2	2	4.03	76	30.7	980	0.76	31.1	4.14	1.06	
Batch 3	1.5	3.42	86	27.5	1040	0.78	29.8	4.13	0.95	Organic modification: hexanol,
Batch 4	3	5.78	73	30.9	1012	0.77	30.5	4.19	1.03	Organic modification: benzyl alcohol,
Batch 5	4	10.19	97	27.2	1037	0.75	29.1	4.08	1.06	Organic modification: methanol undilute cyclohexanol, tert-butanol
Batch 6	6	12.7	80	27.1	1033	0.81	31.6	4.12	1.00	Organic modification: butanol, ethanol, benzyl alcohol - subsequent sulfonation
Batch 7	8	18.6	88	29.7	916	0.74	32.3	4.14	0.88	Not used
Batch 8[C]	8	N/A	N/A	28.4	1052	0.84	31.9	4.18	1.04	Organic modification: benzyl alcohol - subsequent sulfonation
Batch 10	10	23.31	88	28.8	1052	0.78	29.8	4.09	1.16	
ICS	1	2.19	83	26.4	952	0.68	28.4	4.31	0.75	Organic modification: benzyl alcohol, ethanol, phenol
GG[D]			Not known		1007	0.86	34.3	4.15		Post-synthetic iron modification Organic modification: hexanol, propanol, toluene

A; Vp = total pore volume, a = BET surface area
B; relative to the same peak for the sample desigated GG
C; yield not relevant as sample loss during preparation
D; standard material used for comparison for XRD

For most of the samples the position of the 110 diffraction peak varied little compared to the standard material, and a representative sample of these diffraction patterns, along with that of the standard, is shown in figure 3.2.1.

Figure 3.2.1 Typical X-ray diffraction of MCM-41

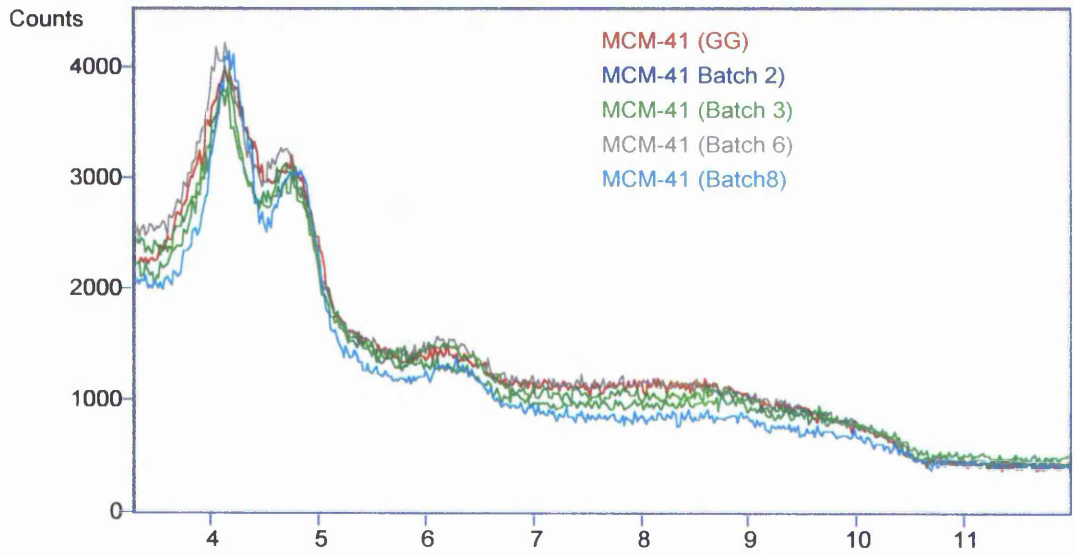

Exceptions were: the batches designated batch 1 and ICS, which were the products of the smallest scale preparations, and batches 5 and 10. These are shown in figure 3.2.2.

In the former two cases there were positive shifts in the position of the 110 diffraction peak of 0.14 and 0.16 $^{o}2\Theta$ respectively, and a lowering of the peak intensity, this suggests a smaller pore size and a more disordered sample. In the latter cases there was a negative shift of 0.07 and 0.06 $^{o}2\Theta$ and a relative increase in the intensity, suggesting a slightly larger pore size, and more order within the pore structure of the samples.

Since there were other differences in the characteristics of the remaining two materials (batches 4 and 7) their diffraction patterns are shown and discussed later in this chapter.

Figure 3.2.2 X-ray diffraction of MCM-41, Batches 1, 5, 10 and ICS

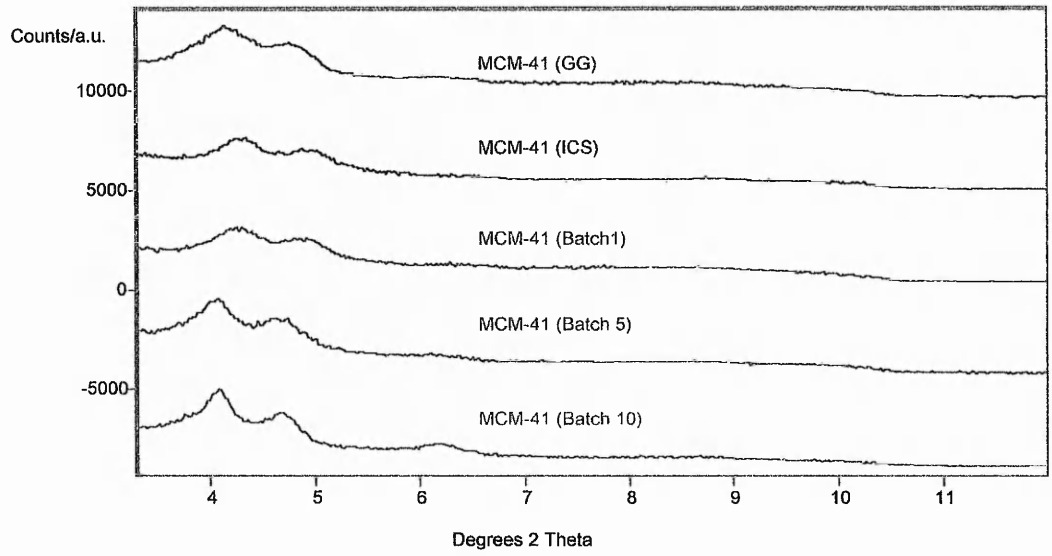

All samples had isotherms characteristic of the BDDT Type IV and most showed an absence of the hysteresis loop which is often associated with the Type IV isotherm. Figure 3.2.3 shows a typical adsorption/desorption isotherm for the parent material.

It has long been observed experimentally that materials of this class with a pore diameter < ca. 40 Å. often lack hysteresis in their nitrogen isotherms[1, 5, 6]. It has been generally accepted that in this type of material with a uniform and non-connecting pore structure hysteresis will be absent, for a given adsorbate at a given temperature, below a critical pore diameter and this type of reversible type IV isotherm has been designated Type IVc[2]. Sonwane and Bhatia have calculated a theoretical value of the pore diameter at which hysteresis is absent in MCM-41 (for nitrogen at 77.4 K). These authors used a modification of the Saam-Cole theory; which has been discussed in chapter one (section 1.5)[2, 7]. It had been previously proposed that if the uncertainty of the intrinsic pore size exceeded $\Delta t'$ (the difference between the instability point for adsorption and desorption) then an absence of hysteresis in MCM-41 could be expected[8]. Sonwane and Bhatia adapted the Saam-Cole approach to take account of additional factors: the difference in interaction potential of an adsorbate molecule

in the presence of the solid adsorbent, compared to the bulk liquid; and the curvature dependence of surface tension[7]. Their calculated diameter of 36 - 38 Å was in fairly good agreement with their own experimental results; where the value lay somewhere between 38 and 43 Å[7].

However Conner et al found nitrogen adsorption hysteresis in samples with much lower pore diameters and, interestingly, found that isotherms could be found to be remarkably similar for samples which were known, from x-ray diffraction data, to be very different, that is, samples known respectively to have ordered and amorphous pore structures[9].

Figure 3.2.3 Nitrogen Adsorption/Desorption Isotherm (at 77 K) for MCM-41

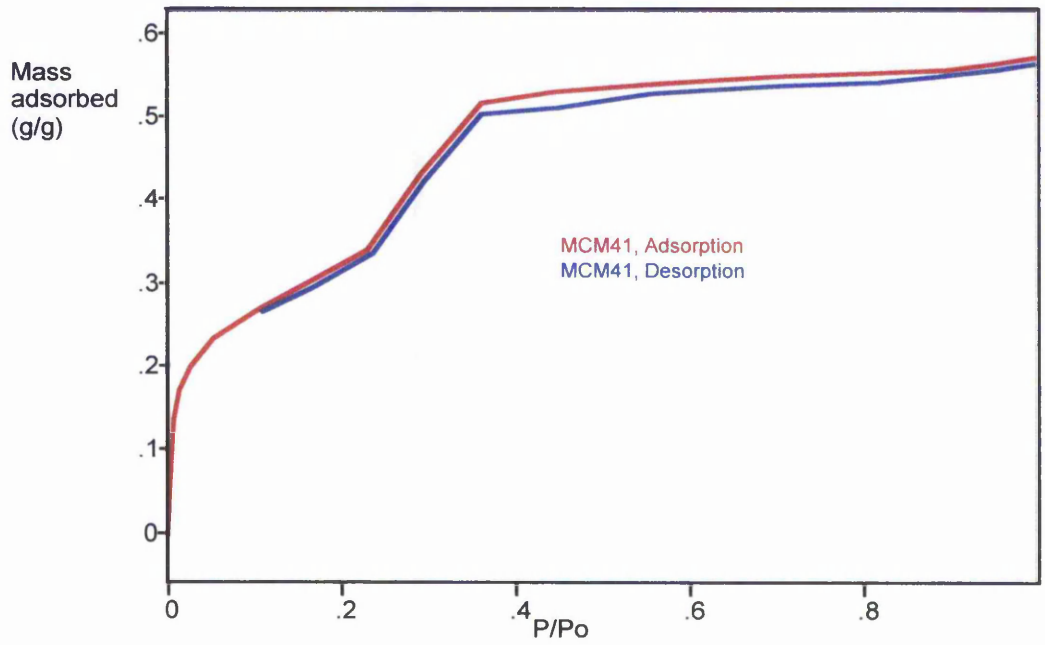

Figure 3.2.3 shows a type IVc reversible isotherm; typical for nitrogen adsorption at 77 K on MCM-41 in this pore size range, and confirms the mesoporous nature of the material

Two batches of the MCM-41 material (batches 4 and 7), however, did show some hysteresis. One batch, batch 7, showed very slight hysteresis of the type classified H_1, which is associated with MCM-41 possessing a higher pore diameter. This is unexpected in this type of system using a surfactant chain length of 16, and neither method of pore size evaluation suggested that this material had a significantly larger pore diameter than those of the other samples.

There was also no shift in the 110 diffraction feature centred around $2\Theta = 4.15°$, but a slight loss in intensity compared with the comparison material. The diffraction patterns of both these samples, batch 4 and 7, are shown in figure 3.2.5. Batch 7 was not used in the subsequent modification described in this work.

The isotherm of the material designated Batch 4, seen in figure 3.2.4, showed significant hysteresis of the type classified H_2, often associated with materials with complex pore structures of different size and shape[2]. This in itself is unusual, as materials of this class, when hysteresis is present, tend to demonstrate type H_1 hysteresis, which is associated with materials with an open pore structure and a very narrow pore size distribution. Selvam et al. report that MCM-41 materials with uniform pore sizes and shapes exhibit type H_1 hysteresis while those with non-uniform pore shapes and sizes exhibit hysteresis of the type H_2[10]. Additionally Kruk and Jaroniec ascribe two different causes to the widening of pore size distributions in MCM-41; either the variation of the diameter across the range of the channels in the material, or the variation of the pore diameter along the length of single channels[11].

Figure 3.2.4 Nitrogen Adsorption/Desorption Isotherm (at 77 K) for MCM-41 Batch 4.

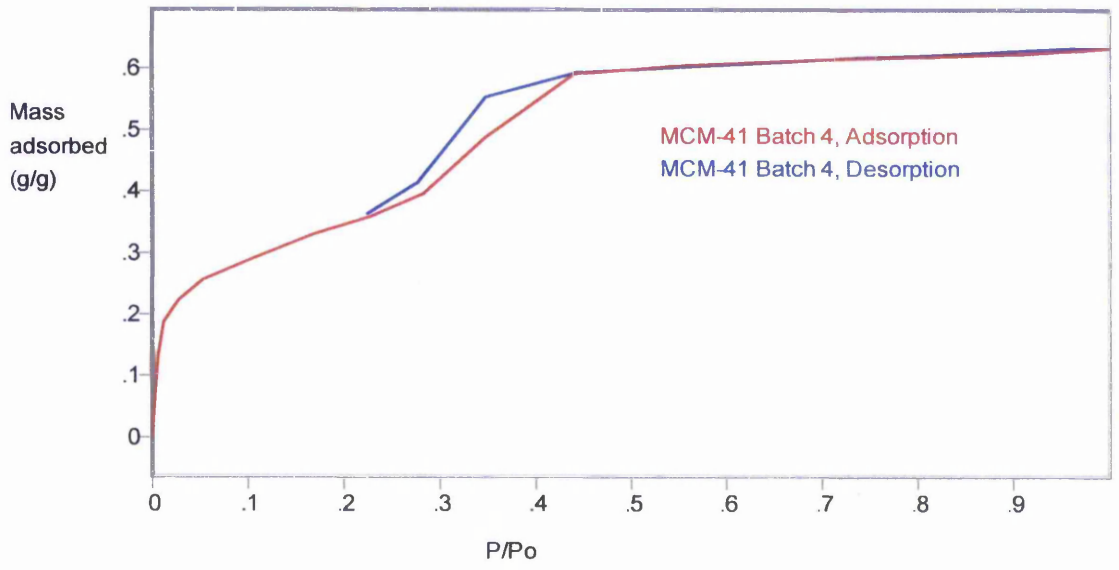

This isotherm also showed a less steep rise between the inflection point (B) and the onset of the plateau; the range associated with mesopore filling/condensation. Since this range of the isotherm is associated with mesopore filling the inflection point can be viewed as filling the smallest mesopores, while the onset of the plateau represents the filling of the largest. Thus the steepness of the rise is an indication of the pore size range[2], and the observations here indicate a broader pore size distribution in this case[10, 11]. These differences in the isotherm were in spite of the fact that this sample showed little difference in the x-ray diffraction pattern (shown below) from the standard MCM-41 material used for comparative purposes. There was a shift in the position of the 110 diffraction feature at $2\Theta = 4.15^{\circ}$ of $+ 0.04^{\circ}$ in Batch 4 compared with the standard material, but the intensity was comparable, indicating no disruption along the length of the pores. The shift itself, if significant, indicates a *smaller* average pore size, which is contradictory to the literature on hysteresis in these materials and may indicate that the reasons for the hysteresis lie in a more disordered pore arrangement.

Figure 3.2.5 X-ray diffraction of MCM-41, Batches 4 and 7.

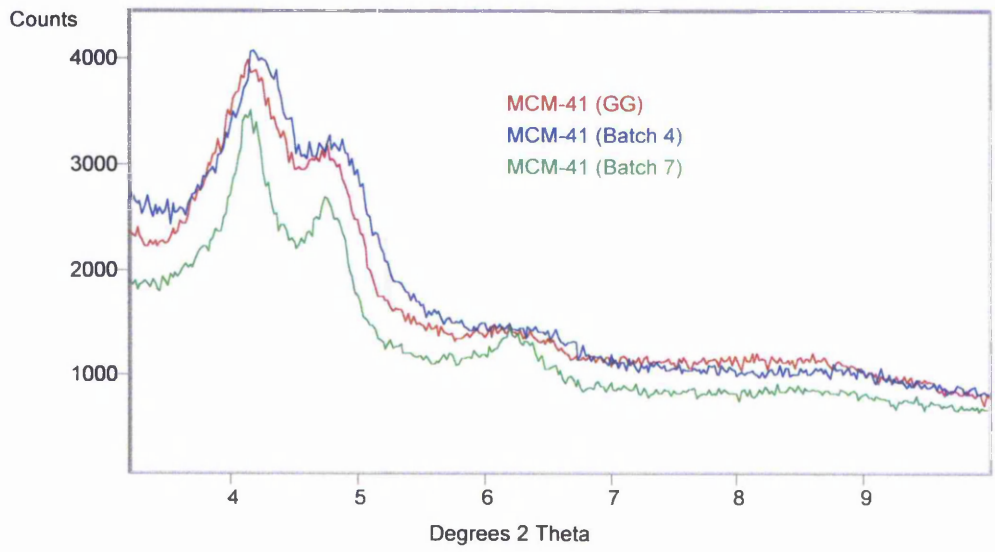

One other sample (which was subsequently used for modification with benzyl alcohol) also showed a shift in the position of the peaks of the x-ray diffraction

pattern; in this case of + 0.16 °2Θ and there was also a considerable loss of intensity of the diffraction from the peaks, suggesting disruption to, or within, the pores in addition to smaller pores. This sample did show the lowest of all the pore volumes and estimated pore diameters, at 0.68 ml/g and 26.4 Å respectively

This sample alone was sent for transmission electron microscopy (by Professor C. J. Kieley of the Department of Materials Science and Engineering, University of Liverpool. A sample of the micrographs are shown in figures 3.2.6 (pores end-on) and 3.2.7 (pores edge-on).

Figure 3.2.6 Transmission Electron Micrograph of MCM-41 Showing Pores End-on.

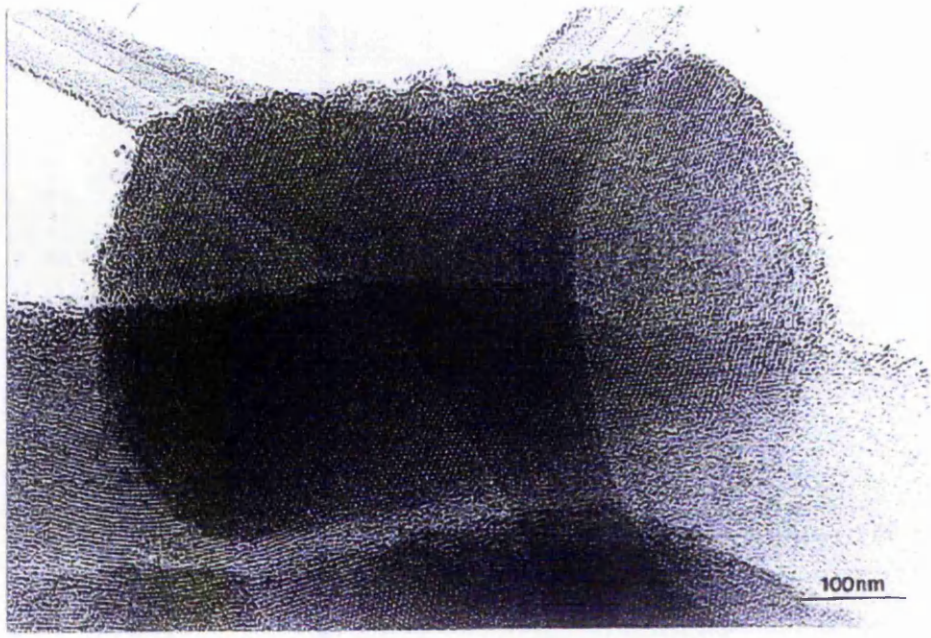

Figure 3.2.7 Transmission Electron Micrograph of MCM-41 Showing Pores Edge-on

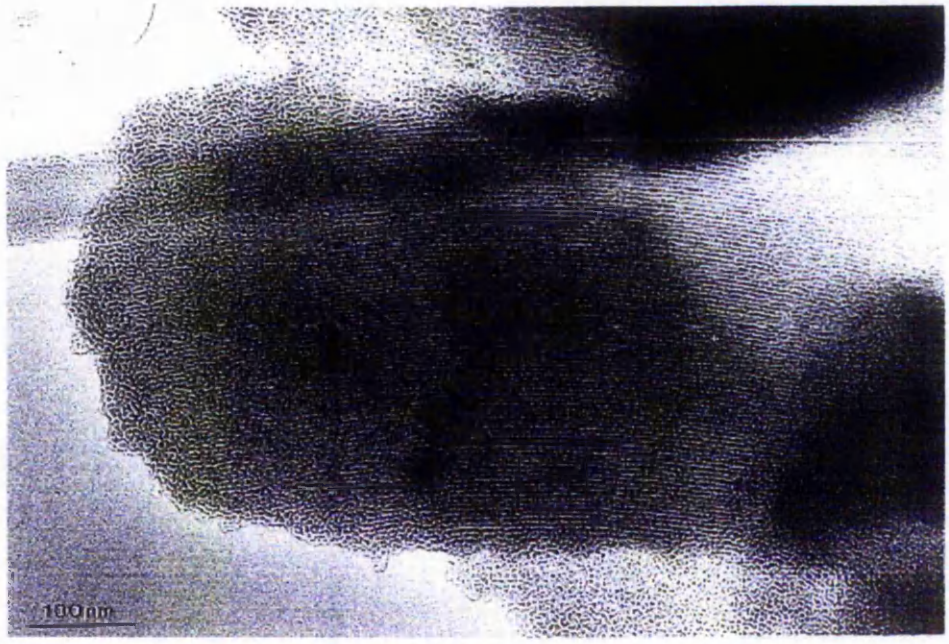

Both these images show a certain amount of disorder in the material, and from inspection of figure 3.2.7 it is clear that there are areas where the pores are neither straight nor parallel.

By observation of the preparation it was possible to make some correlation between certain factors and the quality and consistency of the product obtained. It was found that any marked vortex during stirring was detrimental to the integrity of the final product, and if this occurred the stirring speed was reduced slightly.

3.3 References

1. Grun, M., et al., *Novel pathways for the preparation of mesoporous MCM-41 materials: control of porosity and morphology.* Microporous and Mesoporous Materials, 1999. **27**(2-3): p. 207-216.
2. Rouquerol, F., J. Rouquerol, and K. Sing, *Adsorption by Powders and Porous Solids.* 1999: Academic Press.
3. Grubert, G., et al., *The room temperature, stoichiometric conversion of N2O to adsorbed NO by Fe-MCM-41 and Fe-ZSM-5.* Journal of Catalysis, 2000. **196**(1): p. 126-133.
4. Barrett, E.P., L.G. Joyner, and P.H. Halenda, Journal of the American Chemical Society, 1951. **73**: p. 373.
5. Ciesla, U. and F. Schuth, *Ordered mesoporous materials.* Microporous and Mesoporous Materials, 1999. **27**(2-3): p. 131-149.
6. Jaroniec, M., et al., *Comprehensive characterization of highly ordered MCM-41 silicas using nitrogen adsorption, thermogravimetry, X-ray diffraction and transmission electron microscopy.* Microporous and Mesoporous Materials, 2001. **48**(1-3): p. 127-134.
7. Sonwane, C.G., *Analysis of criticality and isotherm reversibility in regular mesoporous materials.* Langmuir, 1999. **15**(16): p. 5347-5354.
8. Inoue, S., *Prediction of hysteresis disappearance in the adsorption.* Langmuir, 1998. **14**(11): p. 3079-3081.
9. Conner, W.C., et al., *Hysteresis in physical sorption for MCM.* Studies in Surface Science and Catalysis, 1998. **117**(Mesoporous Molecular Sieves): p. 575-581.
10. Selvam, P., S.K. Bhatia, and C.G. Sonwane, *Recent Advances in Processing and Characterisation of Periodic Mesoporous MCM-41 Silicate Molecular Sieves.* Industrial & Engineering Chemistry Research, 2001. **40**: p. 3237-3261.
11. Kruk, M., et al., *Characterization of highly ordered MCM-41 silicas using X-ray diffraction and nitrogen adsorption.* Langmuir, 1999. **15**(16): p. 5279-5284.

4. Aluminium-Containing MCM-41

4.1 Introduction

As early as the introduction of MCM-41 by the scientists at Mobil, aluminium incorporation has been an important facet of the research into the materials. These scientists initially reported the production of aluminosilicate MCM-41 in addition to the purely siliceous materials[1], by the addition of sodium aluminate to the synthesis mixture. Purely siliceous MCM-41 probably has little scope for catalytic application because of its low acid strength[2, 3]. The introduction of a trivalent ion, such as aluminium, can confer acidic properties on the material. The acid sites can arise in two ways: via Brønsted acid (proton donor) and Lewis acid (electron pair acceptor) sites. Using zeolite acidity as an example:

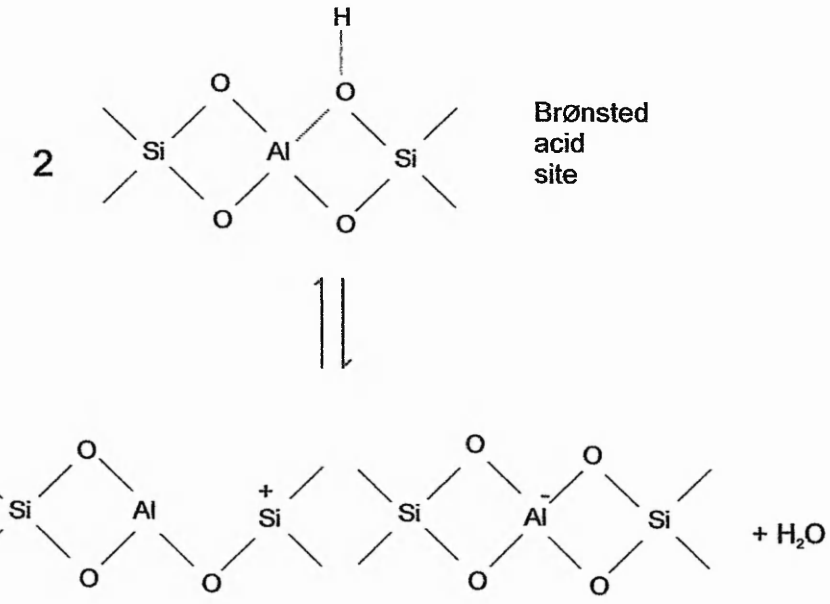

Lewis acid site

The two types of site are interchangeable by hydration or dehydration. In zeolites it is generally observed that acid site strength and number are inversely related. The presence of these, often strongly, acidic sites confers catalytic properties,

for example in initiating carbocation reactions. Additionally zeolites where the hydrogens of the Brønsted acid have been replaced by metal cations can induce reactivity. In this case the nature of the substituting metal will affect catalytic behaviour; for example, differences in electronegativity can produce a partial positive charge on the aluminium atom, giving it some Lewis acid character. However M41S materials are not entirely analogous to zeolites as in this case the silica framework is amorphous whereas zeolites are highly crystalline[1, 4]. Also it has long been considered that even aluminium containing materials lack the high acid strength associated with zeolites[2, 5-7].

Others groups have achieved aluminium introduction by various methods, for example by the incorporation of different aluminium salts such as aluminium sulfate, or alumina, during synthesis[8]. More recently post-synthetic incorporation has been explored, for example by grafting of aluminium isopropoxide[5, 9] or by implantation of aluminium chloride or nitrate[10]. It is considered to be desirable to incorporate aluminium into the silica framework, rather than as extra-framework species, because it is likely that this will result in aluminium which is better structurally defined[11]. It is also more likely that framework aluminium will have tetrahedral rather than octahedral co-ordination; the former being favourable for catalytic activity[7]. Against this there are concerns that aluminium may be embedded so deeply into the framework as to be inaccessible to reactants.

Oumi and co-workers have also developed a post-synthetic alumination process using trimethylaluminium which, they claim, incorporates aluminium into the framework and also significantly improves hydrothermal stability compared to purely siliceous MCM-41[2].

Within our research we have attempted incorporation from aluminium nitrate during synthesis. The activity of the resulting materials has been explored in a reaction well researched within this group[12].

The Friedel-Crafts acylation of aromatic compounds to produce ketones is a key step in the manufacture of many fine chemicals and pharmaceuticals. An example is the preparation of isobutylacetophenone, which is an intermediate in the production of the drug ibuprofen. Traditionally these acylations are carried out using a Lewis acid "catalyst" such as aluminium chloride leading to the need for costly disposal of spent catalyst; this is often, but not always required in

excess. Additionally corrosive hydrogen chloride is a stoichiometric by-product of the reaction.

Acylation reactions are also often performed in halogenated solvents. Because of the environmental undesirability of these solvents they are no longer commercially available, for manufacturing purposes, in this country. Existing stocks are only being allowed to be exploited before removal from chemical processes.

Extensive research within this group has shown this to be a reaction capable of catalysis by zeolite BEA and other zeolites. This research centred around the activity of zeolite BEA into which iron has been introduced by a process resembling exchange, subsequently referred to as Fe-BEA.

4.2 Experimental

4.2.1 Preparation

Aluminium containing samples were prepared by introduction during synthesis only. Incorporation was achieved by the addition of a suitable amount of aluminium nitrate nonohydrate to the surfactant/water mixture. For example, using the original scale of the MCM-41 preparation described in chapter three (10 ml. of Tetraethyl orthosilicate) 0.1869 g was added to achieve a Si : Al ratio of 30. The TEOS was added to the synthesis mixture prior to the addition of ammonia to improve metal distribution within the material as it is believed to form a complex with the metal ions[13].

Nominal aluminium content only is quoted and samples are designated x Al MCM-41, where x represents the Si : Al ratio if the total aluminium in the reaction mixture were incorporated into the final product.

4.2.2 Characterisation

BET surface areas were determined using the automated volumetric apparatus previously described in section 2.1. Subsequently, full nitrogen isotherms were recorded using the vacuum frame apparatus, also described in section 2.1. Powder x-ray diffraction was also performed on the samples as described in section 2.2.
Very recently it has been possible to have x-ray diffraction patterns of some samples recorded over a greater angular range[14].
In these cases x-ray powder diffraction data were collected using a Siemens D-5005 diffractometer equipped with a scintillation detector. A Cu K α x-ray source was used with a Ni filter. The diffractometer operates at 50 kV and 40 mA. Step size was set to 0.02 degrees counting 6 seconds per step between 1 and 10 degrees 2θ.

4.2.3 Catalytic Reactor Testing

Aluminium samples, along with a purely siliceous MCM-41, were tested for activity in the acylation of anisole with acetic anhydride, a reaction normally catalysed by a Lewis acid such as aluminium chloride, but which has been extensively studied within this group using BEA zeolites (see below).
The reaction was carried out in the liquid phase at 333 K in a round-bottomed flask fitted with a condenser with drying tube, a stopper and a thermometer. 42.5 g (0.4 moles) of anisole (Aldrich, 99%), 20.44 g (0.2 moles) of acetic anhydride (Aldrich, 99+%) plus 0.5 g of n-decane (Aldrich 99%), added as an internal standard for analysis purposes, were stirred using a thermostatically controlled heater\stirrer (IKA WERKE RCT Basic) for approximately 5 – 10 minutes at room temperature before a sample was taken from the reaction vessel for analysis. Catalyst samples (~ 300 mg.), previously pre-treated in air at 773 K for 1 hour, were then added to the reaction mixture while they were still hot (> 373 K) and the reaction mixture heated to 333 K, with stirring.

Subsequent samples for analysis were withdrawn at 30 minute intervals; a small amount of the reaction mixture was first withdrawn into a sample bottle to allow to settle and thus avoid contamination of the syringe with the solid catalyst. The progress of the reaction was monitored by gas chromatography using a Shimadzu GC-8A fitted with a packed column (10% OV101 liquid phase on a Chromasorb WHP support). A temperature programme was used over the range 353 - 473 K with a ramp of 8 K/minute and the flame ionisation detector at 623 K was used. The injection volume was 0.2 µl.; from a 0.5 µl. syringe.

Acylation of Anisole With Acetic Anhydride

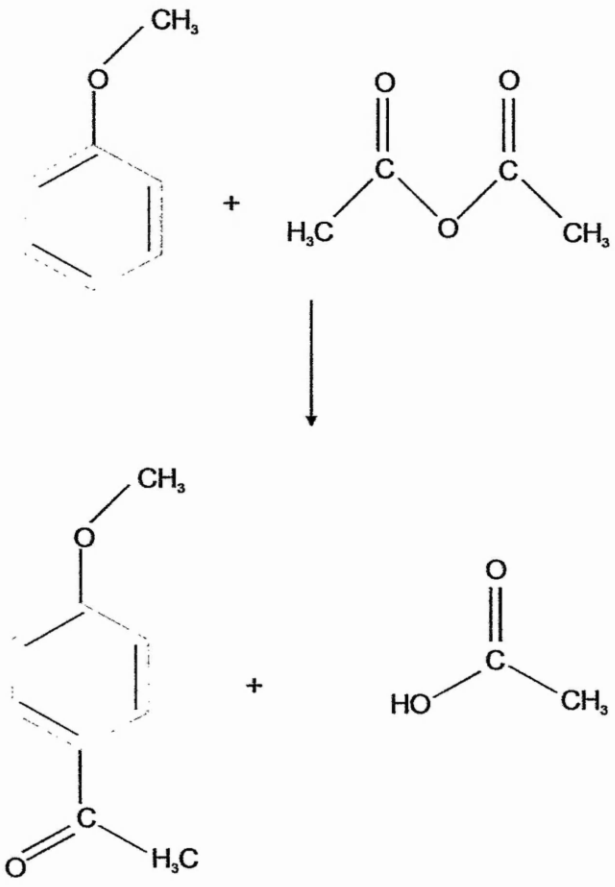

4.3 Results and Discussion

4.3.1 Characterisation

The x-ray diffraction patterns (shown in figure 4.3.1.1, below) of the aluminium containing samples show a loss of ordering in the pore system. No peak attributable to the hexagonal pore arrangement can be observed for any of these materials.

Figure 4.3.1.1 Powder X-Ray Diffraction Patterns for Siliceous and Aluminium Containing MCM-41

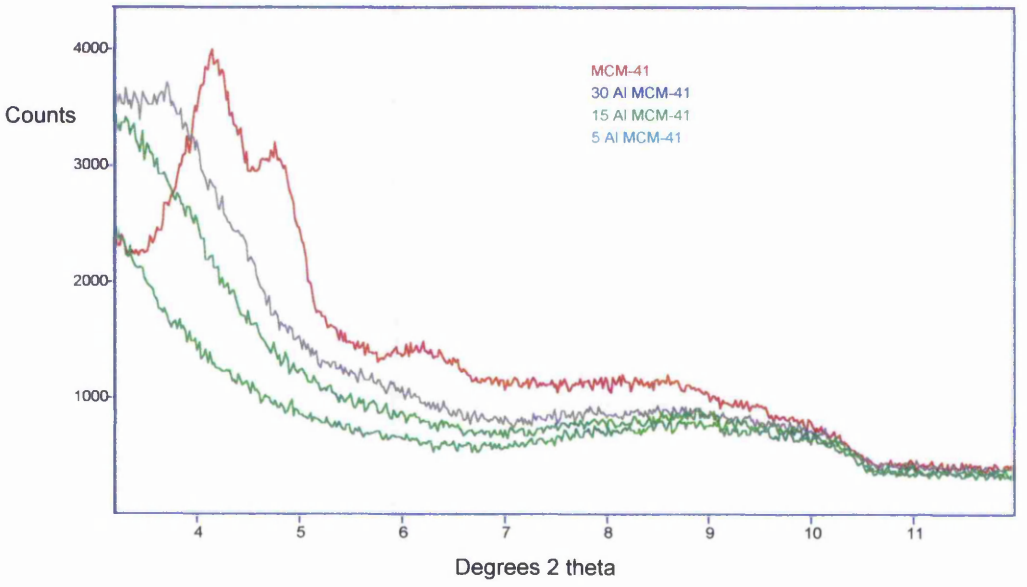

Figure 4.3.1.2 shows the x-ray diffraction patterns of the materials, along with an aluminium free sample, recorded over a greater angular range elsewhere[14].

Figure 4.3.1.2 X-Ray Diffraction Patterns for Siliceous and Aluminium Containing MCM-41

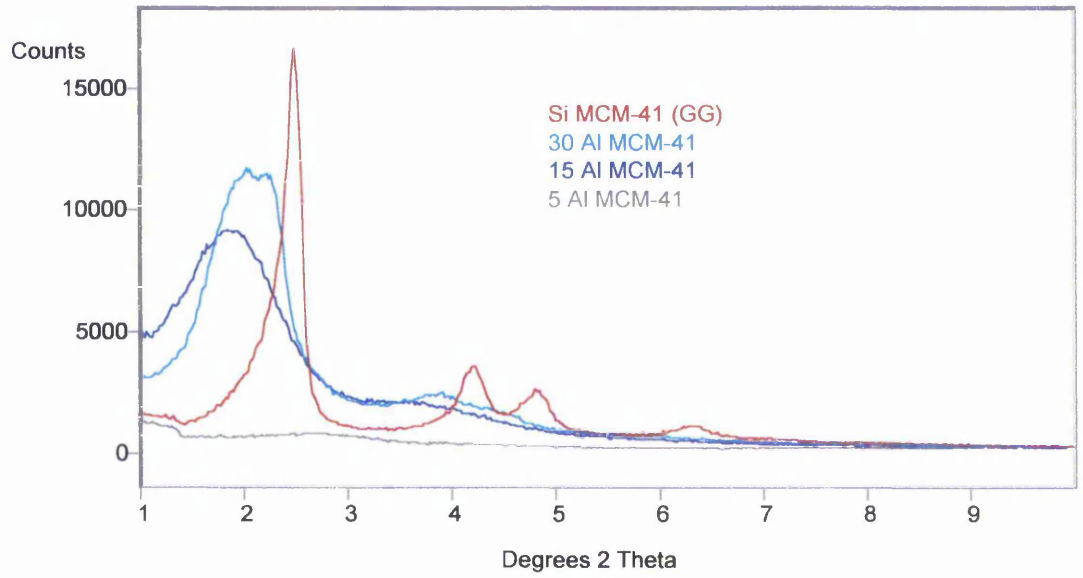

The pattern of the siliceous MCM-41 exhibits a sharp, narrow, reflection at 2.49 °2Θ (hkl 100). Further peaks can be observed at 4.21, 4.81 and 6.33 degrees 2Θ; these correspond to the reflections with Miller indices of 110, 200 and 210 respectively. The sharpness of the 100 peak, along with the presence of the 210 reflection, which is not always seen for MCM-41, indicates that this sample has a high degree of pore ordering[15]. For the aluminium containing samples the 100 peak is observed to lose intensity and broaden. Only one of these samples exhibits any further peak; the sample designated 30AlMCM-41 (the lowest aluminium content) has a very broad, low intensity 110 reflection centred around 3.9 °2Θ. This broadening of the 100 peak is progressive with increasing aluminium content. In the sample containing most aluminium (5 Al MCM-41) this peak also is absent, or occurs at an angle less than 1 °2Θ. This indicates increasing loss of order with aluminium content in line with the findings from our own results.

Luan et al studied the structural effects of aluminium incorporation using different aluminium sources. They found that the only source which introduced aluminium only into the framework, aluminium sulfate, also caused the maximum disruption to the pore system[4].

It is also observed that the main diffraction peak shifts to lower 2Θ values with increasing aluminium content; which indicates an increase in pore size, if wall thickness is constant. Additionally the peak for 30AlMCM-41 appears to consist of a doublet; which indicates a bimodal pore size distribution.
The repeat distance, a, between pore centres can be calculated from the relationship:

$$a = \frac{2\,d_{100}}{\sqrt{3}}$$

The results of these calculations are summarised in table 4.3.1 1

Table 4.3.1.1 Structural Parameters of Aluminium MCM-41

Sample	Position of 100 diffraction peak/°2θ	d-spacing/ Å	a/Å
GG (Al free)	2.49	35.5	40.9
30AlMCM-41(doublet)	2.03 2.21	43.4 39.9	50.1 46.0
15AlMCM-41	1.84	47.9	55.3
5AlMCM-41	Either < 1° 2Θ or absent		

Table 4.3.1.2 shows the effects on the measured BET surface area of increasing aluminium incorporation. The measured surface area of an aluminium free sample is included for comparison purposes.
From this it is apparent that there is a marked lowering of the surface area with even the lowest aluminium content and that this is progressive; with the highest aluminium content giving rise to a surface area of only 330 m^2/g. This is very similar to the findings of Luan and co-workers[16] who used aluminium sulfate. Although they reported a very high surface area (990 m^2/g for Si : Al = 30) this still represented a loss in surface area of ca 20% from their siliceous sample. Chuah et al.[9], by contrast, found an increase in surface area when

incorporating aluminium during synthesis with a decrease only found on post synthetic grafting.

Table 4.3.1.2 BET Surface Areas of Aluminium Containing MCM-41

Sample	Si : Al Ratio	BET Surface Area / $m^2 g^{-1}$
MCM-41	N/A	960
30 Al MCM-41	30	770
15 Al MCM-41	15	600
5 Al MCM-41	5	330

Nitrogen adsorption isotherms are shown in figure 4.3.1.3. The adsorption and desorption branches coincided within experimental error and no hysteresis was observed.

Figure 4.3.1.3 Nitrogen Adsorption Isotherms for Siliceous and Aluminium Containing MCM-41

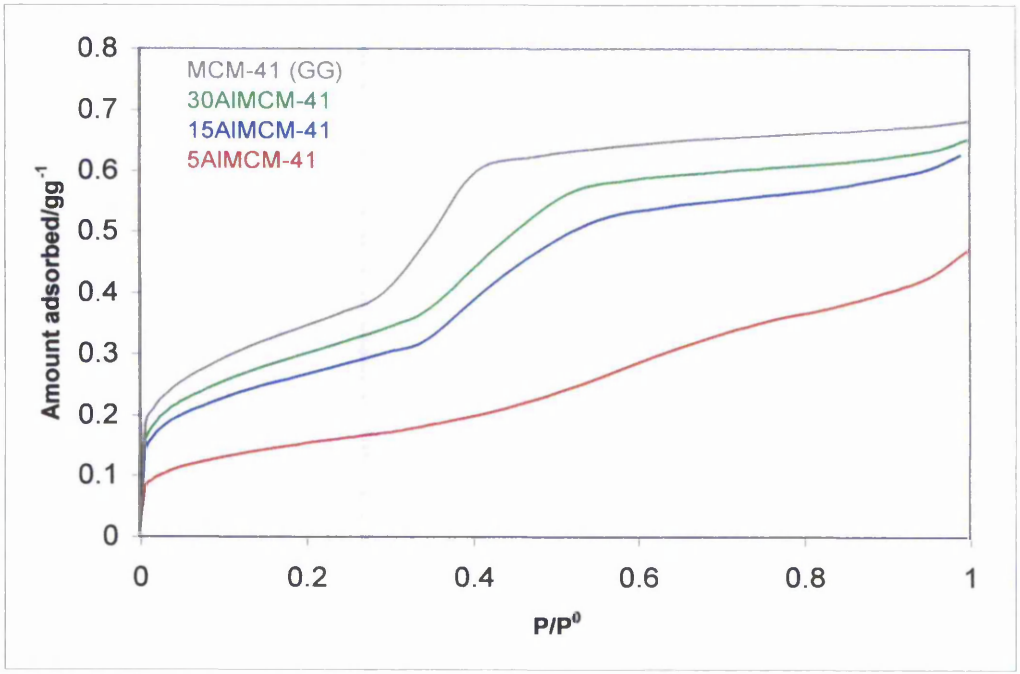

From the isotherms it can be observed that as aluminium content increases a number of effects occur. Alongside a decrease in total pore volume there is a shift to higher values of P/P^o for the onset of the upturn in the isotherm associated with capillary condensation. This indicates an increase in pore size. There is also a decrease in the gradient of the slope, which suggests a broader pore size distribution. These observations agree with the findings of the x-ray diffraction.

For the highest aluminium content sample the isotherm loses the type IV shape, and more resembles a type II isotherm. This type of isotherm is characteristic of a non-porous or macroporous material. The latter case cannot be excluded on the evidence available. From the x-ray diffraction it is possible that the 100 diffraction peak does occur below 1^o 2θ, and, with an angle of, for example, 0.9 °2θ, this would indicate a pore size in the macroporous region. All of these isotherms gave linear BET surface area plots.

From three of these isotherms it is possible to estimate the pore diameter by use of the Kelvin equation as described in chapter three (section 3.2). Using this estimate in conjunction with the XRD results a value for pore wall thickness can also be obtained. A summary of information gathered from the isotherms is contained in table 4.3.1.3.

Table 4.3.1 3 Structural Parameters of Aluminium MCM-41

Sample	BET Surface Area/m^2g^{-1}	Total Pore Volume/ mlg^{-1}	a/Å	Estimated Pore Diameter (Kelvin)/Å	Pore Wall Thickness/Å
GG (Al free)	1007	0.84	40.9	29.3	11.6
30AlMCM-41	857	0.78	50.1	37.7	12.4
(XRD peak doublet)			46.0	37.7	8.3
15AlMCM-41	775	0.73	55.3	38.2	17.1
5AlMCM-41	438	N/A	N/A	N/A	N/A

The results show that, while there is some evidence of pore wall thickening with aluminium incorporation, pore diameter does, in fact, also increase. Pore wall thickening may be expected since the bond length of Al-O is longer than that of Si-O[2].

The increase in pore size is contrary to the findings of some groups who have studied the incorporation of aluminium into these materials. It has been observed that pore diameter tends to decrease with increasing aluminium incorporation during synthesis[3, 6]. From our own work we have observed pore size decreases with the inclusion of even very small amounts of iron into these materials during synthesis[17]. Sulikowski et al report a slight increase in repeat distance with aluminium incorporation. However, since pore size is not reported in their paper it is unclear as to whether this is the result of wall thickening, which is observed here[18].

None of these syntheses are directly comparable to the one used for this work; and Cesteros and Haller have reported that several factors, such as aluminium source, and aging, affect the structural parameters of the materials produced[19].

One possible explanation for this could be provided by the findings of Luan et al. This group report that their as-prepared aluminosilicate materials have the same mesopore diameter as purely siliceous MCM-41. However they observed a macroporous system, secondary to the still present mesopores, developing on heating of the aluminium containing samples due to their lower thermal stability[16]. However this is not entirely consistent with our observations, as there is only slight evidence of a bimodal pore size distribution in a single sample here.

An alternative possibility, which would account for the progressive nature of the pore size increase observed here, concerns the possibility of a side reaction in our synthetic system. In the original work on MCM-41 presented by the scientists at Mobil large pored, and less well ordered materials were synthesised by the addition of auxiliary organic molecules to the reaction mixture[1, 20]. Because of their hydrophobic nature these become trapped in the hydrocarbon portion of the template micelle, resulting in swelling, and, therefore, pore enlargement.

In aqueous solution aluminium is easily hydrolysed if complexing anions are absent. The species produced are dependant on experimental factors such as

pH, and concentration but vary from mononuclear species such as $[Al(OH)(H_2O)_5]^{2+}$ and $[Al(OH)_2(H2O)_4]^{+}$ to polynuclear species; for example: $[Al_2(OH)_2(H_2O)_8]^{4+}$, $[Al_3(OH)_4(H_2O)_{10}]^{5+}$ and $[Al_{13}O_4(OH)_{24}(H_2O)_{12}]^{7+}$[21, 22]. If such polynuclear species were produced in our synthesis they could feasibly act as micelle swelling agents. That this effect is not observed elsewhere could be due to differences in the experimental conditions; including the choice of silica source, as this could provide an anion to complex with the aluminium, thus preventing hydrolysis[21]. It is known that the nitrate anion, present here, shows little complexing behaviour with aluminium[21, 23].

4.3.2 Catalytic Reactor Testing

Figure 4.3.2.1 shows the yield of para-Methoxyacetophenone from the acylation of anisole over aluminium containing MCM-41. The siliceous MCM-41 gave no product and is therefore not shown.

Figure 4.3.2.1 Activity of aluminium containing MCM-41, ZSM-5 and mordenite in the acylation of anisole with acetic anhydride.

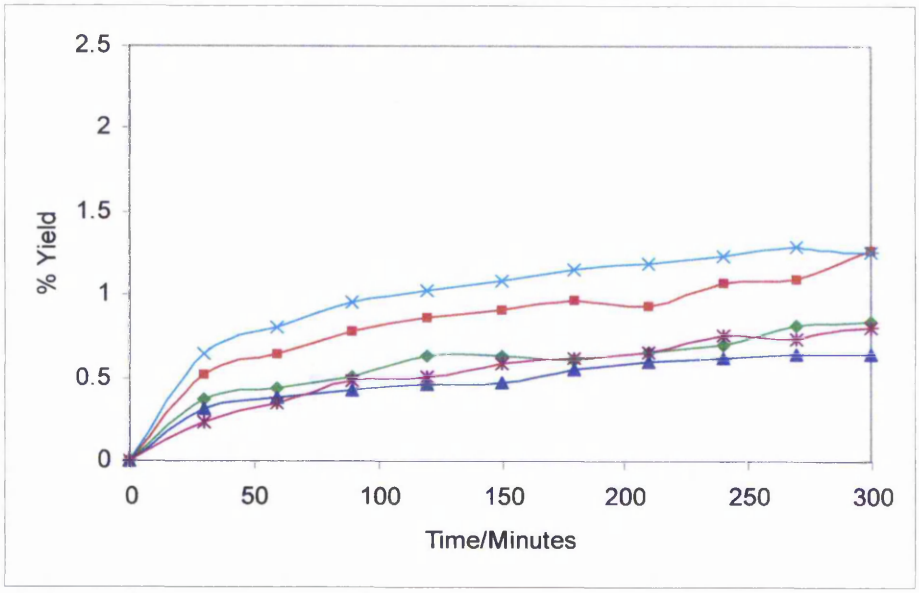

- 30 Al MCM-41 - 15 Al MCM-41 - 5 Al MCM-41
- ZSM-5 -Mordenite

While activity is low compared to that of zeolite BEA [12] the highest aluminium content MCM-41 was found, in this work, to be comparable to other zeolites; as demonstrated in figure 4.3.2.1. These findings strongly suggest that high acid strength is not the decisive factor in activity for this reaction. It also seems that diffusion limitations are not a factor since the mesoporous MCM-41 shows similar activity to the much smaller pored ZSM-5 and mordenite. The findings of x-ray diffraction and nitrogen adsorption suggest that for these samples the pore system is disordered with a wide range of pore sizes, indeed one sample may be non-porous. These results therefore show that a well defined pore system is not necessary for this reaction.

Table 4.3.2.1 Shows Initial Rates of Reaction for the Aluminium Containing MCM-41

Sample	Initial Rate ($mols^{-1}$)
30 Al MCM-41	7.4×10^{-7}
15 Al MCM-41	9.0×10^{-7}
5 Al MCM-41	1.6×10^{-6}

Figure 4.3.2.2 Variation of initial rate with aluminium content of MCM-41

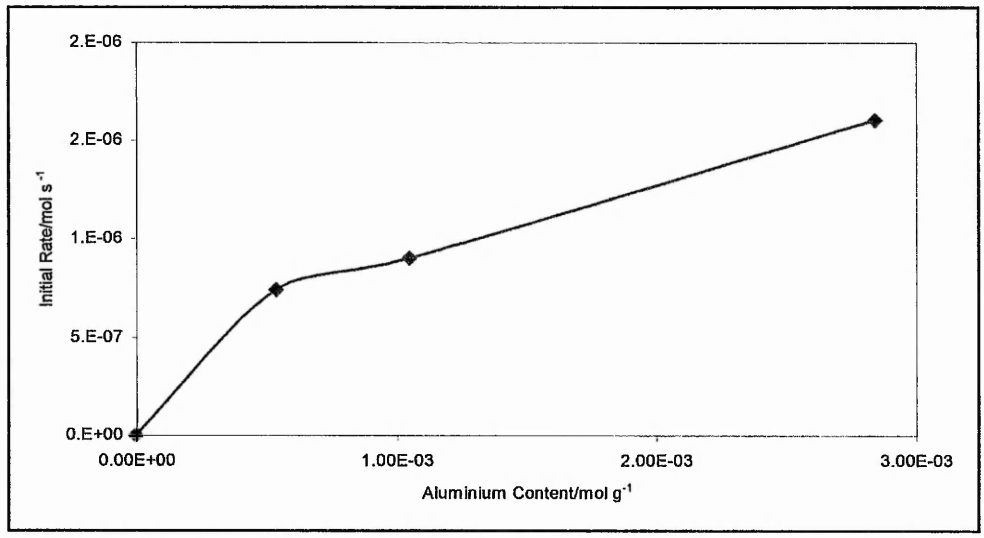

From figure 4.3.2.2 it can be seen that initial rate rises with increasing aluminium content.

The near linearity could suggest that the accessibility of the aluminium sites changes little with aluminium content. This is particularly interesting in light of the findings from the x-ray diffraction and isotherms which show some wall thickening in the samples that retain mesoporosity. It may suggest that the aluminium is incorporated close to the surface of the materials.

Calculation of turnover numbers (see table 4.3.2.2) for the initial 30 minute reaction period, however, does show that activity per aluminium atom falls. This would be expected and suggests that some of the additional aluminium sites show lower or no activity in the reaction.

Table 4.3.2.2 Initial turnover numbers (after 30 minutes) for the production of para-Methoxyacetophenone over MCM-41.

Sample	TON/ molecules Al atom^{-1} s^{-1}
30 Al MCM-41	3.91×10^{-3}
15 Al MCM-41	2.47×10^{-3}
5 Al MCM-41	1.22×10^{-3}
MCM-41	0

It was concluded from the research into zeolite Beta that the presence of tetrahedrally co-ordinated aluminium species capable of transition to an octahedral environment was the most influential characteristic of materials showing activity[12]. Pak and Haller have observed chromium incorporated into MCM-41 to have an easily reversible co-ordination change between tetrahedral and octahedral. If the conclusions drawn by Paine are correct, then it suggests that the incorporation method employed does incorporate aluminium in tetrahedral co-ordination, and that this occurs progressively even at higher aluminium loadings.

4.4 Conclusions

The chosen method of aluminium incorporation has significant effects on the structural integrity of the material produced; causing broadening of the pore size distribution, loss of the hexagonal pore arrangement and larger pore sizes. In the high aluminium content sample this resulted in total loss of the regular pore structure and either a non-porous or a mesoporous material. There is significant loss of surface area, which is progressive as more aluminium is incorporated. This is in agreement with the findings of others investigating synthetic alumination of MCM-41[3, 8, 16]. Ryoo and co-workers attribute this to the embedding of aluminium into the pore wall in synthetic samples as against greater amounts of surface aluminium in post-synthetically modified samples[10].

However, we have produced a material which is catalytically active in a reaction where siliceous MCM-41 shows no activity. Furthermore both the initial rate of reaction and the final yield rise with increasing aluminium content.

Since the reaction itself has been studied extensively[12] these findings suggest progressive incorporation of aluminium active sites.

4.5 References

1. Beck, J.S., et al., *A New Family of Mesoporous Molecular-Sieves Prepared with Liquid-Crystal Templates.* Journal of the American Chemical Society, 1992. **114**(27): p. 10834-10843.
2. Oumi, Y., et al., *Novel post-synthesis alumination method for MCM-41 using trimethylaluminium.* Microporous and Mesoporous Materials, 2001. **44-45**: p. 267-274.
3. Matsumoto, A., et al., *Novel route in the synthesis of MCM-41 containing framework aluminum and its characterization.* Microporous and Mesoporous Materials, 1999. **32**(1-2): p. 55-62.
4. Luan, Z.H., et al., *Mesopore Molecular-Sieve Mcm-41 Containing Framework Aluminum.* Journal of Physical Chemistry, 1995. **99**(3): p. 1018-1024.
5. Mokaya, R. and W. Jones, *Post-synthesis grafting of Al onto MCM-41.* Chemical Communications, 1997: p. 2186.
6. Chen, L.Y., et al., *A comparison of post-synthesis alumination and sol-gel synthesis of MCM-41 with high framework aluminum content.* Microporous and Mesoporous Materials, 1999. **27**(2-3): p. 231-242.
7. Selvaraj, M., et al., *Synthesis, characterization and catalytic application of MCM-41 mesoporous molecular sieves containing Zn and Al.* Applied Catalysis, A: General, 2003. **242**(2): p. 347-364.
8. Cesteros, Y. and G.L. Haller, *Several factors affecting Al-MCM41 synthesis.* Microporous and Mesoporous Materials, 2001. **43**(2): p. 171-179.
9. Chuah, G.K., et al., *Surface properties of mesoporous catalytic supports.* Applied Surface Science, 2001. **169**: p. 253-258.
10. Ryoo, R., et al., *Generalized route to the preparation of mesoporous metallosilicates via post-synthetic metal implantation.* Chemical Communications (Cambridge), 1997(22): p. 2225-2226.
11. Corma, A. and D. Kumar, *Studies in Surface Science and Catalysis.* 1998. **117**(Mesoporous Molecular Sieves 1998): p. 201-222.
12. Paine, G.S., *Active Sites in the Acylation of Anisole with Acetic Anhydride over Zeolite Beta*, in *Chemistry*. 2002, Nottingham Trent University.

13. Stockenhuber, M., et al., *Transition metal containing mesoporous silicas - redox properties, structure and catalytic activity.* Microporous and Mesoporous Materials, 2001. **44**: p. 367-375.

14. Mathisen, K., *Department of Chemistry, Norwegian University of Science*. 2003: N-7491 Trondheim, Norway.

15. Kruk, M., et al., *Characterization of highly ordered MCM-41 silicas using X-ray diffraction and nitrogen adsorption.* Langmuir, 1999. **15**(16): p. 5279-5284.

16. Luan, Z.H., et al., *Effect of Structural Aluminum on the Mesoporous Structure of Mcm-41.* Journal of the Chemical Society-Faraday Transactions, 1995. **91**(17): p. 2955-2959.

17. Grubert, G., et al., *The room temperature, stoichiometric conversion of N2O to adsorbed NO by Fe-MCM-41 and Fe-ZSM-5.* Journal of Catalysis, 2000. **196**(1): p. 126-133.

18. Sulikowski, B., et al., *Oxidative dehydrogenation of isobutane on MCM-41 mesoporous molecular sieves.* Applied Catalysis, A: General, 2002. **232**(1-2): p. 189-202.

19. Cesteros, Y. and G.L. Haller, *Several factors affecting Al-MCM-41 synthesis.* Microporous and Mesoporous Materials, 2001. **43**(2): p. 171-179.

20. Kresge, C.T., et al., *Ordered Mesoporous Molecular-Sieves Synthesized by a Liquid- Crystal Template Mechanism.* Nature, 1992. **359**(6397): p. 710-712.

21. Robinson, G.H., *Co-ordination Chemistry of Aluminium*. 1993, New York: VCH Publishers, Inc.

22. Cotton, F.A. and G. Wilkinson, *Advanced Inorganic Chemistry.* 5th ed. 1988, New York: Wiley-Interscience.

23. Downs, A.J., *Chemistry of Aluminium, Gallium, Indium and Thallium*. 1st ed. 1993, London: Blackie Academic & Professional.

5. Iron-Modified MCM-41

5.1 Introduction

Because of their variable oxidation states and the facility of transfer between them transition metals are well established in catalysis. For reasons discussed in chapter one, such as health and safety and recoverability, supported transition metal catalysts offer advantages over homogeneous catalysts. Additionally by supporting on a high surface area material, such as MCM-41, it is possible to achieve a high dispersion of available active sites for reaction, and thus enhance the activity per centre of the transition metal. There is also an associated cost benefit as this leads to savings in the necessary quantity of a relatively expensive catalyst component.

Iron has a broad range of catalytic applications; from the Haber process to biological examples in enzymes such as peroxidases and cytochromes[1]. It is particularly attractive as a catalyst where safety is an issue because of its low toxicity. Indeed iron was among the earliest industrially applied catalysts. Fe_3O_4 is a well established high temperature water gas shift catalyst in the process referred to above for the synthesis of ammonia[2]. More recently research has shown that Fe_2O_3 can catalyse carbon monoxide oxidation[3] while Pillai and Sahle-Demessie have used iron supported on silica clay for the oxidation of alcohols[4]. Iron has also been shown to be an effective promoter for a copper/silica catalyst in the reverse water gas shift reaction, both increasing activity and lowering catalyst deactivation[5].

Research into iron-containing zeolites, particularly their preparation and characterisation, is well established and iron-containing zeolites have been found to have applications in redox reactions. For example FeZSM-5 has been shown to be active in the selective catalytic reduction of NO_x[6, 7] and the water gas shift reaction[8], iron-containing zeolite beta in the acylation of anisole and both beta and ferrierite, with incorporated iron, in the decomposition of N_2O and reduction of N_2O and NO by ammonia[9].

The advent of the M41S class of materials gave scope in the field of transition metal catalysis. The larger pore size should allow for reaction of larger

molecules; for example bulky organic species, and if reactions of this type are not intrinsically linked to the acidity of the host material, the low acidity of the silicate need not be a disadvantage.

5.2 Experimental

5.2.1 Preparations

Iron containing MCM-41 samples had been previously prepared both by incorporation during synthesis and by post-synthetic modification
Iron was incorporated during MCM-41 synthesis by the addition of iron (III) nitrate nonohydrate to the reaction mixture. In this case the tetraethyl orthosilicate (TEOS) was added to the reaction mixture prior to the addition of ammonia in order to achieve a better distribution of the iron within the material as the former is thought to form a complex with iron[10].
Post synthetic modification was carried out using iron (III) acetylacetonate [$Fe(acac)_3$] in toluene, a method developed by Kenvin and co-workers for the incorporation of metal ions onto silica[11]. Siliceous MCM-41 (5 g) was suspended in toluene (Aldrich, 99.8%, 200 ml.) and the appropriate amount of the iron salt (Aldrich, 99%) was added. The required iron mass for a desired weight percentage is calculated by:

$$g\,Fe = \left[\frac{Wt\%}{100} \times \frac{100}{(100 - Wt\%)} \right] \times 5$$

Mass of the iron (III) acetylacetonate (molecular weight 353.18) given by:

$$Mass = g\,Fe \times \frac{353.18}{55.85}$$

The mixture was stirred for ca. 24 hours, filtered, washed with toluene and calcined at 823 K for 12 hours.
In both cases samples with a range of iron concentrations were prepared (from 0.4 – 12wt% for synthetically modified samples, from 0.1 – 3.2wt% for post-synthetically modified ones).

5.2.2 Characterisation

The iron content of samples was determined by dissolution of the host in a mixture of nitric, hydrochloric and hydrofluoric acids followed by atomic absorption spectroscopy.
BET surface areas of some samples were determined using the automated volumetric apparatus described in section 2.

Temperature Programmed Reduction

Selected samples were characterised by temperature-programmed reduction (TPR). TPR is a commonly used technique, which measures the reducibility of species in catalysts or other materials. The catalyst is exposed to a flow of hydrogen in an inert gas while being heated at a linear ramp rate; hydrogen consumption is monitored and plotted against sample temperature. Integration of reduction peaks gives a quantitative evaluation of the reducible species, while the temperature of maximum reduction (t_{max}) provides a comparison of the reducibility of different species.

Monti and Baiker[12] developed an equation for optimising hydrogen flow rate if the amount of reducible species can be estimated. This reduces artefacts which can occur in TPR profiles[12, 13]. This defines a characteristic K value, which should be kept within the outer limits of 55-140 s; from this suitable flow rates of reducing gas are determined:

$K = S_0 / (C_0 . V)$

Where:

S_0 = Concentration of reducible species / mmol

C_0 = Initial concentration of reducing gas / mmol ml^{-1}

and

V = Flow rate /ml s^{-1}

A schematic diagram of the TPR equipment used is shown in figure 5.2.2.1.

Figure 5.2.2.1 Apparatus for Temperature Programmed Reduction

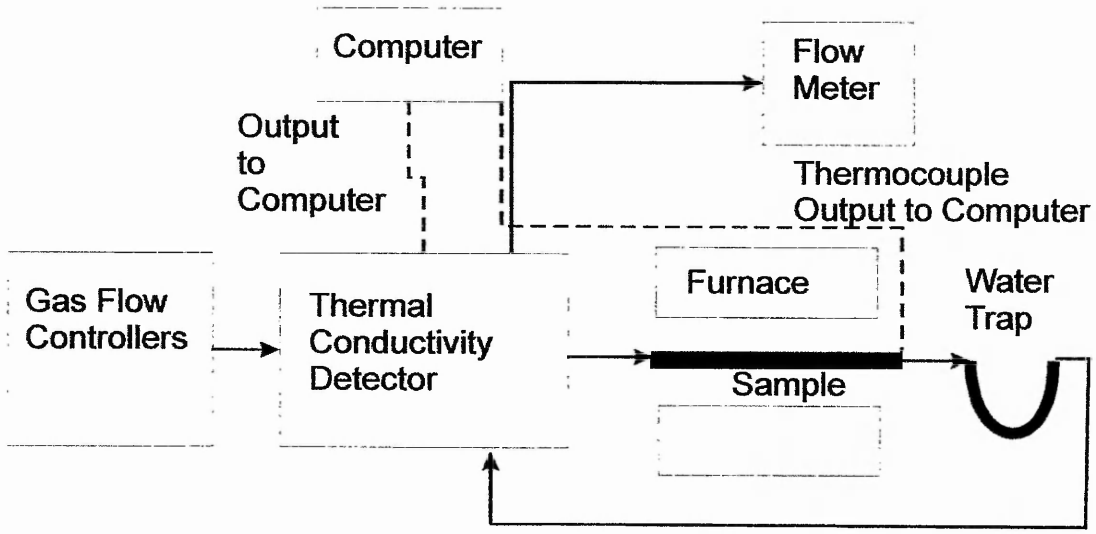

Powdered samples (~ 50 mg, accurately weighed) were placed in a silica sample tube within a furnace (Carbolite, fitted with a Eurotherm temperature controller). The sample was wedged between two plugs of silica wool. Dead space on the exit side of the tube was reduced by the insertion of silica tubing, both to reduce time to reach the detector and to prevent the movement of the sample bed; this ensures that discrepancies between the detector reading and the measured temperature are kept to a minimum.

Samples were first pre-treated at 773 K (ramp rate 5 K/min.) in a flow of nitrogen or air (BOC Gases). These pre-treatments respectively either reduce or oxidise the accessible metal species. The samples were then reduced in a flow of hydrogen (5% or 2%) in argon (Air Products) over the range 293 – 1273 K (293 – 1373 K in later cases) with a ramp rate of 5 K/min. Flow rates were calculated using the Monti-Baiker equation, to give a K value of around 100 s. Hydrogen consumption was monitored through the use of a thermal conductivity detector (Gow Mac Instruments model 40-202). Because of the differences in thermal conductivity of the mixed gases the lowering hydrogen concentration is accompanied by a change in the thermal conductivity of the gas in the exit stream, giving rise to a signal. Water produced in the reduction was removed from the exit stream by a water trap immersed in a slurry of isopropanol and dry ice. Output from the thermal conductivity detector and a thermocouple positioned close to the sample bed was monitored using a personal computer equipped with a Quicklog PC software package (Strawberry Tree Incorporated).

Calibration of the TCD was performed for each flow rate used by the reduction of copper (II) oxide (10 mg., Aldrich 99+%), which exhibits a single, two electron, reduction to copper metal.

X-Ray Photoelectron Spectroscopy

X-Ray Photoelectron Spectroscopy (XPS) is a surface analytical technique whereby samples of material are bombarded with monochromatic x-rays, causing photoelectrons to be ejected from the surface region (2-20 atomic layers depending on the material), as illustrated in figure 5.2.2.2.

Figure 5.2.2.2.X-ray Photoelectron Spectroscopy

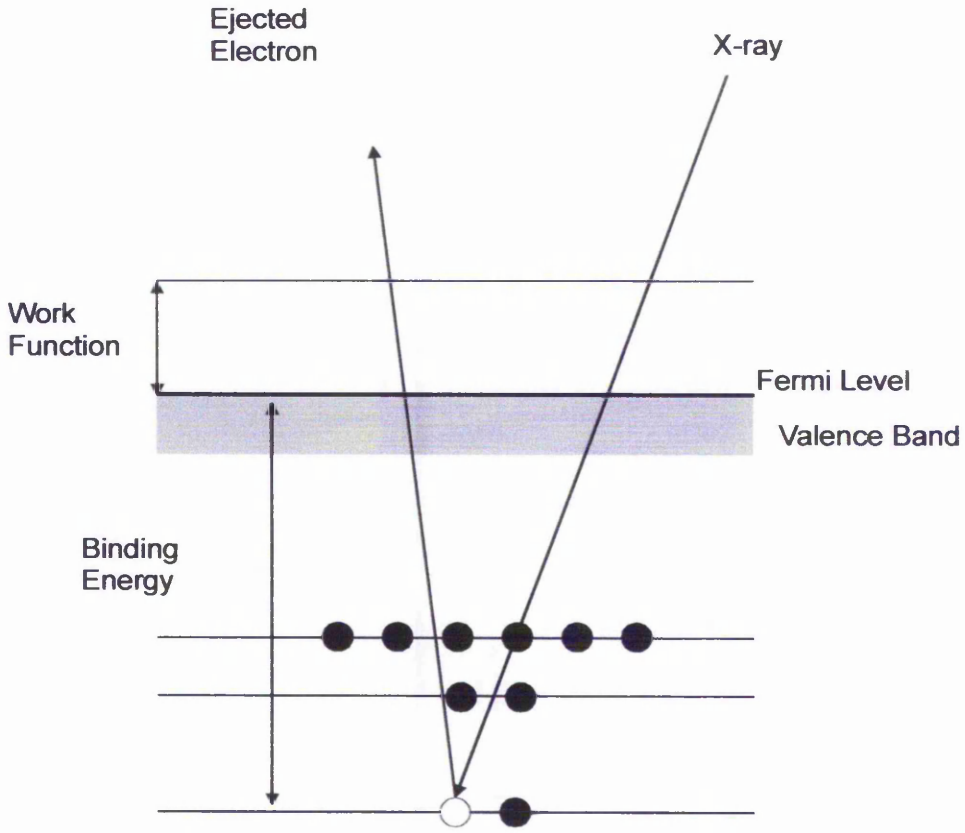

From figure 5.2.3.2.it is evident that the kinetic energy of the ejected electron is related to the photon energy in the manner:

$$E_{k.} = hv - E_{B.} - \phi$$

Where:

E_k = The kinetic energy of the ejected electron

hv = The photon energy

E_B = The binding energy of the ejected electron

ϕ = Work function

Therefore the species present in the sample can be identified from the kinetic energy of the ejected electrons, which is characteristic of the emitting atom.

The number of detected electrons is given by the equation:

$$N_{tot} = k.\lambda.F.C.S.D_E$$

Where:

k = A constant

λ = The escape depth: the depth from which a photoelectron has a probability of 1/e of escaping with no loss of energy.

F = X-ray flux

C = Concentration of the species

S = The photoexcitation cross section

D_E = A spectrometer function

Therefore relative concentrations of elements in the sample can be quantified from the intensity of the peaks.

Figure 5.2.2.3 Photoelectron Spectrometer (schematic)

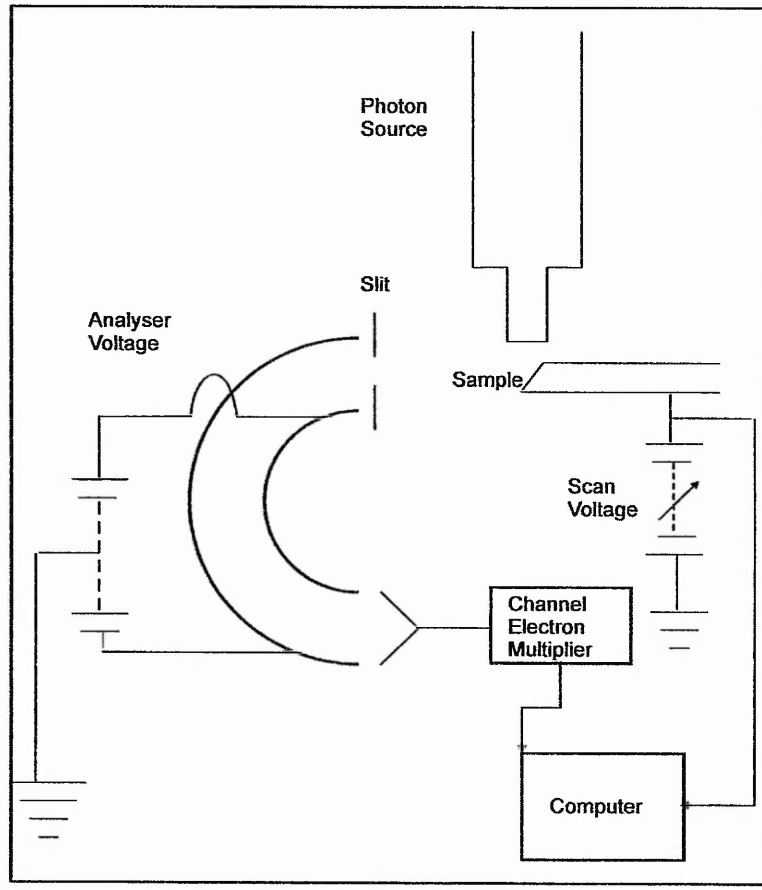

XPS was performed with a Vacuum Generators ESCA 3 Spectrometer. The sample was evacuated to ca. 10^{-7} mbar before photoelectron bombardment using a Mg radiation source with an emission current of 40 mA and an accelerating voltage of 12 kV. Surface Si : Fe ratios are calculated from[8]:

$$\left(\frac{Si}{Fe}\right)_{xps} = \frac{nSi}{nFe} = \frac{I_{Si}.\sigma_{Fe}.\lambda_{Fe}.D_{Fe}}{I_{Fe}.\sigma_{Si}.\lambda_{Si}.D_{Si}}$$

Where:

I = Peak intensity

σ = Cross section of emission

λ = Escape depth

D = Detection efficiency of spectrometer

Photoexcitation cross sections are taken as reported by Scofield[14] and the detection efficiency for the spectrometer is given by:

$D = E_K^{0.6}$ where E_K is the kinetic energy of the emitted electrons.

5.2.3 Catalytic Reactor Testing

Samples were tested for activity in the oxidation of carbon monoxide. A schematic diagram of the reactor used is shown in figure 5.2.3.1.

Catalyst samples were pressed and then granulated to provide pellets of 250 –500 μm in diameter and the sample was placed in the silica glass reactor tube within the furnace (Carbolite, fitted with a Eurotherm Temperature Programmer). The sample (300 mg., 1ml.) was held in place by means of silica wool plus and a length of narrower silica tubing on the exit side.

Samples were pre-treated in 20% oxygen in helium (40% O_2 in He, BOC Gases; He 99.996% BOC Gases, 50:50 Mix) for 1 hour at 623 K (ramp 5 K/min.). The sample was then cooled and carbon monoxide oxidation was carried out over the temperature range 573 – 723 K with a carbon monoxide concentration of

4.5% (BOC 5% CO in He Certified Grade – 4.81%), oxygen concentration of 2.4% (BOC 40% O_2 in He).and a gas hourly space velocity of 19,800 $hour^{-1}$. Gas flows were controlled by Brooks 5878 mass flow controllers and a Brooks 5850 control unit.

Figure 5.2.3.1 Carbon monoxide oxidation reactor

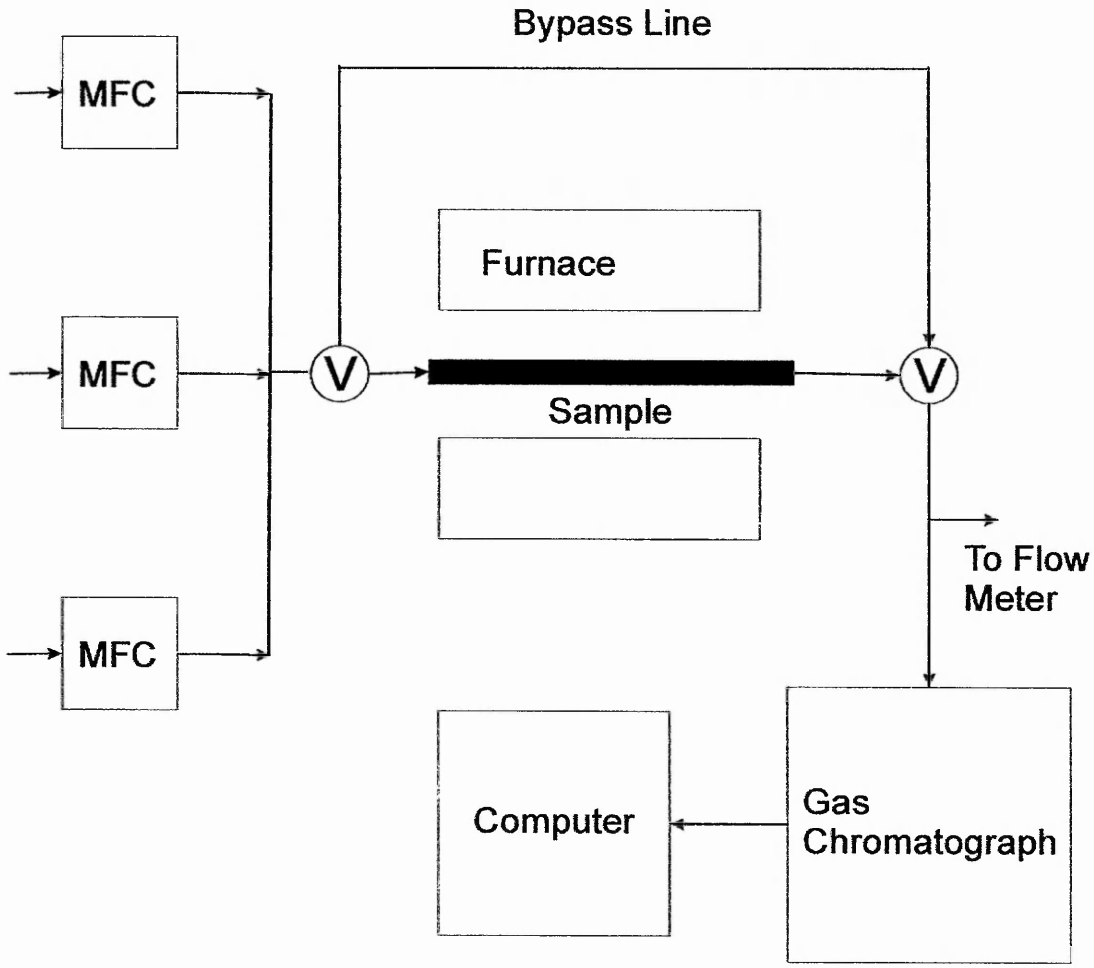

MFC - Mass Flow Controller

Carbon monoxide and carbon dioxide concentrations were monitored at 25 K temperature increments after 40 minutes on stream at each temperature. Analysis was performed using gas chromatography by a Varian Star 3400 gas chromatograph fitted with an Alltech CTR 1 column using the thermal

conductivity detector and recording via a personal computer with the Varian Star software supplied by the manufacturers. A column temperature of 308 K was used and both the injector and the detector were kept at a temperature of 393 K. Calibration of the GC was performed using a mixture of helium, carbon monoxide (as for the reaction) and carbon dioxide (BOC CP grade) over a suitable concentration range.

5.3 Results and Discussion

5.3.1 Characterisation

The most extensively studied of the iron-containing samples were the materials, both synthetically (designated Syn) and post-synthetically (designated PS) modified, containing moderate amounts of iron (ca.4wt%). At this level of iron incorporation only minor degreases of the BET surface area occur and these are summarised in table 5.3.1.1. In both cases there is a lowering of the surface area of 5-10% compared to the parent MCM-41, but there is no significant difference dependant on whether the iron was incorporated during synthesis or later.

Table 5.3.1.1 BET surface areas of Iron-MCM-41

Sample Designation	Iron Content/ Wt.%	BET Surface Area/ $m^2 g^{-1}$
MCM-41	0	960
FeMCM-41(Syn)	3.5	900
MCM-41Fe(PS)	3.2	880

5.3.1.1 Temperature Programmed Reduction

Figures 5.3.1.1 and 5.3.1.2 show TPR profiles for synthetically modified Fe-MCM-41 (iron content 3.51wt.%) pre-treated in nitrogen and air respectively. As shown in figure 5.3.1.2 this sample was also subjected to pre-treatment in air at 1273 K (1 hour, ramp rate 5 K/min.).

These profiles are representative of the lower iron-content synthetically modified samples. Under normal pre-treatment regimes (773 K) a reduction feature was observed centred around ca. 680 K with no further reduction before the onset of the second, larger reduction feature, usually at temperatures above 1170 K. Integration of the lower temperature reduction peak gives a molar ratio of H_2 : Fe of 0.43 and 0.45 for the samples pre-treated in nitrogen and air at 773 K respectively. Reduction of iron III to iron II would require 0.5 moles of hydrogen gas per mole of iron. As the uptake observed here is less than that this suggests that reduction does not proceed beyond the +2 oxidation state at these lower temperatures. This shows the remarkable stability of the redox sites in these catalysts and suggests that the iron is present in a highly dispersed state. These findings are similar to those reported by Joyner and Stockenhuber for the exchange of iron into ZSM-5, from aqueous and methanolic solutions. They report their samples exhibiting only a small reduction feature around 750 K. Szegedi and co-workers[15] also commented on the high stability of their iron containing MCM-41s, however with their samples (synthetically modified using iron (III) sulphate as iron source) the onset of total reduction occurs at considerably lower temperatures than observed here; suggesting that our method of incorporation leads to singularly stable materials.

Pre-treatment in air at 1273 K results in a 0.49 molar ratio of H_2 : Fe suggesting that all the iron present as iron (II) can be oxidised to iron (III) by this pre-treatment. It does, however, result in a slight additional reduction feature in the TPR around 1110 K, which may indicate that this rigorous pre-treatment results in the formation of other iron species to some degree

At higher iron content (5.9wt.%) this slight extra reduction feature is present in synthetically modified samples subjected to either standard pre-treatment (773 K, air/nitrogen), again suggesting additional iron species in these samples.

Figure 5.3.1.1 TPR profile of synthetically modified iron MCM-41 pre-treated in nitrogen at 773 K

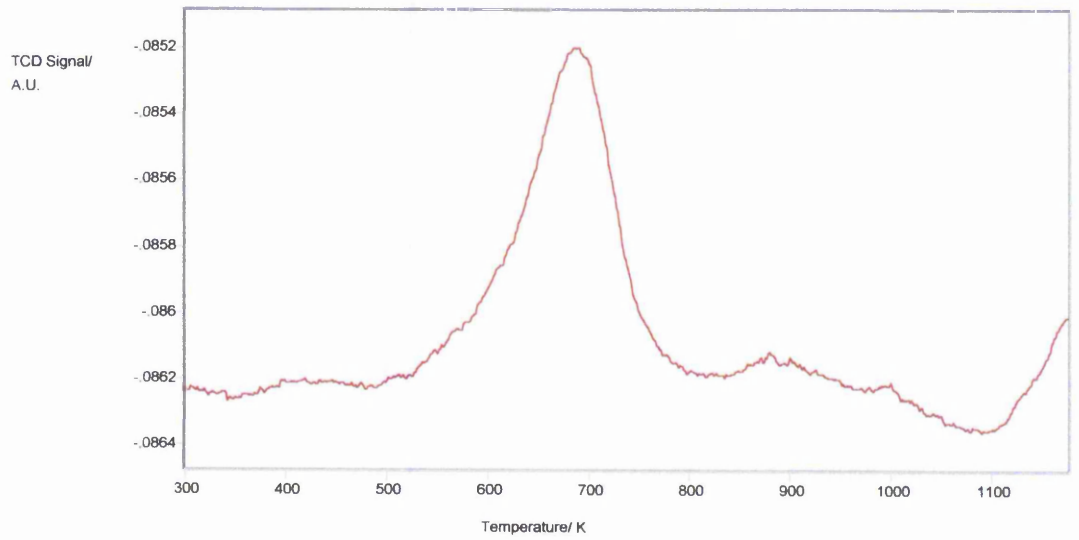

Figure 5.3.1.2 TPR profiles of synthetically modified iron MCM-41 pre-treated in air

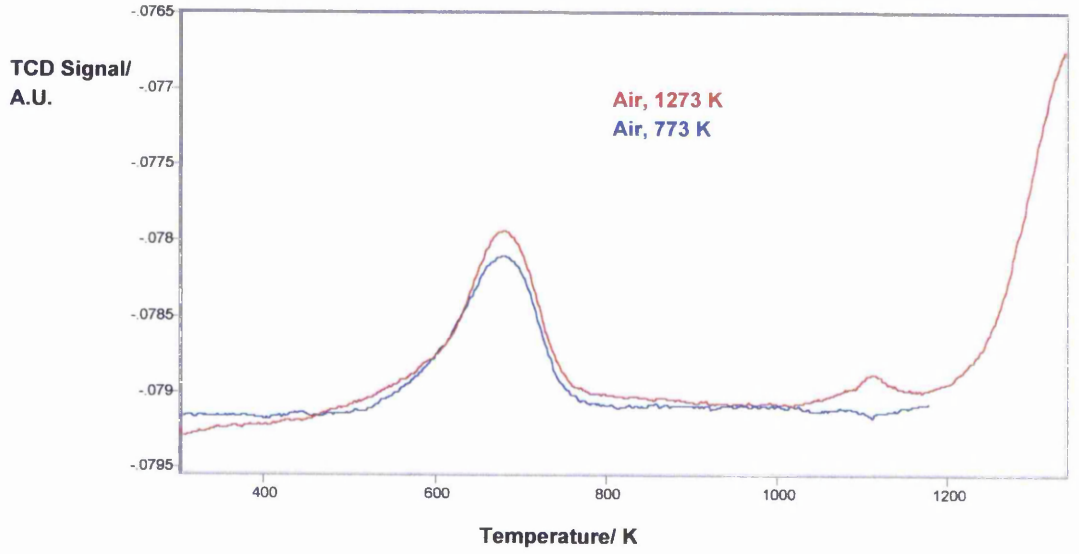

Profiles of the post synthetically modified samples (see figure 5.3.1.3) were similar but with two noteworthy differences. Firstly, in the case of the post-synthetically modified samples the pre-treatment showed a more marked effect on the hydrogen uptake. Pre-treatment in nitrogen resulted in a H_2 : Fe molar ratio of just 0.3 suggesting a greater stability of iron in oxidation state two in these samples. Secondly the small extra reduction feature before the onset of total reduction occurs at lower iron concentrations (3.2wt%, but not 2.45wt%) suggesting the presence of additional species even at moderate incorporation levels.

Figure 5.3.1.3 TPR profiles of post-synthetically modified iron MCM-41 pre-treated in air and nitrogen at 773 K

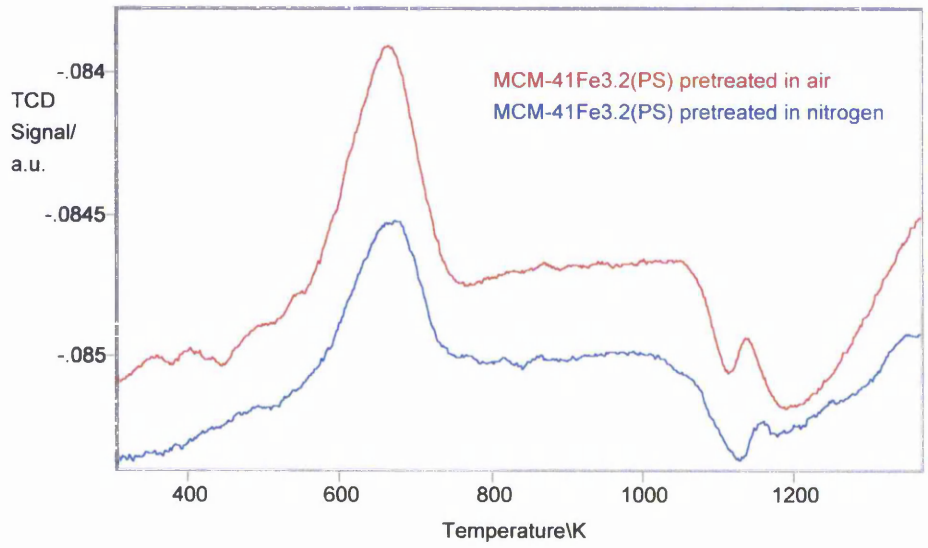

Further to the general TPR investigation, FeMCM-41 (Syn, 3.51wt%) was also reduced in 5% hydrogen for an hour at 1373 K (ramp rate 5 K/minute) cooled and subsequently re-oxidised in air (773 K 1 hour, ramp rate 5 K/minute). This resulted in extra reduction peaks between 520 and 1110 K (see figure 5.3.1.4, below). Integration of the total area gives a molar ratio of H_2 : Fe of 1.49 and represents full reduction of the iron to the metal.

Figure 5.3.1.4 TPR profile of synthetically modified iron MCM-41 reduced in 5% hydrogen and re-oxidised

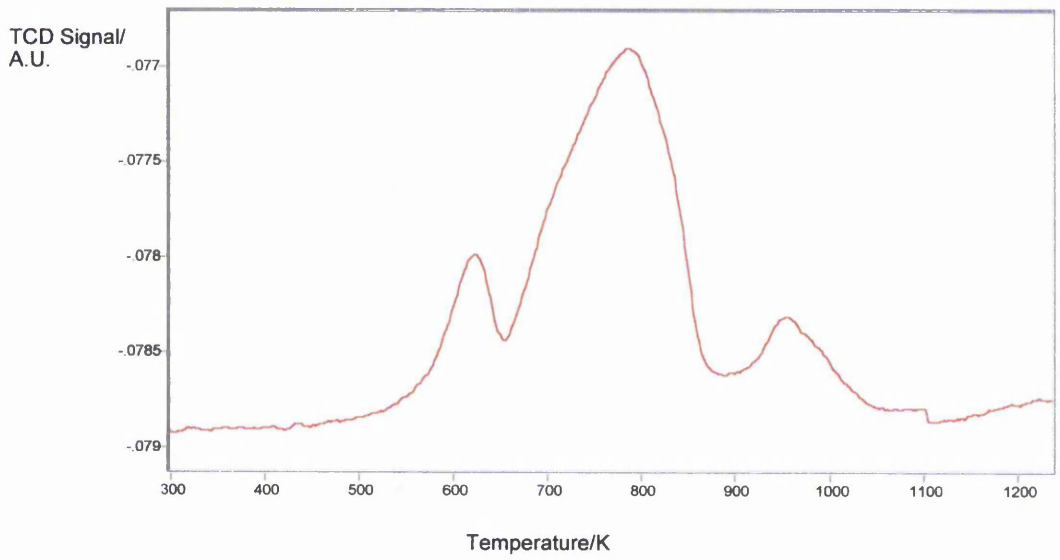

The reduction profile and temperatures are similar to those of Fe_2O_3[15, 16]. Although there are similarities, differences exist, Wimmers et al studied the reduction of Fe_2O_3 under different conditions and observed two reduction features. The first, small, feature at ca 620 K is attributed to the reduction of Fe_2O_3 to Fe_3O_4 and the second, much larger, feature is attributed to the total reduction of Fe_3O_4 to metallic iron. The exact position of these features is dependent on the wetness of the conditions and the heating rate[16]. Szegedi et al observed the same two peaks at ca 620 K and 850 K respectively[15]. The appearance of a third peak in this case can be explained in terms of the K value calculated from the Monti-Baiker equation. The hydrogen flow was calculated to give a K value of around 100 s assuming a one electron reduction, as is the normal case for these samples. The reduction of Fe_3O_4 to metallic iron represents a reduction equivalent to 8/3 electrons, thus giving a K value of ca 37.5 s. Artefacts produced in TPR profiles include the production of apparent double peaks from a single reduction if an insufficient K value is applied[13]. This suggests breakdown of the material under these conditions resulting in the

aggregation of the dispersed iron particles to produce extended iron oxide species.

Samples of this material pre-treated in the same fashion (reduced and re-oxidised) and in air at elevated temperatures (1273 K and 1373 K) were therefore subjected to surface area measurement and x-ray diffraction as described in chapter 2.

It was found that the surface area of the reduced and re-oxidised sample had decreased to ca. 90 m^2/g suggesting a full breakdown of the pore structure, however the samples of the material heated in air at 1273 K and 1373 K had BET surface areas of 960 and 670 m^2/g respectively. The former value is an increase in surface area over the original iron containing parent material. This cannot indicate collapse of the pore walls so that several small pores create one larger one as described by Landau et al for the breakdown of MCM-41[17]. It could indicate roughening of the internal surface of the pores or pore enlargement, wall thinning. The latter, much smaller, value is consistent with the type of collapse described above and suggests that the onset of breakdown is beginning to occur. However much of the pore volume is still intact after treatment under these conditions.

The x-ray diffraction pattern of the treated samples (shown in figure 5.3.1.5), by contrast, shows the absence of any of the peaks attributable to the hexagonal pore arrangement in *any* of the treated samples, so while the surface areas are strongly supportive of the material retaining porosity when treated at elevated temperatures in air it is apparent that the uniform MCM-41 pore structure has been modified by this treatment.

The treated samples were also examined over a wider range to look for any additional diffraction peaks and the results are shown in figure 5.3.1.6, below (this pattern has been smoothed using the Grams 32 v 5.1 software package because of the high signal to noise ratio with these less intense peaks). The reduced and re-oxidised sample alone gives rise to extra peaks in the diffraction pattern the four highest intensity of these peaks, at 33.0, 35.5, 49.4 and 54.1 $^{o}2\theta$ correspond to the four highest intensity peaks in the diffraction pattern of hematite with d-spacings of; 2.70 (100%, hkl 104), 2.52 (70%, hkl 110), 1.84 (40%, hkl 024) and 1.69 (45%, hkl 116). The absence of these peaks in all but the reduced and re-oxidised sample suggests that despite the apparent partial

breakdown of the pore system the iron species are not significantly affected by treatment in air at elevated temperatures, and that no bulk iron oxide species are formed. Complete reduction followed by re-oxidation, however, does result in the total loss of porosity and the formation of the iron oxide, hematite, as suggested by the results of the TPR on this sample. This, again points to high stability of the iron containing samples.

Figure 5.3.1.5 X-ray diffraction pattern of synthetically modified iron MCM-41 pre-treated under different conditions

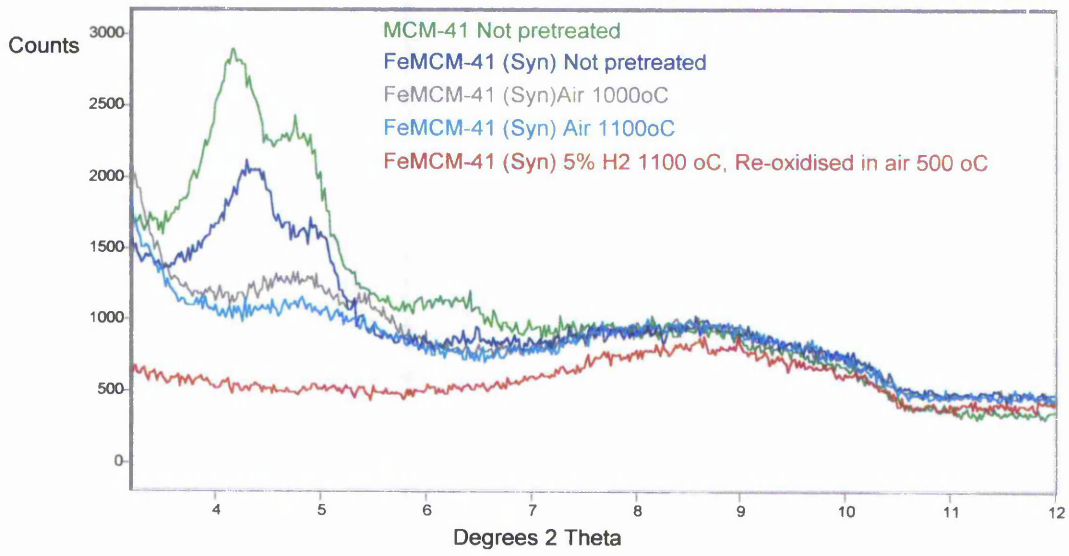

Figure 5.3.1.6 X-ray diffraction pattern of synthetically modified iron MCM-41 pre-treated under different conditions

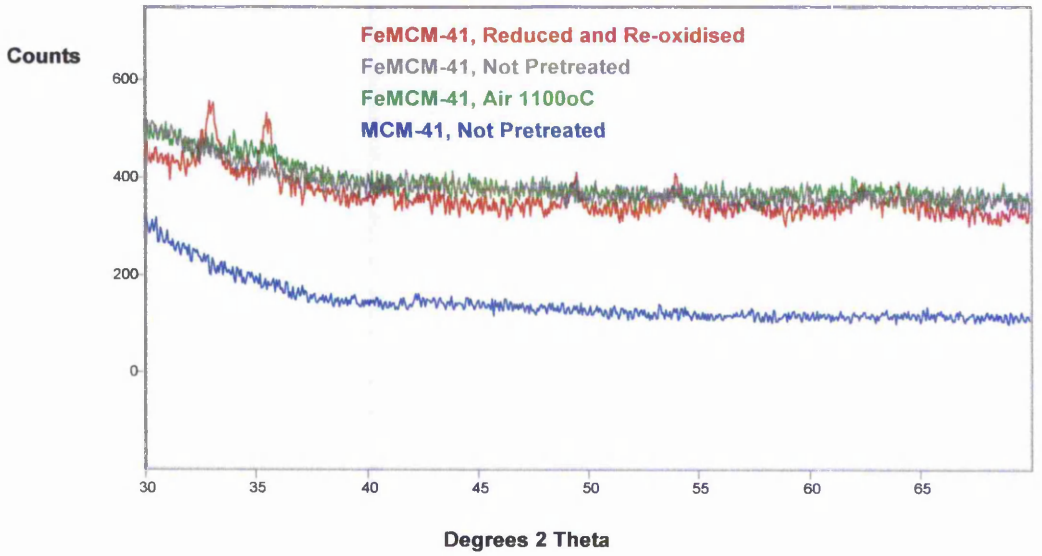

5.3.1.2 X-Ray Photoelectron Spectroscopy

XPS results for the two well-characterised samples (FeMCM-41(Syn), 3.51wt% and FeMCM-41(PS), 3.2wt%) showed a lowering of the surface Fe : Si ($Fe2p_{3/2}$: Si2p) compared with the bulk ratios. The synthetically modified sample had a surface ratio of 0.015 compared to its bulk ratio of 0.039 while the post-synthetically modified material had a surface ratio of 0.032 compared to 0.035 in the bulk. This suggests that a greater proportion of the iron in both materials may be located away from the external surface.

The difference between the synthetically modified material and the post-synthetically modified one suggests iron species are in different positions as a result of the incorporation method used. It would seem likely that an electron would be more likely to be ejected (that is, the escape depth be greater) from a position close to a pore opening than from deep within a pore or from the bulk of the silicate walls. This, therefore, suggests that for the synthetically modified materials the iron is either very deep within the pores, or incorporated into the

walls of the MCM-41. We, have observed, however, from the results of TPR, that these species that these species are nonetheless accessible for reaction.

5.3.2 Catalytic Reactor Testing

Results in this section are reported mainly in terms of the yield of the expected product, carbon dioxide. However, there are a few points worth discussion. Firstly there is the possibility of systematic error. If there is a systematic error in the quantification of either carbon monoxide or carbon dioxide then the figures reported would be systematically skewed. Results can be stated in terms of carbon monoxide conversion:

$$\%\ CO\ Conversion \quad = \quad \left(\frac{CO_{in} - CO_{out}}{CO_{in}} \right) X 100$$

or by carbon dioxide yield:

$$\%\ CO_2\ Yield \quad = \quad \left(\frac{CO_{2\,out}}{CO_{in}} \right) X 100$$

Systematic error would normally manifest itself so that one set of figures was consistently higher. This type of error is more likely to occur in the calculation of carbon monoxide concentration. Using the experimental parameters described the carbon monoxide peak, with a retention time of ca 16 minutes, is very broad and difficult to integrate. The carbon dioxide peak, by contrast, has a retention time of 3 minutes and is sharp. This peak broadening with increasing retention time is a feature of chromatography and results from the diffusion of the analyte in the mobile phase.

There is some evidence of such a systematic error in this case. The figures calculated for carbon monoxide conversion are in the region of 10% lower than

those calculated for carbon dioxide yield. There is also some evidence that this stems from a low value for the carbon monoxide figures rather than a high one in the case of carbon dioxide. For reasons which will be discussed later, single values of negative conversion are not in themselves impossible. However it was observed here that for the samples with low conversions using the figures for carbon monoxide conversion resulted in negative values across the whole temperature range, even where the product was consistently and clearly evident. This is unlikely to represent the true situation.

For these reasons to report carbon dioxide yield was considered more representative.

However, reporting carbon dioxide yield assumes a single reaction:

$$CO + \tfrac{1}{2} O_2 \longrightarrow CO_2$$

Whereas, in fact, the following reaction may be occurring at some, or all, temperatures:

$$2\,CO \longrightarrow C + CO_2$$

All the iron-containing MCM-41s were physically examined for evidence of the second reaction, for example sample darkening or blackening, after carbon monoxide reactor testing. With the exception of a single sample there was no evidence of this. This sample was the one with the highest iron loading (12wt%) and did show some blackening after reaction. This sample, itself, had certain other differences to the other samples, which will be discussed later. From the visible evidence it is apparent that the second reaction is not occurring to any degree overall with the other samples.

It is worth noting that if the second reaction were taking place alongside the first this would show itself in the results in such a way that the figures calculated from carbon monoxide conversion would be *higher* than those from carbon dioxide yield because of the 2.: 1 stoichiometry in the latter case.

In some cases the profile of the carbon monoxide conversion did not follow that of carbon dioxide yield. This is shown in figure 5.3.2.1.
In most of these cases an initially high conversion is followed by a drop at higher temperatures. Conversion subsequently rises again. In two of these cases there is evidently a negative conversion. This situation could arise if initial conversion follows both the paths described above; to produce both carbon dioxide and carbon deposits. At higher temperatures the carbon deposits may then be oxidised, again there are two possible reactions:

$$C + O_2 \longrightarrow CO_2$$

and,

$$C + \tfrac{1}{2} O_2 \longrightarrow CO$$

If the second of these reactions is taking place to a significant extent then it would be possible for a negative conversion to be a true value. However, these four samples do not show a trend. Two of the samples are ones where the iron was introduced during MCM-41 synthesis, yet they have vastly different iron loadings; one contains just 0.4wt% iron, while the other is the 12wt% iron sample mentioned previously. None of the samples with iron loadings between these values exhibit this phenomenon. The other two samples are post-synthetically modified; 1wt% and 2.45wt% iron. In this case there are similar samples with iron loadings lower, higher and intermediate where this is not seen. Given these facts it seems likely either that these downturns are in some way the product of experimental error. Alternatively this may be occurring with all the samples but, for some reason, is being masked in the other cases, however this seems unlikely.

Figure 5.3.2.1 Carbon Monoxide Conversion for Selected Iron MCM-41s

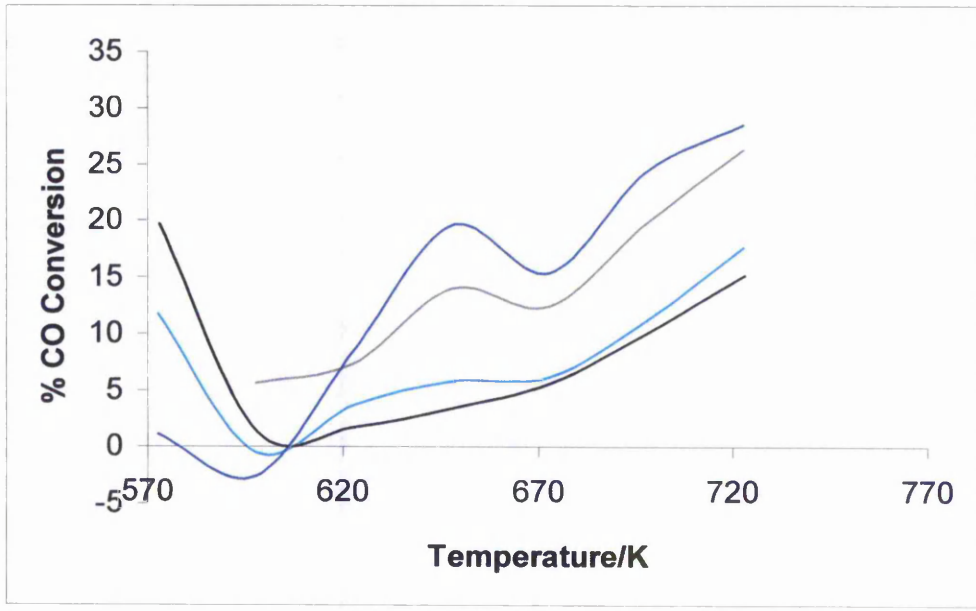

- FeMCM-41(Syn, 12wt%)
- FeMCM-41(Syn, 0.4wt%)
- FeMCM-41(PS, 2.45wt%)
- FeMCM-41 (PS, 1wt%)

Figures 5.3.2.2 and 5.3.2.3 show carbon dioxide yields for synthetically modified and post-synthetically modified iron MCM-41 respectively.
These show remarkable similarities in behaviour between the synthetically and the post-synthetically modified samples. Activities are similar for samples with similar iron content; regardless of the method of incorporation. This suggests that the accessibility of the iron species is similar, which is in keeping with the findings of TPR reported earlier. This may indicate that even in the synthetically modified samples the iron is not buried very deeply within the silica walls of the MCM-41, and is thus accessible to the reactants.

Figure 5.3.2.2 Carbon Dioxide Yield for Synthetically Modified Iron MCM-41

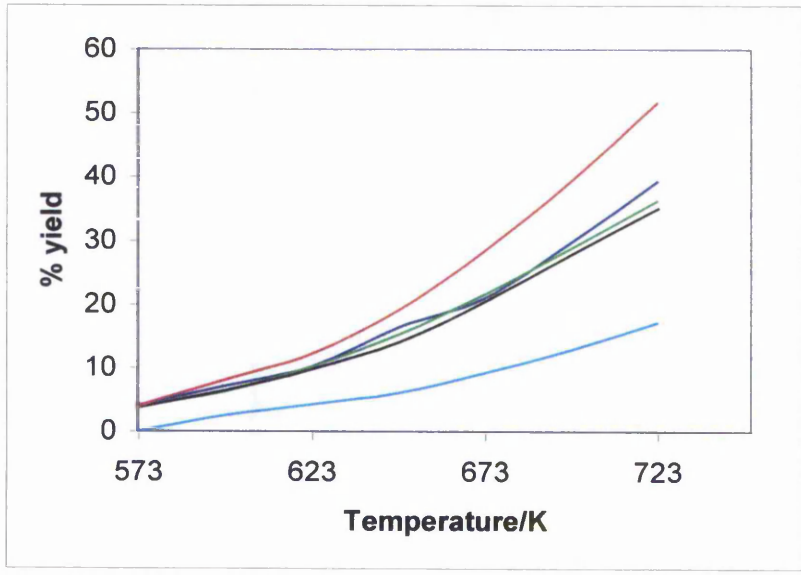

- FeMCM-41(Syn, 12wt%)
- FeMCM-41(Syn, 3.51wt%)
- FeMCM-41(Syn, 0.4wt%)
- FeMCM-41(Syn, 5.93wt%)
- FeMCM-41(Syn, 1.96wt%)

Figure 5.3.2.3 Carbon Dioxide Yield for Post-synthetically Modified Iron MCM-41

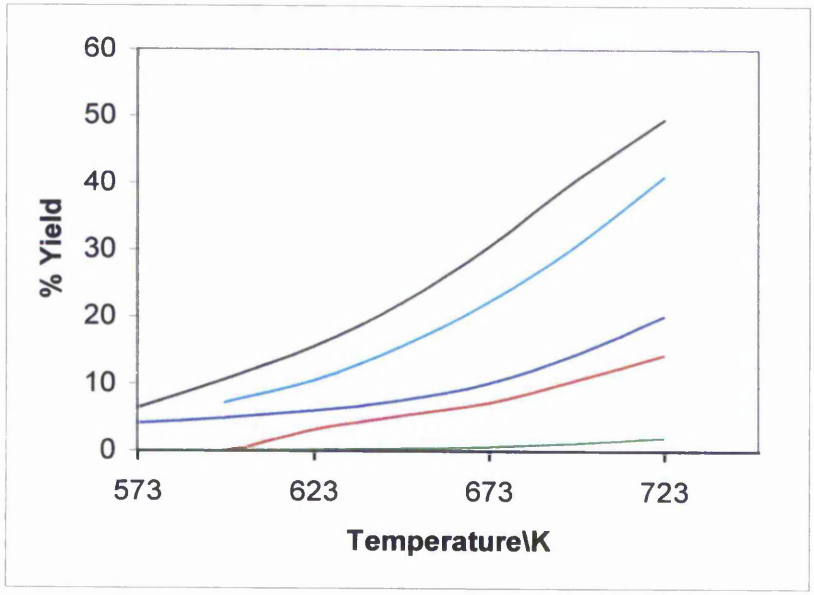

- FeMCM-41 (PS, 3.2wt%)
- FeMCM-41 (PS, 1wt%)
- FeMCM-41 (PS, 0.1wt%)
- FeMCM-41 (PS, 2.45wt%)
- FeMCM-41 (PS, 0.5wt%)

There are, however, some differences. The synthetically modified iron MCM-41 shows an increase in activity from the very low iron content materials (0.4wt%) to the sample containing ca. 2wt% iron. After this there is a plateau for the samples containing approximately 4 and 6wt%. This is in keeping with the findings of Szegedi and co-workers who found that for iron weightings over 4.4wt% (Si : Fe = 20) there was no further increase in activity[15]. However, their conversions were considerably higher than observed here, reaching over 80% at 690 K for their best performing sample (4.4wt%). In contrast to the findings of that group our highest iron content sample (12wt%) did show a higher activity, but this sample has a significantly different appearance to the other samples exhibiting a range of colours (brown, orange and grey), rather than the uniform pale brown of the other samples. This is suggestive of the presence of bulk iron oxide species and it has been previously reported[3] that Fe_2O_3, for example, is active in the oxidation of carbon monoxide. This sample represents a significantly higher iron content than Szegedi's highest loading. That group also concluded that there were only isolated iron species present in their samples. The presence of isolated metal entities at low levels of incorporation with bulk oxide species at higher loadings is also in keeping with the findings of Lang and co-workers who incorporated vanadium and titanium post-synthetically into MCM-41[18]. They found that both these metals are present mainly as isolated species at low levels of incorporation, but that at higher metal content extended oxide species were produced.

Examination of activity per iron species, however, shows that, with the exception of the sample containing 0.5wt% iron the activity of the post synthetically modified samples varies little with iron content, showing a slight fall as iron loading increases. By contrast the synthetically modified samples show a dramatic decrease in activity per site with increasing iron incorporation.

Figure 5.3.2.4 Turn Over Number (TON), molecules per molecule /s (at 723 K) for iron MCM-41

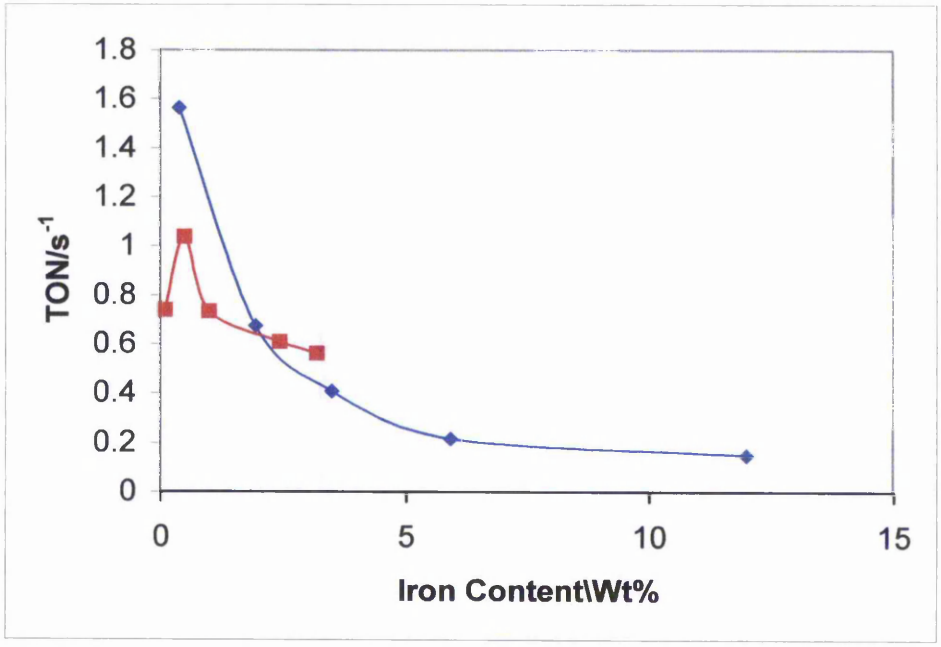

Synthetically modified iron MCM-41

Post-synthetically modified iron MCM-41

Figure 5.3.2.4 also shows that at low loadings the synthetically modified materials are more active than the post-synthetically modified whereas at loadings higher than ca. 2wt% the post synthetically modified samples perform better.

Arrhenius type plots for the synthetically and post-synthetically modified samples with iron content of ca. 3.5wt% are shown in figure 5.3.2.5.

Figure 5.3.2.5 Arrhenius Plot for Carbon Monoxide Conversion over Synthetically Modified Iron MCM-41 (Blue) and Post-synthetically Modified Iron MCM-41 (Red)

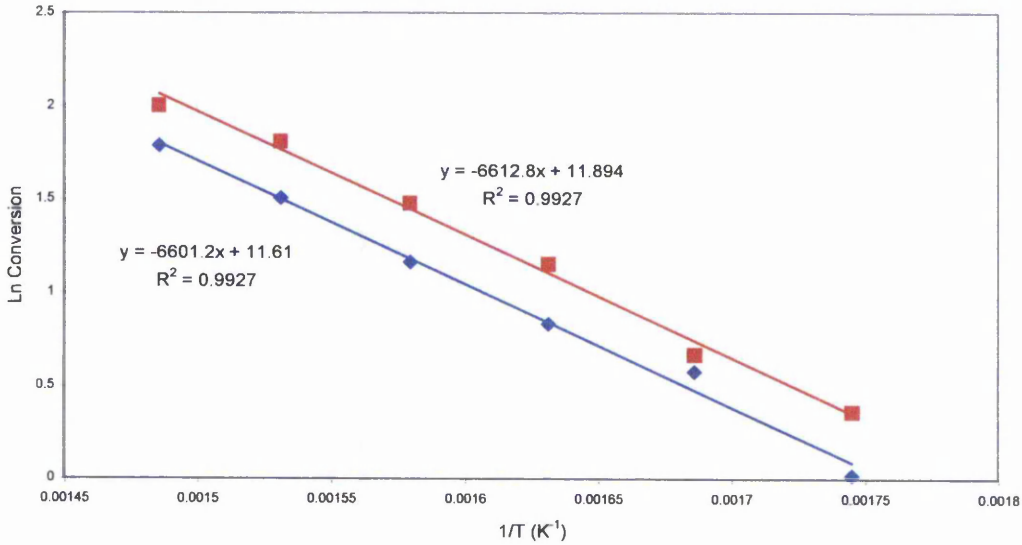

From these the apparent activation energy is calculated as 54.9 kJ/mole for the synthetically modified sample and 55.0 kJ/mole for the post-synthetically modified one. Again these are remarkably similar between the two methods of iron incorporation, however, it should be noted that the latter sample has an actual iron content ~ 8.5% lower than the former. Both these figures are considerably lower than the 165.7 kJ/mole for the gas phase reaction and 110.5 kJ/mole over bulk Fe_2O_3 reported by Li et al[3]. This group tested the activity of NANOCAT superfine Fe_2O_3 nanoparticles in this reaction and found an apparent activation energy of 60.7 kJ/mole. They attributed the increase in activity to the small particle size.

5.4 Conclusions

Iron can be introduced into MCM-41 effectively either by synthetic inclusion from iron (III) nitrate or post-synthetic treatment with iron (III) acetylacetonate. Neither method leads to significant changes in surface area of the host material at moderate levels of incorporation (ca 4wt%).

Both of these methods result in remarkably stable, probably isolated, iron species, which are, however, easily converted between the +2 and +3 oxidation states. Both the resultant materials show activity in the catalytic oxidation of carbon monoxide.

X-ray photoelectron spectroscopy suggests that the iron is in different locations in the two types of sample, with the iron introduced during synthesis probably incorporated in the silica walls. However the redox behaviour of both types of samples is remarkably similar, as seen from TPR and catalytic testing.

Treatment of the synthetically modified samples in air at very high temperatures brings only partial modification of the MCM-41 structure but complete reduction followed by re-oxidation leads to total pore break down and the formation of Fe_2O_3.

5.5 References

1. Kaim, W. and B. Schwederski, *Bioinorganic Chemistry : Inorganic Elements in the Chemistry of Life An Introduction and Guide.* Inorganic Chemistry A Textbook Series, ed. G. Meyer and A. Nakamura. 1991: John Wiley and Sons.
2. Pearce, R. and W.R. Patterson, *Catalysis and Chemical Processes.* 1981, Glasgow: Leonard Hill.
3. Li, P., et al., *The Removal of Carbon Monoxide by Iron Oxide Nanoparticles.* Applied Catalysis B-Environmental, 2003. **43**: p. 151-162.
4. Pillai, U.R. and E. Sahle-Demessie, *Oxidation of alcohols over Fe^{3+}/montmorillonite-K10 using hydrogen peroxide.* Applied Catalysis A: General, 2003. **245**: p. 103-109.
5. Chen, C.-S., C. Wu-Hsun, and L. Shou-Shiun, *Enhanced activity and stability of a Cu/SiO_2 catalyst for the reverse water gas shift reaction by an iron promoter.* Chemical Communications, 2001. **18**: p. 1770-1771.
6. Chen, H.Y. and W.M.H. Sachtler, *Activity and durability of Fe/ZSM-5 catalysts for lean burn NOx reduction in the presence of water vapor.* Catalysis Today, 1998. **42**(1-2): p. 73-83.
7. Joyner, R.W. and M. Stockenhuber, *Preparation, Characterization and Performance of Fe-ZSM-5 Catalysts.* Journal of Physical Chemistry B, 1999. **103**: p. 5963-5976.
8. Mahay, A., et al., *Deoxygenation of Methanol with Carbon Monoxide over Fe/ZSM-5 Catalysts.* Journal of Catalysis, 1986. **103**: p. 480-491.
9. Guzman-Vargas, A., G. Delahay, and B. Coq, *Catalytic decomposition and catalytic reduction of N_2O and N_2O + NO by NH_3 in the presence of O_2 over Fe-zeolite.* Applied Catalysis B: Environmental, 2003. **42**.
10. Stockenhuber, M., et al., *Transition metal containing mesoporous silicas - redox properties, structure and catalytic activity.* Microporous and Mesoporous Materials, 2001. **44**: p. 367-375.
11. Kenvin, J.C., M.G. White, and M.B. Mitchell, *Preparation and Characterisation of Supported Mononuclear Metal Complexes as Model Catalysts.* Langmuir, 1991. **7**(6): p. 1198.

12. Monti, D.A.M. and A. Baiker, Journal of Catalysis, 1983. **83**: p. 323.

13. Fierro, G., et al. *Temperature-Programmed Reduction in Catalysis: A Critical Evaluation of the Method.* in *10th International Congress on Catalysis.* 1992. Budapest: Elseiver.

14. Scofield, J.H., *Hartree-Slater Subshell Photoionization Cross Sections at 1254 and 1487 eV.* Journal of Electron Spectroscopy and Related Phenomena, 1976. **8**: p. 129-137.

15. Szegedi, A., G. Pal-Borbely, and K. Lazar, *Comparison of the redox properties of iron incorporated in different amounts into MCM-41.* Reaction Kinetics and Catalysis Letters, 2001. **74**(2): p. 277-287.

16. Wimmers, O.J., P. Arnoldy, and J.A. Moulijn, *Determination of the Reduction Mechaism by Temperature-Programmed Reduction: Application to Small Fe_2O_3 Particles.* Journal of Physical Chemistry, 1986. **90**: p. 1331-1337.

17. Landau, M.V., et al., *Wetting stability of Si-MCM-41 mesoporous material in neutral and basic aqueous solutions.* Microporous and Mesoporous Materials, 1999. **33**: p. 149-163.

18. Lang, N., P. Delichere, and A. Tuel, *Post-synthesis introduction of transition metals in surfactant-containing MCM-41 materials.* Microporous and Mesoporous Materials, 2002. **56**: p. 203-217.

6. Modification of Siliceous MCM-41 by Attachment of Organic Species

6.1 Introduction

Among other approaches to conferring catalytic activity on the M41S class of materials there has been work by a number of groups on the tethering of organic molecules to the silica surface and inside the pore walls. There are possibilities of benefits with this strategy; should it be possible to attach a bulky or sterically hindered organic species, the possibility of introducing some degree of size or shape selectivity into the uniform pores arises.

A popular and widely used method has involved the post synthetic grafting of organosilanes onto the surface: although there is the possibility of the formation of multiple species because of binding through more than one Si-O-Si group; attachment of oligomeric silanes, and the presence of physisorbed species. Organic loading may be also be low resulting in the use of large quantities of catalyst[1]. The synthetic procedures involved are often relatively complicated and lengthy. Other groups have preferred the direct incorporation of organosilanes into the silica framework during synthesis[2-4]. This is effectively a co-polymerisation, which may result in a very thermally stable inorganic-organic hybrid with the potential for very high loadings of the organic material[1], but does not necessarily result in surface organic species.

Previous work in this laboratory, however, suggests an alternative, more simple, and less costly, approach. During iron incorporation, with methanol as the solvent, it has been observed that methoxy groups have become strongly bonded to the surface of the MCM-41 material[5]. Attachment occurred merely by stirring the host material in the solvent. As has been discussed in chapter one of this work, it is established that alcohols react with both oxides and hydroxides of silica; indeed this is the basis of the production of the metal alkoxides[6]. Also Iler has reported the attachment of alcohols to silicas[7, 8]. However, it is the ease of attachment in this case and the surprising stability of the resultant groups (up to 725 K in air) that make this interesting and potentially useful. This

stability, in itself, is somewhat surprising given the susceptibility of metal hydroxides to hydrolysis; this has also been discussed in chapter one. If the method could be extended to other alcohols it would open a route for a remarkably simple method of attaching a hydrocarbon species to form an organic-inorganic hybrid. Not only is no special equipment necessary the synthesis time is low.

It was, therefore, of interest to study the extension of this approach from methanol to other alcohols.

The location of the organic attachment is of some interest because the preferred aim is to create surface organic groups within the pores of the material.

6.2 Experimental

Preparations

In a series of experiments attempts were made to attach a series of straight chain, saturated, primary alcohols (C = 1-6), cyclohexanol, benzyl alcohol and phenol to the mesoporous MCM-41 host.

The straight chain alcohols and benzyl alcohol (100 ml) were stirred briskly (> 500 rpm) at room temperature in a three necked flask fitted with a reflux condenser with an inert gas bubbling through (Ar/N_2, flow 3-5 L/hour) for ca. 1 hour, after which time the MCM-41 was added and stirring continued over a period of 24 hours. The resulting material was filtered over a sinter and dried at 383 K overnight.

In the case of cyclohexanol and phenol attachment was attempted from 0.1 molar and 0.5 molar solutions (in toluene) following the procedure outlined

above; except that the resultant material was washed with toluene prior to drying.

Attachment of the alcohols was studied and confirmed by infra-red spectroscopy at atmospheric pressure on a self-supporting wafer of the sample using a Mattson Polaris FTIR in transmission mode. Spectra were converted to absorbance using the Grams 32 computer programme.

Characterisation

BET surface areas of the modified materials were determined by the computer controlled apparatus described in section 2.1.2.

Thermogravimetric analysis (TGA) was performed on the materials in order to estimate the organic content. This was performed both in dry nitrogen and atmospheric air as the facility for performing this in dry air or oxygen was not available. A Stanton Redcroft TG 760 Series Thermal Balance was used. The sample (ca. 3-5 mg) was heated in a flow of nitrogen/air of 3 L/hour from 295 to 1100 K (ramp 5 K/minute).

For the butanol, pentanol, hexanol and benzyl alcohol modified samples temperature programmed removal of the organic species was attempted in the apparatus designed for temperature programmed desorption, previously described in chapter 2. This apparatus is equipped with a mass spectrometer as its detection system, as described in that chapter; which may enable some identification of the products of removal.

A simplified, schematic, diagram of a mass spectrometer is shown in figure 6.2.1. Briefly this comprises of: an ionisation chamber, with a source of ionisation, an analyser, which separates the ions according to their mass/charge (m/z) ratio and a detection system. The ionisation, separation and detection methods in the present case are electron impact ionisation, a quadrupole analyser and an electron multiplier respectively.

Figure 6.2.1 Schematic Diagram of a mass Spectrometer

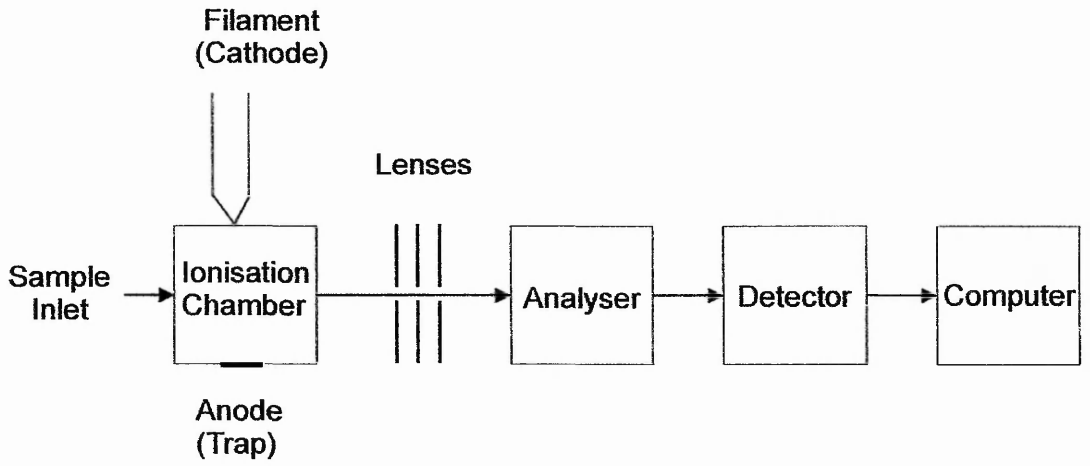

In electron ionisation a stream of high energy electrons is accelerated from the cathode at the gas phase molecule in the ionisation chamber. Collision can result in the loss of an electron from the molecule.

$$M + e^- \longrightarrow M^{\cdot+} + 2e^-$$

High energy electrons	Radical + Thermal Cation + electrons

The ions formed are vibrationally excited and therefore may fragment to form a charged fragment ion and a neutral radical species.

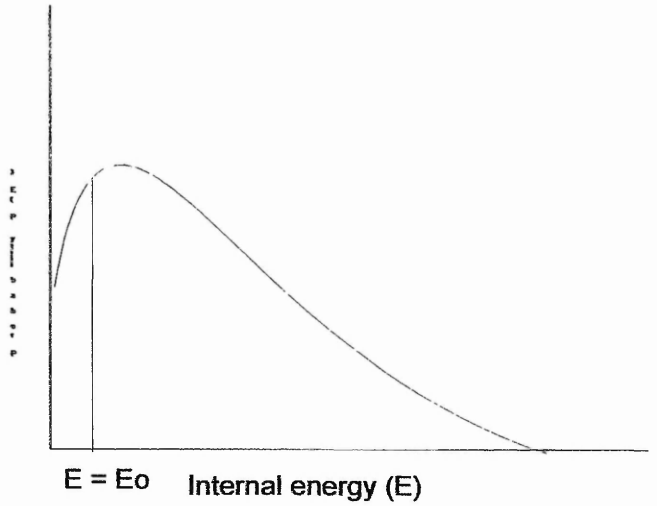

E_o represents the energy required to break the weakest bond in a given molecule, any molecule possessing a lower internal energy than this will appear as the parent (or molecular) ion. E_o is typically in the region of 10-15 eV for an organic molecule. In the case of electron impact ionisation fragmentation is often extensive, not only because of the relatively high energy ionisation, but also because the parent ion formed, as a radical, is unstable. For these reasons the molecular ion is often absent or in very low abundance in electron impact mass spectra[9]. This can be observed from the expected fragmentation patterns reproduced in the results section of this chapter.
The fragmentation process is characteristic of the strength of the bonds, and therefore of the molecule itself. Because of this the presence of given fragments in the mass spectrum can be used for identification and to support the presence of a particular molecular species.

Samples (ca. 500 mg) were heated from 303 K to 873 K with a ramp rate of 5 K/minute with the mass spectra being recorded at intervals of ca. 5 K. The resulting mass spectra were examined for fragments present in the spectra of: the alcohol, the corresponding saturated hydrocarbon and the α-unsaturated hydrocarbon.
For the shorter chain aliphatic alcohols the limitation arose of being able to identify suitable unambiguous fragments in the mass spectra.
Additionally most of the organically modified samples were subjected to powder x-ray diffraction using the approach described in chapter 2.

6.3 Results and Discussion

Infra-red spectroscopy confirmed the presence of hydrocarbon on all the MCM-41 materials modified with straight chain alcohols. The relevant section of the infra-red spectra of these materials is shown in figure 6.3.1.

Figure 6.3.1 Infra-red spectra of alcohol-modified MCM-41

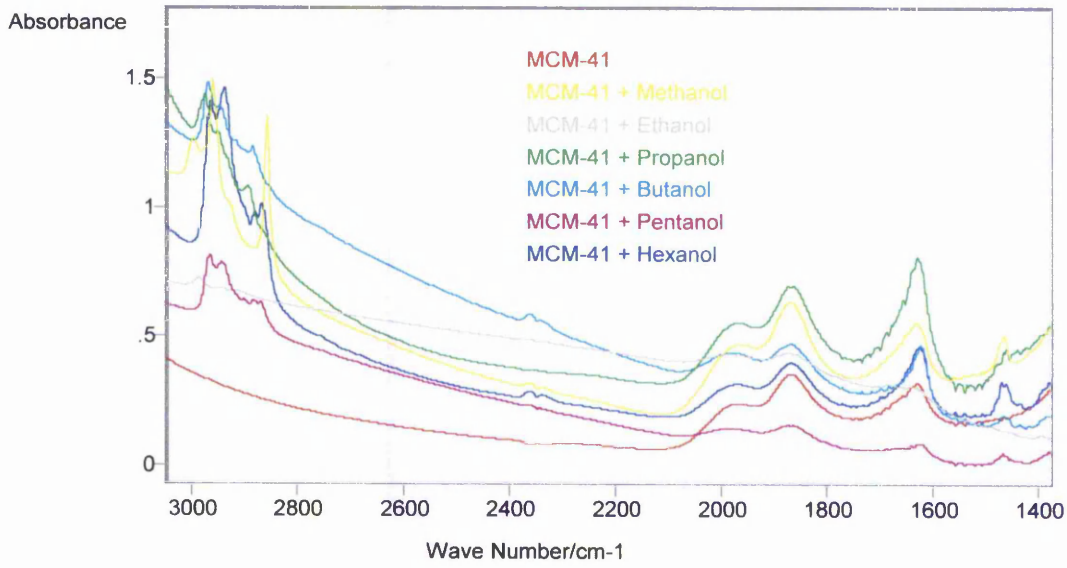

For all samples the bands expected from the silica host were present: a sharp band ca. 3740 cm^{-1} attributed to terminal –OH groups, a broad band centred around ca. 3550 cm^{-1} attributed to silanol nests and the bands between ca. 2100 cm^{-1} and 1700 cm^{-1} attributed to the SiO_2 overtones of the MCM-41. In addition up to four extra bands were observed in the C-H vibration region and up to three weak extra bands in the deformation region. A summary of all bands in these samples is presented in table 6.3.1. It should be noted that some of the weaker bands are not observed in all cases; this is not surprising since the quantity of hydrocarbon is likely to be small compared to the host material.

Table 6.3.1 Infra-red band assignment for Alcohol-modified MCM-41

Attaching Alcohol	Wave Number/ cm^{-1}	Possible Assignment	Comments
Methanol	3740	MCM-41 terminal OH	
	3688-3046	MCM-41 Silanol nests, adsorbed water	Very broad
	2997		Medium
	2959	CH_3 Asymmetric stretch	Strong, shoulder at 2928cm^{-1}
	2857	CH_3 Symmetric stretch	Strong
	1464	CH_3 Asymmetric deformation	Weak
	2090-1570	MCM-41 SiO_2 overtones	
Ethanol	3741	MCM-41 terminal OH	
	3688-3046	MCM-41 Silanol nests, adsorbed water	Very broad
	2985	CH_3 Asymmetric stretch	
	2940	CH_2 Asymmetric stretch	
	2070-1600	MCM-41 SiO_2 overtones	
Propanol	3741	MCM-41 terminal OH	
	3695-3040	MCM-41 Silanol nests, adsorbed water	Very broad
	2972	CH_3 Asymmetric stretch	
	2947	CH_2 Asymmetric stretch	Shoulder at 2931 cm^{-1}
	2889	CH_3 Symmetric stretch	
	1464	CH_3 Asymmetric deformation	
	2080-1560	MCM-41 SiO_2 overtones	
Butanol	3743	MCM-41 terminal OH	
	3710-3005	MCM-41 Silanol nests, adsorbed water	Very broad
	2966	CH_3 Asymmetric stretch	
	2944	CH_2 Asymmetric stretch	
	2883	CH_3 Symmetric stretch	
	1470	CH_2 Symmetric deformation	
	1457	CH_3 Asymmetric deformation	
	1386	CH_3 Symmetric deformation, C-C vibration	
	2060-1570	MCM-41 SiO_2 overtones	
Pentanol	3742	MCM-41 terminal OH	
	3690-3030	MCM-41 Silanol nests, adsorbed water	Very broad
	2964	CH_3 Asymmetric stretch	
	2940	CH_2 Asymmetric stretch	
	2880	CH_3 Symmetric stretch	
	2868	CH_2 Symmetric stretch	
	1470	CH_2 Symmetric deformation	
	1462	CH_3 Asymmetric deformation	
	1382	CH_3 Symmetric deformation, C-C vibration	
	2070-1570	MCM-41 SiO_2 overtones	
Hexanol	3744	MCM-41 terminal OH	
	3705-3020	MCM-41 Silanol nests, adsorbed water	Very broad
	2962	CH_3 Asymmetric stretch	
	2935	CH_2 Asymmetric stretch	
	2880	CH_3 Symmetric stretch	
	2866	CH_2 Symmetric stretch	
	1471	CH_2 Symmetric deformation	
	1464	CH_3 Asymmetric deformation	
	1382	CH_3 Symmetric deformation, C-C vibration	
	2070-1570	MCM-41SiO_2 overtones	

Two other features are worthy of note. Firstly, that the methanol-modified sample, alone, has an extra band at 2997 cm^{-1} that is neither expected in the spectrum of an alkane nor observed in the spectrum of the other modified MCM-41 materials. Nakanishi reports that, in the case of organic ethers (R-O-R, with which these materials are analogous) the methoxyl group (-O-CH_3) exhibits extra bands in this area, which are absent in -O-C_2H_5[10]. Secondly, regarding the weak band at ca. 1380 cm^{-1}: this can be attributed to CH_3 symmetric deformation but it falls in an area of the spectrum where C-C vibrations, if present, are to be expected[11]. It seems likely that in these samples the latter attribution is the correct one. The band is noticeably absent from the spectrum of the methanol-modified sample, where the bands (all attributable to CH_3) are very clear and well defined; this material is not expected to contain a C-C bond. Furthermore it appears only in the spectra of the longer chain alcohols and does not become smaller compared to peaks attributed to CH_2. This could be due to a relative increase in the intensity of the band with increasing alkyl chain length. There are two possible reasons for this. Firstly, and simply, the presence of a greater number of C-C bonds; however there may be another factor involved. Generally for a given infra-red vibration the more polar a bond the more intense will be the band arising from that vibration[12]: since alkyl groups are electron donating an increase in the chain length will increase the polarity of the C-C bonds[13]. All these observations are the opposite of that which would be expected if the former attribution (to CH_3) were correct. Additionally, this band is present in the spectrum of the cyclohexanol-modified sample (see next paragraph); where no CH_3 is to be expected.

For the cyclohexanol-modified sample (see figure 6.3.2), bands were observed at 2943 cm^{-1}, with a shoulder at 2913 cm^{-1}, and 2865 cm^{-1}, which are attributed to asymmetric and symmetric stretch of –CH_2–. Additionally weak band attributed to symmetric bending of –CH_2 can be observed at 1455 cm^{-1}, as can the band at 1380 cm^{-1}, previously discussed, which may be attributed to C-C vibrations. No bands attributable to toluene were observed.

The additional bands in the spectra of all these alcohol-modified samples are in keeping with what one would expect to observe in the free alcohol except that they all lacked the band at 3650-3590 cm^{-1} attributed to free –OH in alcohols[9, 14, 15]. However, since this appears in an area of the spectrum which is

dominated by the broad band attributed to silanol nests and adsorbed water in the parent MCM-41, this band may be present but obscured.

Figure 6.3.2 Infra-red spectra of cyclohexanol-modified MCM-41

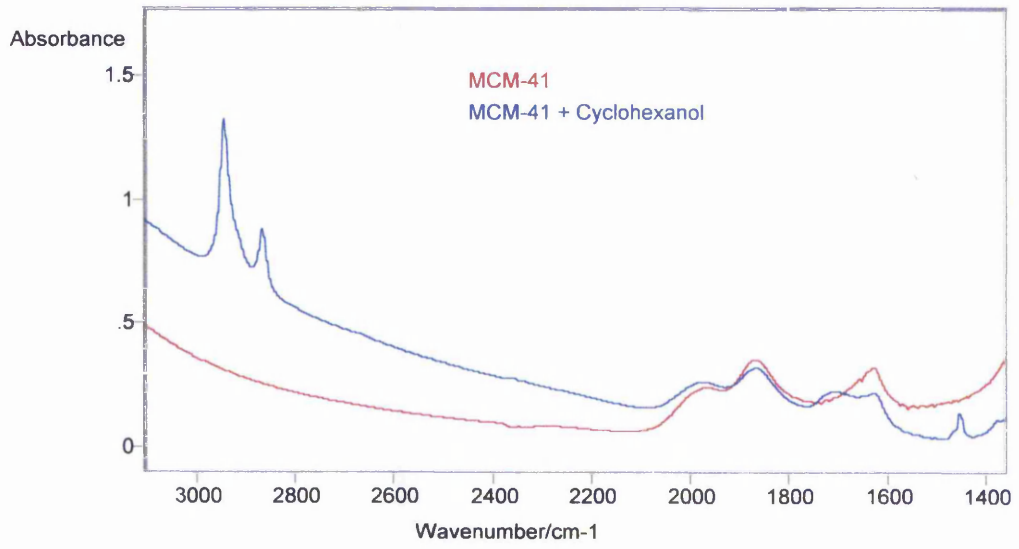

The spectrum of the benzyl alcohol modified MCM-41, along with the corresponding spectra for both MCM-41 alone and liquid phase benzyl alcohol (KBr disc, recorded under the same conditions), are shown in figure 6.3.3.

Figure 6.3.3 Infra-red spectra of MCM-41, benzyl alcohol-modified MCM-41 and benzyl alcohol

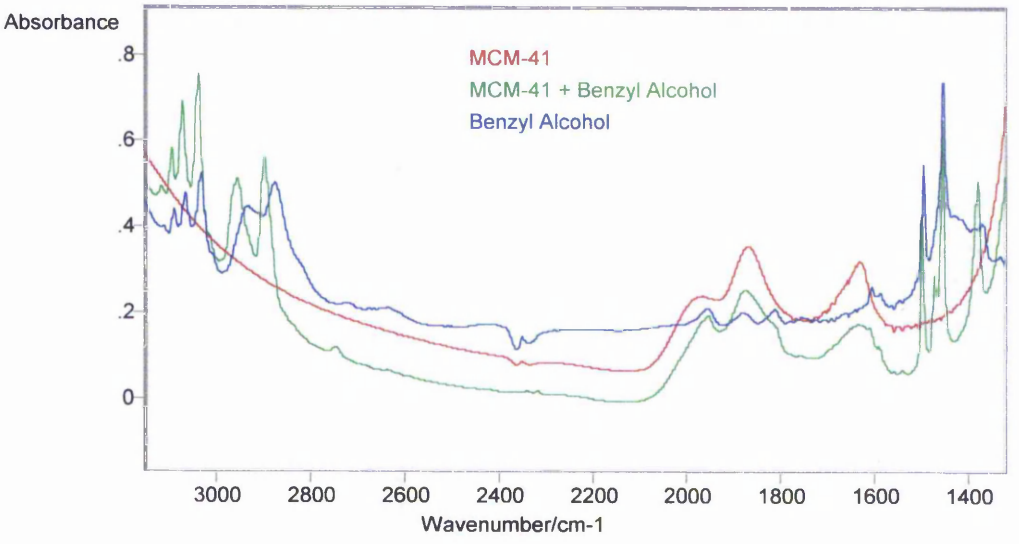

Additional bands are observed as follows: four bands at 3110 cm^{-1}, 3093 cm^{-1}, 3071 cm^{-1} and 3037 cm^{-1}, attributed to the =C-H stretch of the aromatic ring, two bands at 2955 cm^{-1} and 2896 cm^{-1}; attributed to the asymmetric and symmetric stretch of the $-CH_2$ group, bands at 1498 cm^{-1} and 1456 cm^{-1}; attributed to C=C stretching of the aromatic ring, a band at 1473 cm^{-1} attributed to CH_2 symmetric deformation and a band at 1380 cm^{-1}; attributed to C-C vibration (as discussed in the section on straight chain alcohols). A summary can be found in table 6.3.2.

Table 6.3.2 Infra-red band assignment for Benzyl Alcohol-modified MCM-41

Wave Number/cm-1			Possible Assignment	Comments
MCM-41	Benzyl Alcohol Modified MCM-41	Benzyl Alcohol		
3741	3741		MCM-41 terminal OH	
3690-3120	3720-3130		MCM-41 Silanol nests, adsorbed water	Very broad
	3630		O-H Stretch	Sharp
		3341	O-H Stretch	Very broad
	3115	3110	CH stretch (benzene ring)	
	3093	3088	CH stretch (benzene ring)	
	3071	3065	CH stretch (benzene ring)	
	3037	3031	CH stretch (benzene ring)	
	2955	2934	CH_2 Asymmetric stretch	
	2896	2874	CH_2 Symmetric stretch	
2085-1570	2090-1570		MCM-41SiO_2 overtones	
	1498	1496	C=C Stretch	
	1473		CH_2 Symmetric deformation	
	1456	1453	C=C Stretch	
	1380		C-C vibration	

This sample alone exhibited a band at 3630 cm^{-1} which could be attributable to free O-H stretching of the alcohol, indicating at least some adsorbed benzyl alcohol. This is also supported by the results of the temperature-programmed removal, which is reported later in this chapter. However this band is significantly different in appearance and position in the modified material compared to the free alcohol. In the free alcohol it appears as a broad band centred around 3340 cm^{-1}, whereas in the modified MCM-41 a sharp peak is observed at 3630 cm^{-1}. Although the latter band (in the benzyl alcohol modified-MCM-41) is more typical of free O-H stretch in alcohols the experimentally observed band is to be expected for benzyl alcohol [11].

Another feature of the modified MCM-41 material is a shift to higher wave number of approximately 20 cm^{-1} for the CH_2 stretching modes and ca. 5 cm^{-1} for the =C-H stretch of the aromatic ring on attachment. This shift to higher

frequency is indicative of a higher energy vibration; which suggests a strengthening of the C-H bonds within the organic molecule. It is also evident that this strengthening is greatest in the C-H bands closest to the silica host, diminishing throughout the molecule.

For both the phenol samples (0.1 molar, 0.5 molar) there was no evidence in the infra-red of any additional bands attributable to phenol, and there was no evidence from the infra-red of damage to the MCM-41 material. In order to rule out concentration effects the experiment was repeated substituting a 0.1 molar solution of benzyl alcohol in toluene, and attachment, albeit to a reduced degree, was confirmed. The same infra-red bands were present as in the previous preparation, but reduced in intensity. Although it is not possible to normalise to wafer thickness completely accurately the reduction was significant and normalisation to the SiO_2 overtones at 1870 cm^{-1} and 1960 cm^{-1}, followed by integration of the bands at 1498 $cm^{-1}$and 1456 cm^{-1} attributed to C=C stretching of the ring, indicates a lesser attachment by a factor of 3 - 4.
Significantly, therefore, phenol failed to attach to the MCM-41 material at a concentration five times higher than that which results in the attachment of both benzyl alcohol.and cyclohexanol. This may indicate a functional group specificity to alcohols which are not strongly acidic. The other notable difference between the two cases is the absence of a hydrogen atom directly bonded to the hydroxyl carbon; if this hydrogen were involved in the reaction mechanism, then this absence would explain the non-attachment of phenol. In order to clarify this the preparation was repeated with the smallest tertiary alcohol, tertiary butanol, and there was evidence, both in the infra-red and thermogravimetric analysis (see later) of attachment. This suggests that this hydrogen is not involved in the reaction mechanism, unless different mechanisms are occurring in the two cases.

Characterisation

Results of TGA of the straight chain alcohol-modified materials over the total range, from room temperature to 1100 K, show some correlation to chain length. The loss, expressed in terms of mole%, decreases with increasing alcohol chain length for the alcohols from methanol to pentanol. There is a slight rise in the case of hexanol, but it is possible that this is an aberrant result. This decrease would be expected merely on the basis of molecular size; the surface of the MCM-41 is likely to be more accessible to smaller molecules. The case of benzyl alcohol is exceptional, the material having similar molar content to that of the methanol modified material. This would not be expected on the grounds of physical accessibility since the molecule is both bulky and, because of the aromatic ring, rigid.

However, since it is known that alcohols adsorb onto materials of this type[16, 17], and results from temperature-programmed removal (reported later in this chapter) indicate the removal of significant quantities of intact alcohol at temperatures that suggest adsorption a report of the total weight loss during TGA in the range 295 – 1100 K would be likely to considerably overstate amount of bonded material. For this reason weight loss below a given temperature should be excluded from the results of the TGA. Examination of the profiles of the hydrocarbon fragments in the temperature-programmed removal shows, in most cases, two distinct removal peaks. The first, which is likely to arise from adsorbed material, centres around ca. 385 K and removal is complete by ca. 450 K. The second, centred around ca. 800 K has its onset no lower than 650 K. Between these two peaks removal of hydrocarbon fragments is, in most cases, negligible. It was, therefore, decided to choose a temperature somewhere within this plateau, below which weight loss would be disregarded, in order to minimise contribution from any adsorbed alcohol. This can provide an *estimate* of the quantity of alcohol bonded to the host but also allows comparison between the different materials. It was considered more important to be confident of excluding a contribution from adsorbed alcohol from the reported results than a possible, slight, underestimation of the quantities of *bonded* material. For this reason a temperature of 575 K was chosen. In a study of the interaction adsorption of methanol on alkali metal exchanged zeolites. Lercher et al have performed

temperature-programmed removal. The desorption reported from those materials was similar to that observed here; with desorption complete below, but close to, 575 K[18].

A summary of the results of TGA in nitrogen and air is shown in table 6.3.3; only weight loss above 575 K is reported, as outlined above.

Table 6.3.3 Summary of results of thermogravimetric analysis in nitrogen and air for organically-modified MCM-41

Attaching Alcohol	% Weight Loss > 575 K	
	Air	N2
MCM-41	1.2	2.1
Methanol	3.4	3.7
Ethanol	1.0	3.2
Propanol	2.6	4.8
Butanol	2.4	3.9
Pentanol	0.9	4.9
Hexanol	6.4	7.9
Hexanol	3.4	7.4
Cyclohexanol	4.4	5.2
Benzyl Alcohol	20.8	20.2
Benzyl Alcohol	9.0	11.1
Benzyl Alcohol	15.0	15.6

From this it can be seen that in all cases, including the unmodified MCM-41 heating in atmospheric (undried) air the weight loss is lower than that for heating in dry nitrogen. It is possible that the composite materials are more stable in air than they are in nitrogen; this, in turn, would suggest that they are more vulnerable to reduction than oxidation. However this is unlikely in view of the experimental conditions (dry nitrogen, undried. air) and the susceptibility of the Si-O-C bond to hydrolysis[6, 8].

One possible explanation is that in wet air the process involves the addition of water. This is in agreement with the conclusions of others, who suggest that

problems with the hydrothermal and long-term stability of MCM-41 are the result of the hydrolysis of strained siloxane bonds[19-21].

Another possibility is the formation of carbonaceous deposits on the material heated in air; this would mean that the weight loss does not represent the total removal of the organic material.

Therefore, the results of the thermogravimetric analysis performed in nitrogen provide a better estimate of the amount of bonding alcohol. However it is an estimate of the minimum since it is possible that under these experimental conditions the alcohol would be incompletely removed. In fact, examination of some of the samples after TGA confirmed incomplete removal since there was a brown residue suggesting incompletely combusted material.

Results of nitrogen TGA are shown in table 6.3.4. Again only weight loss above 575 K is reported, for the reasons previously discussed and are additionally adjusted to weight loss of a parent MCM-41 under the same conditions which lost 2.1 weight%.

Table 6.3.4 Summary of results of thermogravimetric analysis in nitrogen for organically modified MCM-41 (Corrected figures refer to weight loss minus weight loss in pure MCM-41 over the same temperature range).

Attaching Alcohol	Weight Loss > 575 K (Wt%)	Corrected Weight Loss > 575 K (Wt%)	Corrected Weight Loss > 575 K (Mole%)
Methanol	3.7	1.6	5.7
Methanol	3.6	1.5	5.4
Ethanol	3.2	1.1	2.2
Propanol	4.8	2.7	3.6
Butanol	3.9	1.8	1.9
Pentanol	4.9	2.8	2.3
Hexanol	7.9	5.8	4.1
Hexanol	7.4	5.3	3.8
Cyclohexanol (0.1 molar)	5.2	3.1	2.2
Benzyl Alcohol	11.1	9	5.9
Benzyl Alcohol	15.6	13.5	9.1
Benzyl Alcohol	20.2	18.1	12.4
Benzyl Alcohol (0.1 molar)	5.2	3.1	2.0
Tert-butanol	4.5	2.4	2.5

The corrected values show an attachment of 1-6% (by weight) of organic material to the MCM-41 for most of the straight chain alcohols. Normalisation to molecular weight of the hydrocarbon leaving group (see temperature programmed removal) shows ca. 2-4 mol% loss. The exception amongst these was the methanol sample with had a higher attachment, ca 6 mol%.
However, with the benzyl alcohol samples, the organic attachment rose to 6-18 wt% for different samples (6-12 mol%). The cyclohexanol sample was similar to the straight chain alcohols, with 2.3 mol% corrected weight loss. However, this sample had been prepared from a 0.1 molar solution. A further cyclohexanol sample was prepared by stirring in the liquid alcohol, and analysis of this showed an uncorrected weight loss of 6.5 wt%, equivalent to. 3.1 mol% when corrected. This suggests that cyclohexanol attachment is similar to that of straight chain alcohols and discounts the possibility that increased attachment in benzyl alcohol is a function of larger molecular size (increased residence time in the pores of the material).
The benzyl alcohol sample prepared from a 0.1 molar solution showed a corrected weight loss of 3.1 weight%, equivalent to 2 mol%, which is a similar attachment from a dilute solution to that of many of the aliphatic alcohols undiluted.
It appears that there is no trend with increasing carbon chain length of the straight chain alcohols. However, as can be seen from the results of the TGA, for some of the alcohols more than one value is reported; these are the results of repeat preparations. This shows that even for the same alcohol the preparations themselves are subject to variability in the amount of alcohol attaching. There are a number of factors which could influence this behaviour.
Firstly, samples were not necessarily prepared from the same batch of parent MCM-41. This could mean that some differences in attachment are a function of the parent material, rather than just the attaching alcohol. Characteristics of the MCM-41 which could influence in this respect are, for example, degree of condensation in the original material and particle size effects. In the former case if attachment is solely or primarily as a result of condensation between the alcohol and the silanol groups of the MCM-41 an increase in condensation of the host would lower the number of sites available to the alcohol. In the latter case, MCM-41, as prepared, is a solid after calcination; in order to produce the powder

desired the material was ground. Since there are no controls on this a difference in particle sizes may result. This can affect accessibility of the internal surface as well as the external, since in smaller particles the pores will be shorter and therefore more accessible. This second factor could even have some effect within a single batch of MCM-41 if the grinding is uneven.

Other experimental factors such as stirring speed and temperature during the alcoholic modification may be of influence. Indeed, it was experimentally observed that attachment was very sensitive to stirring speed. Under mild stirring conditions it proved possible to produce material with no organic material; either adsorbed or attached.

However, in the cases of methanol and benzyl alcohol there is still good evidence of a greater affinity for the surface of the MCM-41 than that of the other alcohols. It is likely that in the case of benzyl alcohol it is energetically favourable for the system to gain aromaticity.

Table 6.3.5 gives the BET surface areas of samples modified by alcohols compared to their parent materials. Results are only reported where it has been possible to compare the modified samples with their particular parent material using the same experimental method, to avoid systematic inaccuracies.

It should be noted, however, that significant attachment of an organic species of different density makes comparison of surface areas difficult; apparent changes in surface area may, in fact, be the result of changes in the density of the material.

Table 6.3.5 BET Surface Areas of Organically Modified MCM-41

Surface Areas

Attaching Alcohol	Surface Area/ m^2/g	Surface Area of Parent/m^2/g	% Change
Propanol	1010	1010	0
Butanol	1030	930	-11
Pentanol	1070	930	-15
Hexanol	970	1010	4
Cyclohexanol	980	930	-5

These results show no trend with chain length, furthermore in some cases the apparent surface area increased while in others it decreased. It is worth noting, however, that the propanol and hexanol samples were prepared from one MCM-41 sample, while the butanol, pentanol and cyclohexanol samples were prepared from another (batch 1). This sample demonstrated an unusually low surface area for this type of material itself and it could be that the original surface area result was suspect or that the organic template had been incompletely removed by calcination. Unfortunately there is no remaining parent material of this batch so neither of these possibilities was investigated. Neither had this parent material, unlike most others used in this section, had its infra-red spectrum recorded. This was also the only MCM-41 batch not to have had its full isotherm recorded.

However this is supported by the results of the x-ray diffraction (see figure 6.3.4, below). Not only did the unmodified MCM-41 in question shown a lower intensity in its diffraction pattern than most but the modified samples have an increased intensity over the parent with a slight shift to lower values of 2θ, the opposite effect to that which one would expect if attaching material inside the pores of the parent. The cyclohexanol sample (not shown) which was also prepared from this MCM-41 did show a small decrease in intensity, which again supports the hypothesis: since this sample was prepared in a dilute solution in toluene it is unlikely that the alcohol could extract unremoved surfactant in the way which undiluted alcohol can. Quaternary ammonium surfactants are generally insoluble in non-polar organic solvents if they have *only one* long hydrophobic chain, as is the case with CTAB; solubility increases, for this type of surfactant, with the number of hydrophobic chains[22].

Figure 6.3.4 Powder X-Ray diffraction patterns for butanol and pentanol modified MCM-41

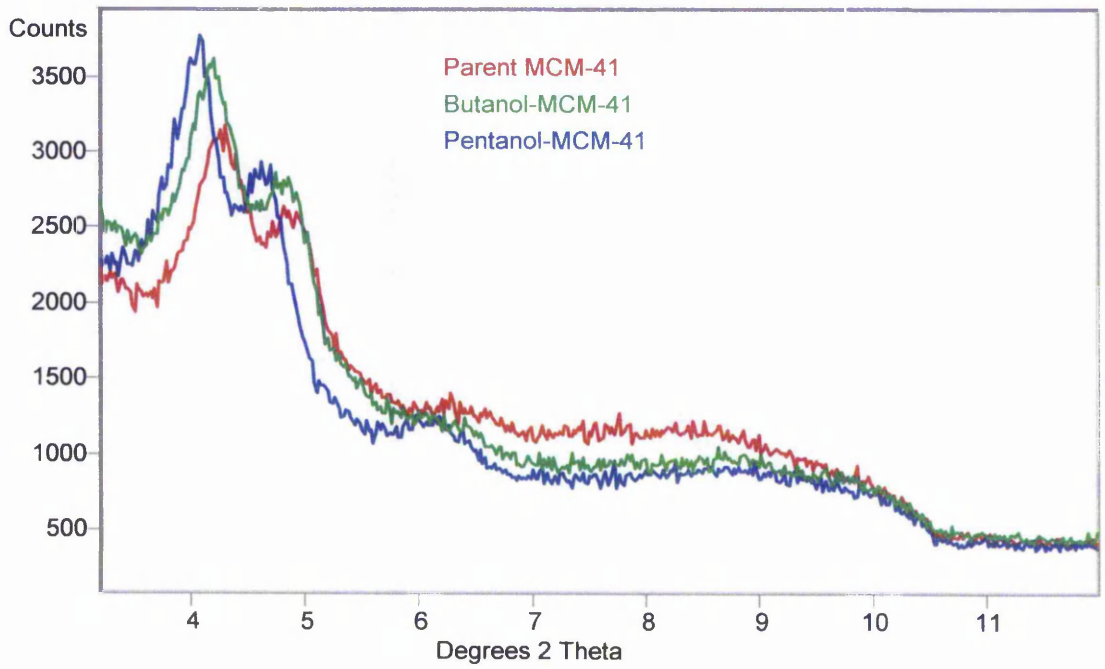

In the case of the hexanol modified sample, prepared from a different parent material the x-ray diffraction pattern (shown below) showed a loss of intensity The attachment of bulky species within the pores of MCM-41 may be expected to show some such effects on the XRD pattern; since it indicates some loss of ordering within the channels of the pores[23, 24]. However it is worth noting that this was very slight, indicating minimal disruption within the pores.

Figure 6.3.5 Powder X-Ray diffraction pattern for hexanol modified MCM-41

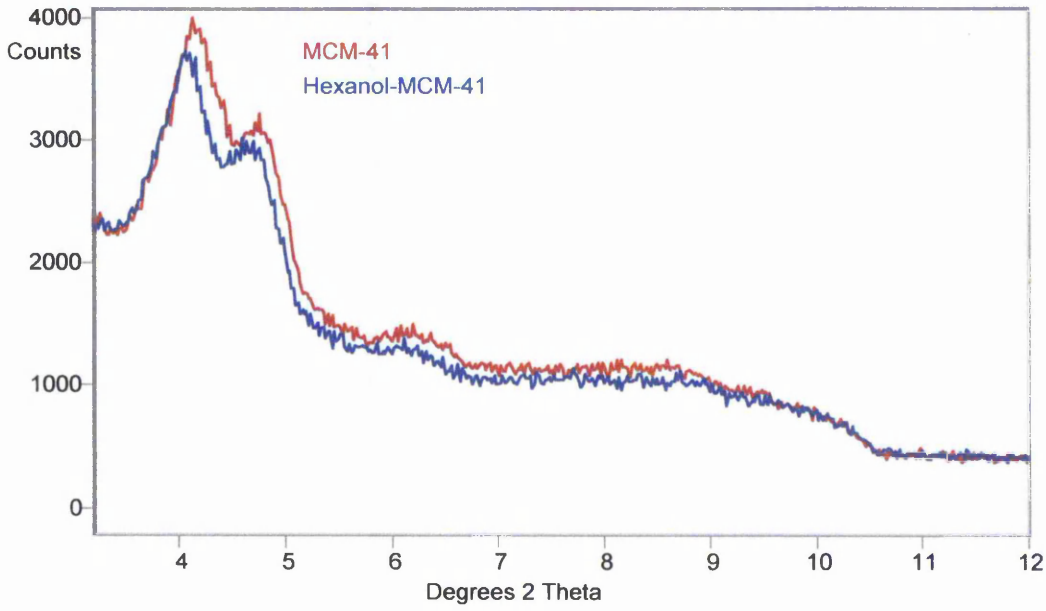

Temperature Programmed Removal

As mentioned previously the apparatus used is equipped with a mass spectrometer allowing some identification of leaving groups. Likely leaving groups for the straight chain materials include the alcohol itself, the fully saturated hydrocarbon and the corresponding alkene.

Tables 6.3.6 shows the expected mass spectral fragments for butanol, butane and but-1-ene[25]. Table 6.3.7 gives designations for the fragments in all cases, along with analysis of the probable neutral leaving groups, which are not detected[9, 26, 27].

As briefly outlined in the experimental section of this chapter in mass spectrometry ionisation results from the loss of an electron from the molecule. This follows the pattern of susceptibility of: lone pair electron > π electron > σ electron. Thus for an alcohol, such as butanol, one of the electrons from an oxygen lone pair will be removed. Fragmentation occurs when the parent (or molecular) ion produced has enough internal energy to break bonds within the

molecule. In the case of alcohols this arises either from direct cleavage of a bond within the parent ion or from rearrangement followed by cleavage. Some examples for butanol follow:

Ionisation:

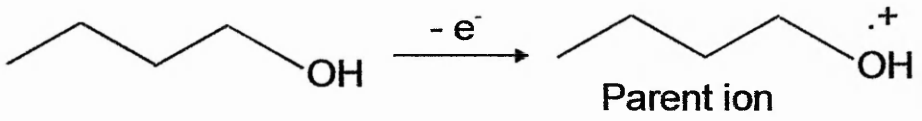

Direct cleavage:

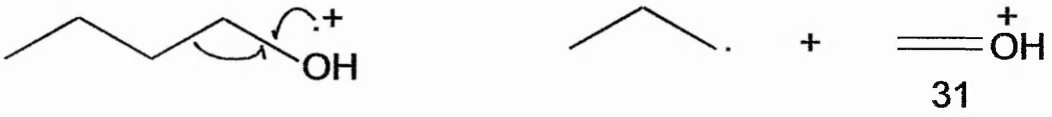

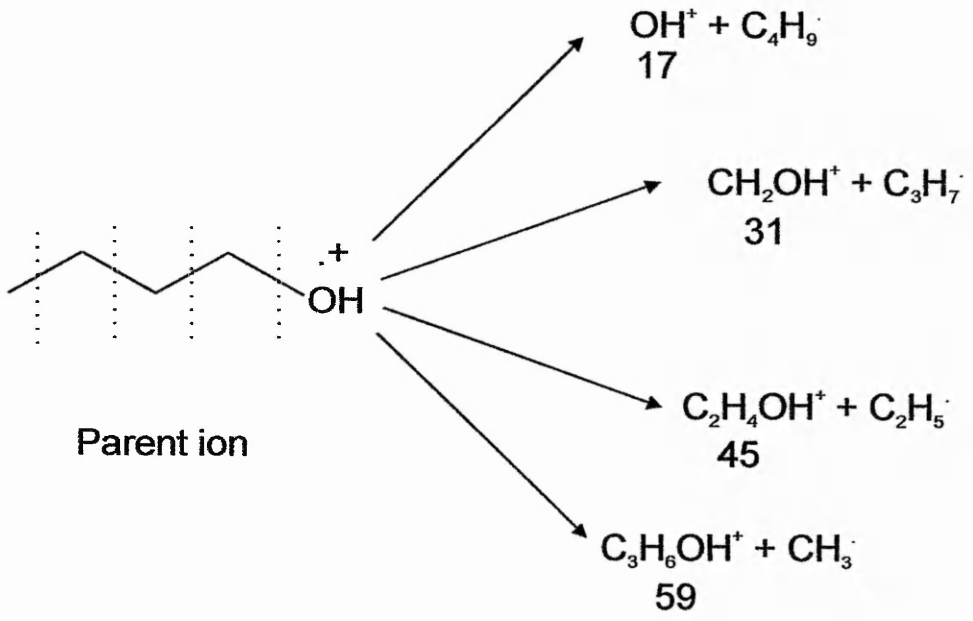

As shown above, direct cleavage of a bond results in cationic fragments with odd m/z ratios. The neutral leaving group is a radical and there is no charge

migration. However in primary alcohols the appearance of oxygen containing ions in the mass spectrum is often low[26, 28].

Rearrangement followed by cleavage:

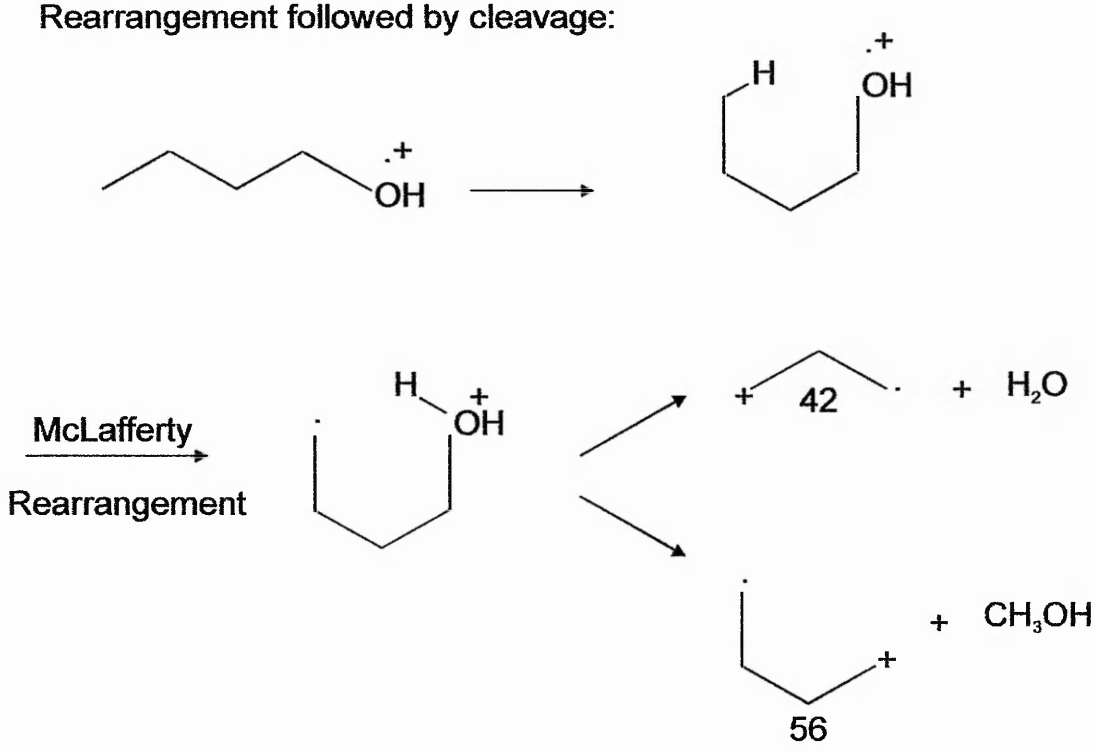

Even fragments result from rearrangement followed by cleavage: the fragments are radicals, and the neutral leaving group is a molecule[26]. This, and the above observation about direct cleavage, conforms to a general rule in mass spectrometry of organic molecules: the even electron rule. This is that where there is no nitrogen present any ion with an even mass has an odd number of electrons and is a radical cation or radical anion. Any ion with an odd mass has an even number of electrons and is a cation or an anion[26, 29].

Table 6.3.6 Mass spectral fragmentation data for possible leaving groups from butanol-modified MCM-41 (expected fragments)[25]

	Fragment m/z ratio									
Butanol	31	56	41	43	27	42	29	39	28	55
Butane	43	29	27	28	41	58	39	42	57	15
Butene	41	56	39	28	27	55	29	26	40	53

Table 6.3.7 Suggested Designations for Possible Mass Spectral Fragments for Butanol-Modified MCM-41

Fragment m/z ratio	Possible Designation			Loss From Molecular ion (neutral fragment)			Comments
	Butanol	Butane	Butene	Butanol	Butane	Butene	
15	N/E	CH_3^+	N/E	N/A	$C_3H_7^{\cdot}$	N/A	
26	N/E	N/E	$C_2H_2^{+\cdot}$	N/A	N/A	C_2H_6	
27	$C_2H_3^+$	$C_2H_3^+$	$C_2H_3^+$	$C_2H_7O^{\cdot}$	$C_2H_7^{\cdot}$	$C_2H_5^{\cdot}$	
				Probably $H_2O + C_2H_5^{\cdot}$	Probably $H_2 + C_2H_5^{\cdot}$		
28	$C_2H_4^{+\cdot}$	$C_2H_4^{+\cdot}$	$C_2H_4^{+\cdot}$	C_2H_5OH	C_2H_6	C_2H_4	
	$CO^{+\cdot}$	N/E	N/E	C_3H_8	N/A	N/A	
29	$C_2H_5^+$	$C_2H_5^+$	$C_2H_5^+$	$C_2H_4OH^{\cdot}$	$C_2H_5^{\cdot}$	$C_2H_3^{\cdot}$	
31	CH_3O^+	N/E	N/E	$C_3H_7^{\cdot}$	N/A	N/A	Strongly indicates alcohol
39	$C_3H_3^+$	$C_3H_3^+$	$C_3H_3^+$	$CH_7O^{\cdot}$	$CH_7^{\cdot}$	$CH_5^{\cdot}$	
				Probably $H_2O + H_2 + CH_3^{\cdot}$	Probably $2H_2 + CH_3^{\cdot}$	Probably $H_2 + CH_3^{\cdot}$	
40	N/E	N/E	$C_3H_4^{+\cdot}$	N/A	N/A	C_2H_2	
41	$C_3H_5^+$	$C_3H_5^+$	$C_3H_5^+$	$H_2O + CH_3^{\cdot}$	$H_2 + CH_3^{\cdot}$	$CH_3^{\cdot}$	
42	$C_3H_6^{+\cdot}$	$C_3H_6^{+\cdot}$	N/E	CH_3OH	CH_4	N/A	
43	$C_3H_7^+$	$C_3H_7^+$	N/E	$CH_3O^{\cdot}$	$CH_3^{\cdot}$	N/A	
53	N/E	N/A	$C_4H_5^+$	N/A	N/A	Probably $H_2 + H^{\cdot}$	
55	$C_4H_7^+$	N/A	$C_4H_7^+$	$H_3O^{\cdot}$	N/A	$H^{\cdot}$	
56	$C_4H_8^{+\cdot}$	N/A	$C_4H_8^{+\cdot}$	H_2O	N/A		Parent ion
57	N/E	$C_4H_9^+$	N/E	N/A	$H^{\cdot}$	N/A	
58	N/E	$C_4H_{10}^{+\cdot}$	N/E	N/A		N/A	Parent ion

N/E Not expected in the mass spectral pattern of this component
N/A Not applicable

The temperature-programmed removal profile of the butanol-modified MCM-41 is shown in figure 6.3.6 (all fragments). This shows a well-defined removal profile with two distinct removal steps. Peak removal temperatures (T_{max}) were 385 K and 800 K. The temperature of removal for the first peak is more typical of adsorption than that expected for the bonded species[5]. This may be indicative of some adsorbed alcohol.

Figure 6.3.6 Temperature Programmed Removal Profile of Butanol-modified MCM-41 (All Fragments)

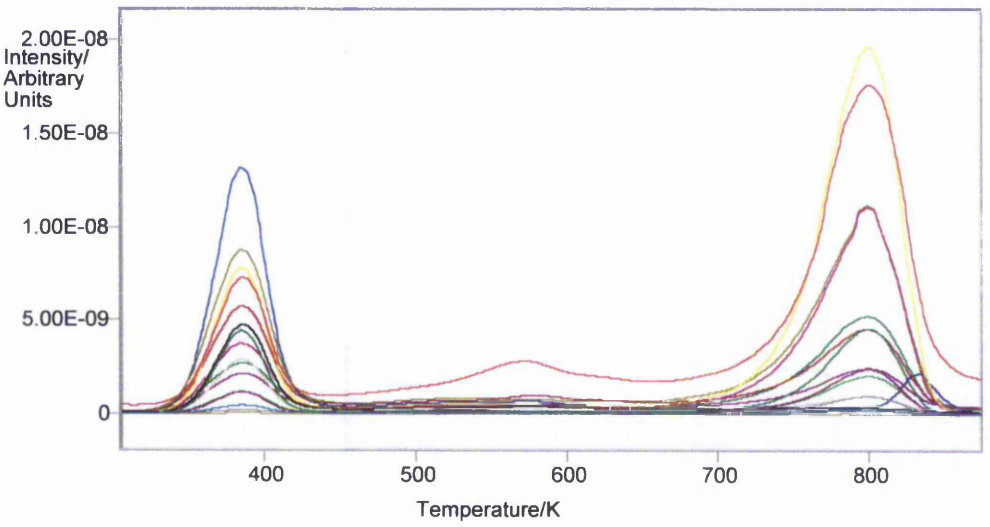

The exception to this general pattern is the fragment with m\z ratio = 28, shown in red above, which shows significant removal in the mid temperature range. However, examination of the mass spectral pattern of the host MCM-41 under the same conditions showed that this continuous loss in the mid-temperature range was a feature of the host material. The profiles from ca. 450 K to 670 K were similar in both the modified and unmodified materials; indeed loss of this fragment at these temperatures was much higher in the unmodified MCM-41. This may suggest some protective effect with the attachment of alcohol. These profiles are shown in figure 6.3.7.

Figure 6.3.7 Temperature Profile of Mass Spectral Fragment m/z = 28 for Butanol-modified MCM-41 and Unmodified MCM-41

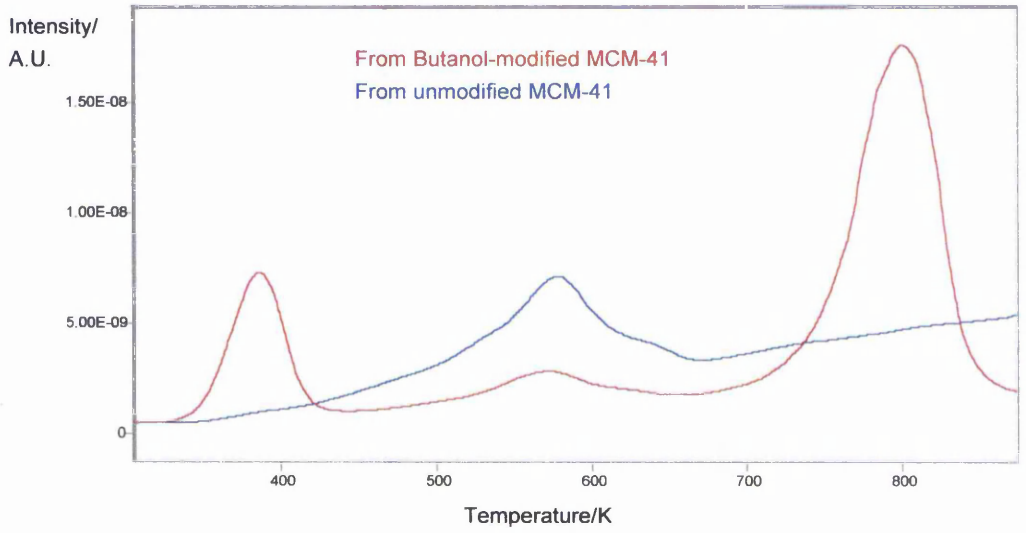

The profile of fragments exclusive to the individual leaving groups is shown in figure 6.3.8 (below). Unfortunately in the case of butanol there is only one such fragment (m/z = 31). Absolute quantification of the leaving groups is not possible, as the degree of fragmentation of the individual components is not known under these experimental conditions. However, it can be observed that the alcohol fragment (m/z =31) dominates the low temperature peak loss along with smaller contributions from the fragments due to both the saturated and unsaturated hydrocarbons. This suggests that there was a large amount of adsorbed alcohol on the material. It cannot be ruled out that the hydrocarbon fragments arise from a reaction of the removing alcohol on heating. However the presence of the m/z = 31 peak, which indicates oxygen does show that the alcohol is being removed at this temperature[30].

At higher temperatures there was evidence of loss of both saturated and unsaturated hydrocarbon and alcohol. Integration shows that alkane fragments are approximately equal in the high temperature peak compared to the low temperature peak. In the case of the alkene fragments the high temperature peak is substantially larger than the one at lower temperature. For the alcohol fragment the high temperature loss is minimal compared to that at 385 K. It is also worth noting that this peak has a higher T_{max} than that of the hydrocarbons

(830 K compared to 800 K). This suggests that the removal of the alcohol may be the result of a different process.

Figure 6.3.8 Temperature Programmed Removal Profile of Butanol-modified MCM-41 (Selected Fragments)

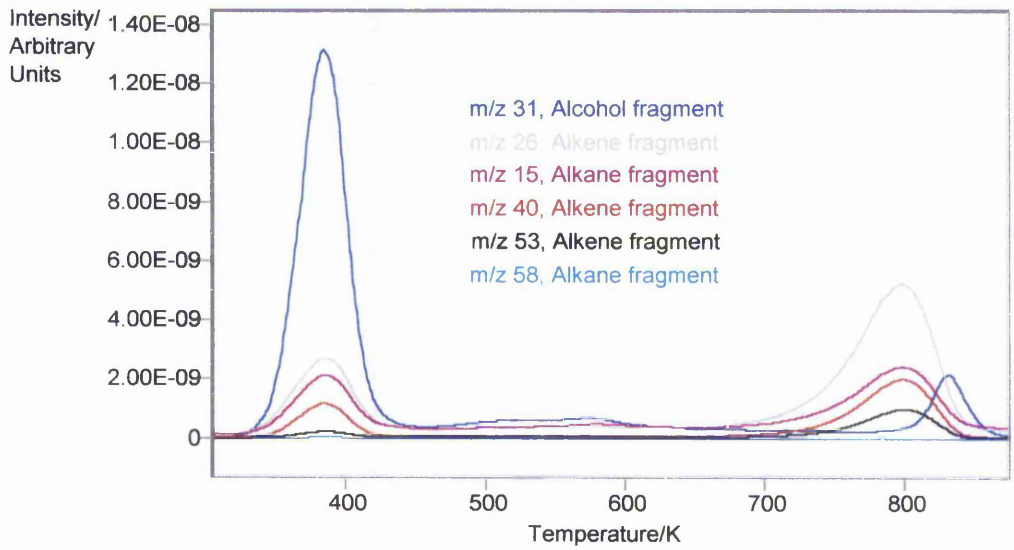

Table 6.3.8 shows the expected mass spectral fragments for pentanol, pentane and pent-1-ene[25]. Table 6.3.9 gives designations for the fragments in all cases, along with analysis of the probable neutral leaving groups[9, 26, 27].

Table 6.3.8 Mass spectral fragmentation data for possible leaving groups from pentanol-modified MCM-41 (expected fragments)[25]

	Fragment m/z ratio									
Pentanol	42	55	41	70	29	31	43	57	44	27
Pentane	43	42	41	27	29	39	57	72	28	15
Pentene	42	55	41	39	27	70	29	40	15	26

Table 6.3.9 Suggested Designations for Possible Mass Spectral Fragments for Pentanol-modified MCM-41

Fragment m/z ratio	Possible Designation			Loss From Molecular ion (neutral fragment)			Comments
	Pentanol	Pentane	Pentene	Pentanol	Pentane	Pentene	
15	N/E	CH_3^+	CH_3^+	N/A	$C_4H_9^\cdot$	$C_4H_7^\cdot$	
26	N/E	N/E	$C_2H_2^{+\cdot}$	N/A	N/A	C_3H_8	
27	$C_2H_3^+$	$C_2H_3^+$	$C_2H_3^+$	$C_3H_8OH^\cdot$	$C_3H_9^\cdot$	$C_3H_7^\cdot$	
				Probably $H_2O + C_3H_7^\cdot$	Probably $H_2 + C_3H_7^\cdot$		
28	N/E	$C_2H_4^{+\cdot}$	N/E	N/A	C_3H_6	N/A	
29	$C_2H_5^+$	$C_2H_5^+$	$C_2H_5^+$	$C_3H_6OH^\cdot$	$C_3H_7^\cdot$	$C_3H_5^\cdot$	
31	CH_3O^+	N/E	N/E	$C_4H_7^\cdot$	N/A	N/A	Strongly indicates alcohol
39	N/E	$C_3H_3^+$	$C_3H_3^+$	N/A	$C_2H_7^\cdot$	$C_2H_5^\cdot$	
					Probably $H_2 + C_2H_5^\cdot$		
40	N/E	N/E	$C_3H_4^{+\cdot}$	N/A	N/A	C_2H_6	
41	$C_3H_5^+$	$C_3H_5^+$	$C_3H_5^+$	$C_2H_7O^\cdot$	$C_2H_7^\cdot$	$C_2H_5^\cdot$	
				Probably $H_2O + C_2H_5^\cdot$	Possibly $H_2 + C_2H_5^\cdot$		
42	$C_3H_6^{+\cdot}$	$C_3H_6^{+\cdot}$	$C_3H_6^{+\cdot}$	C_2H_5OH	C_2H_6	C_2H_4	
43	$C_3H_7^+$	$C_3H_7^+$	N/E	$C_2H_4OH^\cdot$	$C_2H_5^\cdot$	N/A	
44	$C_3H_8^{+\cdot}$	N/E	N/E	C_2H_4O	N/A	N/A	
	$CH_2{=}CH(OH)^{+\cdot}$	N/E	N/E	C_3H_8	N/A	N/A	
55	$C_4H_7^+$	N/E	$C_4H_7^+$	$H_2O + CH_3^\cdot$	N/A	$CH_3^\cdot$	
57	$C_4H_9^+$	$C_4H_9^+$	N/A	$CH_2OH^\cdot$	$CH_3^\cdot$	N/A	
70	$C_5H_{10}^{+\cdot}$	N/E	$C_5H_{10}^{+\cdot}$	H_2O	N/A	Parent ion	
72	N/E	$C_5H_{12}^{+\cdot}$	N/E	N/A	Parent ion	N/A	

N/E Not expected in the mass spectral pattern of this component
N/A Not applicable

The profiles for the pentanol-modified sample are shown in figures 6.3.9 and 6.3.10.

Figure 6.3.9 Temperature Programmed Removal Profile of Pentanol-modified MCM-41 (All Fragments)

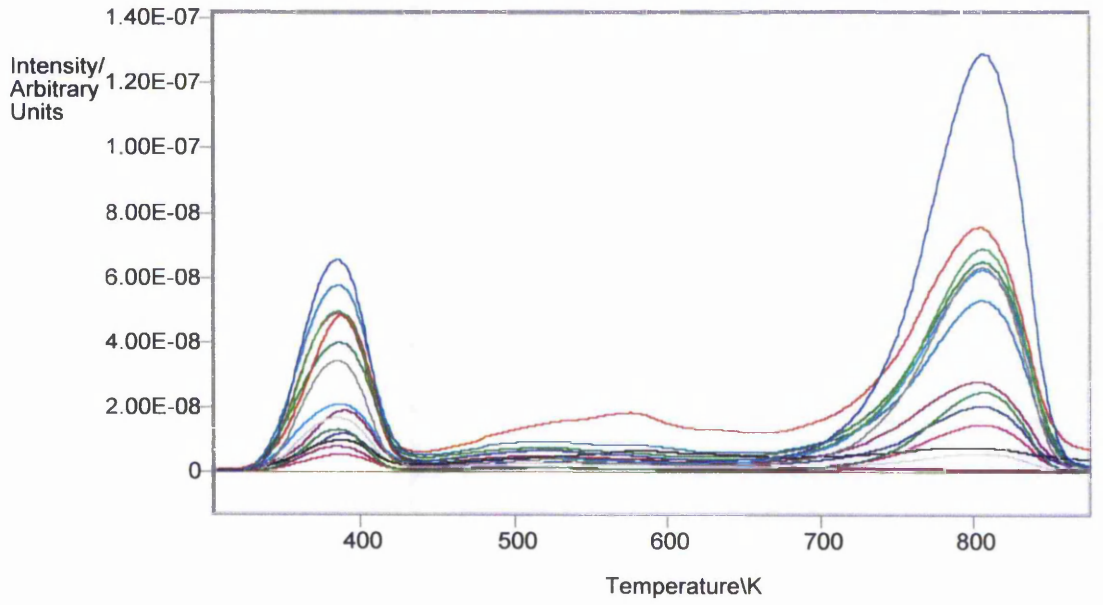

As with the butanol-modified MCM-41, discussed previously, there is a well-defined removal profile with two distinct removal steps. Peak removal temperatures (T_{max}) were also very similar at 385 K and 805 K. Again the fragment with m\z ratio = 28 (red above) is exceptional, showing significant removal in the mid temperature range. However, in the case of the pentanol-modified sample, although the profile from ca. 450 K to 670 K is similar in shape to that of unmodified MCM-41 the loss in the modified material is somewhat higher.

The profile of fragments exclusive to one possible leaving group is shown below in figure 6.3.10.

Figure 6.3.10 Temperature Programmed Removal Profile of Pentanol-modified MCM-41 (Selected Fragments)

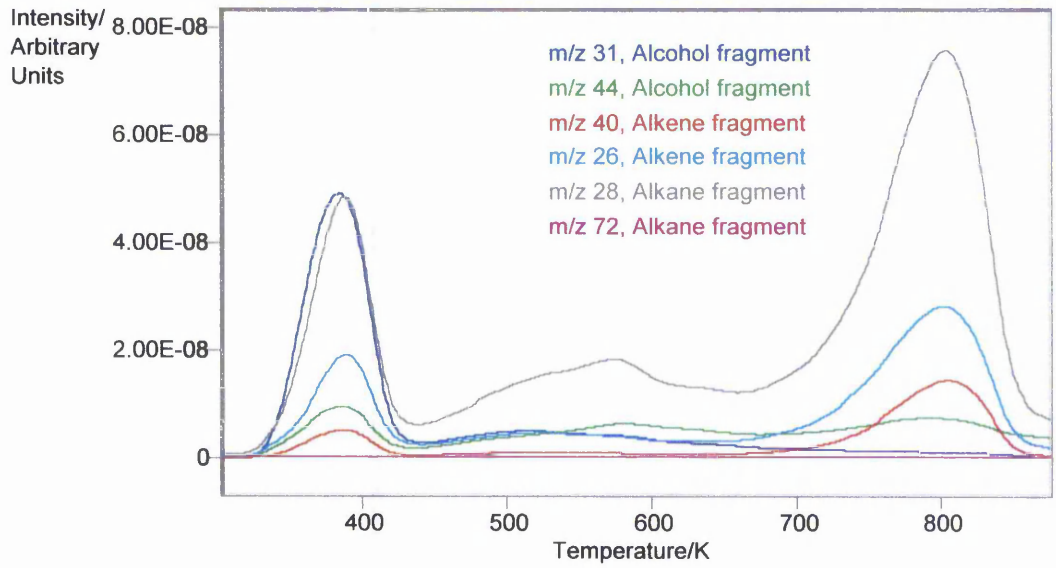

Again there is evidence of significant levels of alcohol removal at a temperature (385 K) suggestive of adsorption along with fragments attributable to both the alkane and alkene. It should be noted that the fragment m/z = 44 could also be attributed to carbon dioxide, however the presence of the fragment m/z = 31 ($CH_2=^+OH$), which is expected in all the spectra of primary alcohols is a strong indication of a primary alcohol[9]

In this case examination of the fragments and integration shows that at the higher temperature peaks attributable to both the saturated and unsaturated hydrocarbons are significantly larger than they are at the lower temperature. There is no corresponding removal peak for fragments attributable to the alcohol at the higher temperature, although there is some continuous loss of the fragment with m/z = 44. As mentioned above this can also be attributed to carbon dioxide, so the absence of the peak with m/z = 31 is perhaps more significant; it would be expected in the mass spectral fragmentation pattern of pentanol, and is present in the lower temperature removal. This strongly

suggests that alcohol is not a product of removal in this sample at the higher temperatures.

In both the above cases there is evidence of significant amounts of adsorbed alcohol. By contrast higher temperature removal, which indicates bonded organic species, occurs with the loss of saturated and unsaturated hydrocarbons, rather than alcohol. Of these two leaving groups the unsaturated product apparently dominates. This is the product of an α-elimination reaction and a mechanism for its formation is suggested below.

Suggested mechanism for the formation of α-unsaturated hydrocarbon from alcohol-modified MCM-41:

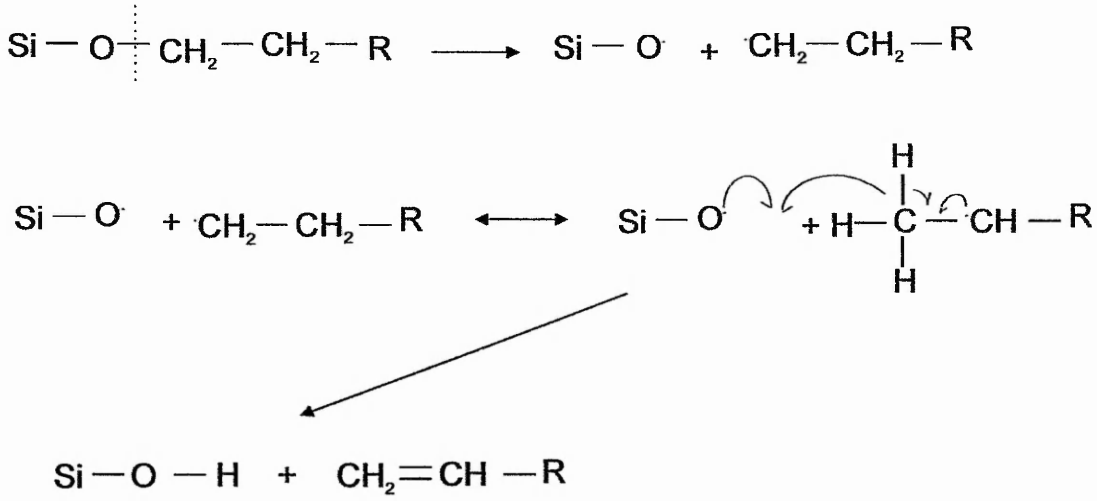

At present we have no clear understanding how the fully saturated product is formed.

Table 6.3.10 shows the expected mass spectral fragments for hexanol, hexane and hex-1-ene[25].

Table 6.3.10 Mass spectral fragmentation data for possible leaving groups from hexanol-modified MCM-41

	Fragment m/z ratio									
Hexanol	56	43	55	41	31	27	42	29	69	28
Hexane	57	43	41	29	27	56	42	39	86	28
Hexene	41	53	42	27	43	55	39	84	29	69

This sample caused a high pressure cut-off of the mass spectrometer before the expected appearance of the high temperature removal peak. Even so, at temperatures up to ca. 675 K it showed a completely different profile. In common with the other two samples, all fragments common to the three leaving groups were present, however there was no clearly defined low temperature removal peak and significant continuous removal of all fragments at temperatures greater than 365 K. The profile is shown in figure 6.3.10.

Figure 6.3.10 Temperature Programmed Removal Profile of Hexanol-modified MCM-41 (All Fragments)

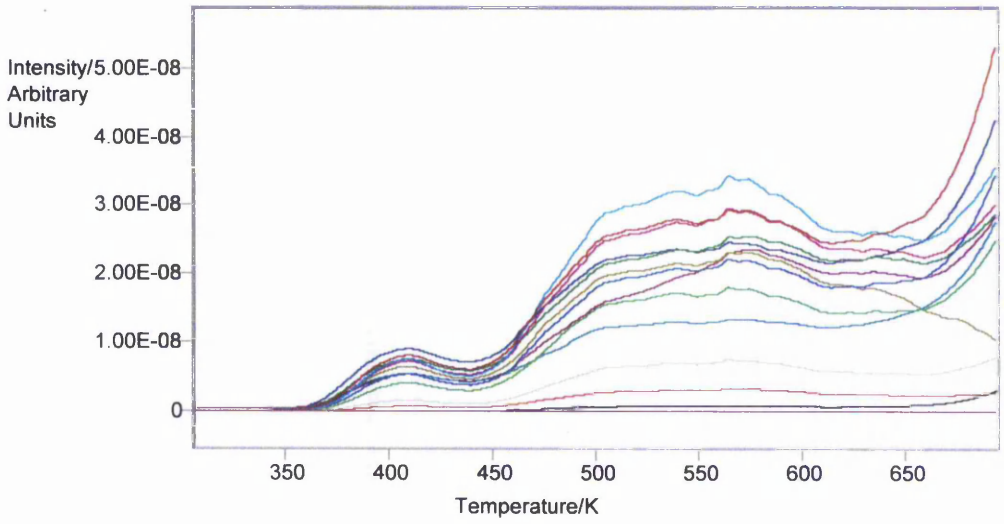

Table 6.3.11 shows the expected mass spectral fragments for benzyl alcohol, toluene and phenol[25]. Table 6.3.12 shows possible designations for these (expected) fragments.

Table 6.3.11 Mass spectral fragmentation data for possible leaving groups from benzyl alcohol-modified MCM-41

	Fragment m/z ratio									
Benzyl alcohol	79	108	107	77	51	39	50	27	29	91
Toluene	91	92	39	65	51	63	90	50	27	38
Phenol	94	39	66	65	40	55	50	63	51	95

Table 6.3.12 Possible designations for mass spectral fragments of benzyl alcohol, toluene and phenol.

Fragment m/z ratio	Possible Designation			Loss From Molecular ion (neutral fragment)			Comments
	Benzyl Alcohol	Toluene	Phenol	Benzyl Alcohol	Toluene	Phenol	
27	$C_2H_3^+$	$C_2H_3^+$	N/E	$C_5H_5O^{\cdot}$	$C_5H_5^{\cdot}$	N/A	
29	$C_2H_5^+$	N/E	N/E	$C_5H_8O^{\cdot}$	N/A	N/A	
	CHO^+	N/E	N/E	$C_6H_7^{\cdot}$	N/A	N/A	
38	N/E	$C_3H_2^{+\cdot}$	N/E	N/A	C_4H_6	N/A	Neutral fragment may be conjugated diene (favourable)
39	$C_3H_3^+$	$C_3H_3^+$	$C_3H_3^+$	$C_4H_5O^{\cdot}$	$C_4H_5^{\cdot}$	$C_3H_3O^{\cdot}$	Aromatic series
40	N/E	N/E	$C_3H_4^{+\cdot}$	N/A	N/A	C_3H_2O	
50	$C_4H_2^{+\cdot}$	$C_4H_2^{+\cdot}$	$C_4H_2^{+\cdot}$	C_3H_5OH	C_3H_6	C_2H_4O	Aromatic series Neutral fragment probably CO+ CH_4
51	$C_4H_3^+$	$C_4H_3^+$	$C_4H_3^+$	$C_3H_5O^{\cdot}$	$C_3H_5^{\cdot}$	$C_2H_3O^{\cdot}$	Aromatic series
55	N/E	N/E	$C_3H_3O^+$	N/A	N/A	$C_3H_3O^{\cdot}$	
63	N/E	$C_5H_3^+$	$C_5H_3^+$	N/A	$C_2H_7^{\cdot}$	$CH_3O^{\cdot}$	Neutral fragment probably H_2 + $C_2H_5^{\cdot}$ for toluene
65	N/E	$C_5H_5^+$	$C_5H_5^+$	N/A	$C_2H_5^{\cdot}$	$CHO^{\cdot}$	Cyclic diene, common in aromatic spectra
66	N/E	N/E	$C_5H_6^{+\cdot}$	N/A	N/A	CO	Cyclic diene, common in aromatic spectra. Loss of neutral CO, favourable.
77	$C_6H_5^+$	N/E	N/E	$CH_3O^{\cdot}$	N/A	N/A	Aromatic series
79	$C_6H_7^+$	N/E	N/E	$CHO^{\cdot}$	N/A	N/A	Aromatic series
91	$C_7H_7^+$	$C_7H_7^+$	N/E	$OH^{\cdot}$	$H^{\cdot}$	N/A	
90	N/E	$C_7H_6^{+\cdot}$	N/E	N/A	H_2	N/A	
92	N/E	$C_7H_8^{+\cdot}$	N/E	N/A	N/A	N/A	Parent ion
94	N/E	N/E	$C_6H_5OH^{+\cdot}$	N/A	N/A	N/A	Parent ion
95	N/E	N/E	$C_6H_5OH_2^+$	N/A	N/A	N/A	Parent ion + $H^{\cdot}$
107	$C_7H_7O^+$	N/E	N/E	$H^{\cdot}$	N/A	N/A	Parent ion - $H^{\cdot}$
108	$C_7H_7OH^{+\cdot}$	N/E	N/E	N/A	N/A	N/A	Parent ion

N/E Not expected in the mass spectral pattern of this component
N/A Not applicable

The profile of the benzyl alcohol exhibited fragments attributable to the alcohol, toluene (saturated hydrocarbon) and phenol at a temperature suggesting adsorption, ca. 400 K, with a distinct removal peak (see figure 6.3.11).
A separate gas phase experiment confirmed that heating benzyl alcohol alone under similar conditions produced fragments associated with toluene and phenol in the temperature range 303-355 K in similar proportions. This suggests that there is a gas phase reaction of the alcohol, on heating, to produce toluene and phenol. The lower temperatures here are merely indicative of the fact that in the former case the limiting process is the desorption of the alcohol from the solid.

Figure 6.3.11 Temperature Programmed Removal Profile of Benzyl Alcohol Modified MCM-41

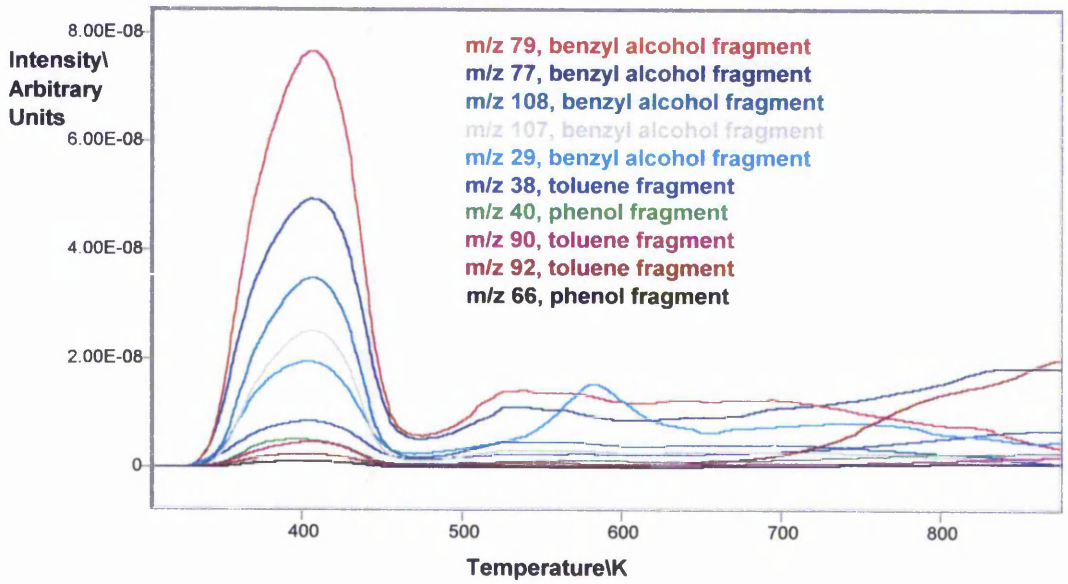

At temperatures above ca. 475 K there is an apparent, slight, continuous alcohol loss and above ca. 710 K a *very* small loss of toluene and phenol fragments. Again the toluene and phenol fragments were in similar proportion to those produced in the gas phase heating of benzyl alcohol, which suggests that the sole leaving group, in this case, is the alcohol. This did not reach a peak or a

temperature of maximum removal up to the limits of the equipment (875 K). Evidence presented in chapter 7 (temperature-programmed infra-red spectroscopy), along with the results of thermogravimetric analysis clearly demonstrate that the benzyl alcohol is still present on the material under these conditions. This suggests that the bonded aromatic group is far more strongly bonded to the MCM-41 surface than are the straight chain hydrocarbons. One possible reason for this additional stability is the inability of this group to produce the α-unsaturated hydrocarbon that features in the removal of the straight chain alcohols. This leaving group is the product of an α-elimination reaction involving a hydrogen atom located on the β carbon [11]. In the case of benzyl alcohol, see below, this carbon does not carry a hydrogen, or any other possible leaving group.

Benzyl alcohol:

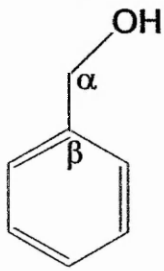

Any elimination reaction would involve losing the aromaticity of the ring system, which is a chemically unfavourable reaction. These findings support the suggestion that the removal of the bonded species is dominated by the α-elimination reaction producing the unsaturated product. The lack of a peak for the saturated product, which is a feature in the case of the straight chain alcohols, suggests that even where this is evident its production is intimately linked with the formation of the unsaturated hydrocarbon. It is worth noting that the other sample that has been shown to possess this high stability; methanol, reported elsewhere[5], shares this inability to form an unsaturated leaving group. The investigation of the benzyl alcohol-modified sample will be covered in greater detail in the next chapter.

6.4 Conclusions

It is easy to attach both aliphatic and non-phenolic alcohols to MCM-41, in the case of benzyl alcohol, both via undiluted benzyl alcohol and from solution. However the more strongly acidic phenol does not attach from solution under conditions where both benzyl alcohol and cyclohexanol do.

This offers a cheap and facile route for the incorporation of organic material into the host.

Attachment of non-aromatic alcohols does occur within the pores of the material yet causes minimal disruption.

The resultant materials are remarkably thermally stable, particularly in the cases of methanol and benzyl alcohol, which appear to have greater stability than the other alcohols. Since these two materials are unable to produce the α-unsaturated hydrocarbon that features in the removal of the straight chain alcohols it would seem that this inability is the reason for this additional stability. This, in turn, suggests that thermal removal is driven by the elimination reaction that produces this product.

6.5 References

1. Clark, J.H. and D.J. Macquarrie, *Catalysis of liquid phase organic reactions using chemically modified mesoporous inorganic solids.* Chemical Communications, 1998(8): p. 853-860.
2. Igarashi, N., K. Hashimoto, and T. Tatsumi, *Studies on the structural stability of mesoporous molecular sieves organically functionalized by a direct method.* Journal of Materials Chemistry, 2002. **12**: p. 3631-3636.
3. Jones, C.W., K. Tsuji, and M.E. Davis, *Organic-functionalized molecular sieves (OFMSs). II. Synthesis, characterization and the transformation of OFMSs containing non-polar functional groups into solid acids.* Microporous and Mesoporous Materials, 1999. **33**(1-3): p. 223-240.
4. Macquarrie, D., et al., *Organically modified hexagonal mesoporous silicas (HMS) - remarkable effect of preparation solvent on physical and chemical properties.* Journal of Materials Chemistry, 2001. **11**: p. 1843-1849.
5. Stockenhuber, M., M.J. Hudson, and R.W. Joyner, *Preparation, characterization, and unusual reactivity of Fe- MCM-41.* Journal of Physical Chemistry B, 2000. **104**(14): p. 3370-3374.
6. Bradley, D.C., R.C. Mehrotra, and D.P. Gaur, *Metal Alkoxides*. 1978, London: Academic Press.
7. Iler, R., K. 1953: U.S. Patent 2,657,149 (E. I. du Pont de Nemours & Co. Inc.).
8. Iler, R., *The Colloid Chemistry of Silica and Silicates.* 1989, Ann Arbor: UMI.
9. Williams, D., H. and I. Fleming, *Spectroscopic Methods in Organic Chemistry*. 5th ed. 1995: McGraw-Hill Book Company.
10. Nakanishi, K. and P.H. Solomon, *Infrared Adsorption Spectroscopy*. 2nd ed. 1977, San Francisco: Holden-Day Inc.
11. McMurray, J., *Organic Chemistry*. 4th Edition ed. 1996: Brooks/Cole Publishing Company.
12. Banwell, C.M. and E.M. McCash, *Fundamentals of Molecular Spectroscopy*. 4th ed. 1994: McGraw-Hill.

13. Sykes, P., *A Guidebook to Mechanism in Organic Chemistry*. 6th ed. 1986, London: Longman.

14. Szymanski, H.A., *Interpreted Infrared Spectra*. Vol. 3. 1967, New York: Plenum Press Data Division.

15. Pouchert, C.J., *The Aldrich Library of Infrared Spectra*. 3rd ed. 1975, Miwaukee: Aldrich Chemical Co.

16. Namba, S., et al., *Pressure Swing Adsorption of Organic Solvent Vapors on Mesoporous Molecular Sieves.* Studies in Surface Science and Catalysis, 1997. **105**(Progress in Zeolite and Microporous Materials): p. 1891-1898.

17. Branton, P.J., P.G. Hall, and K.S.W. Sing, *Physisorption of Alcohols and Water Vapour by MCM-41, a Model Mesoporous Adsorbent.* Adsorption, 1995. **1**: p. 77-82.

18. Rep, M., et al., *Interaction of methanol with alkali metal exchanged molecular sieves. I. IR spectroscopy study.* Journal of Physical Chemistry B, 2000. **104**(35): p. 8624-8630.

19. Zhao, X.S., F. Audsley, and G.Q. Lu, *Irrevesible Change of Pore Structure of MCM-41 upon Hydration at Room Temperature.* Journal of Physical Chemistry B, 1998. **102**: p. 4143-4146.

20. Landau, M.V., et al., *Wetting stability of Si-MCM-41 mesoporous material in neutral and basic aqueous solutions.* Microporous and Mesoporous Materials, 1999. **33**: p. 149-163.

21. Edler, K.J. and J.W. White, *Preparation dependent stability of pure silica MCM-41.* Journal of Materials Chemistry, 1999. **9**: p. 2611-2615.

22. Porter, M.R., *Handbook of Surfactants*. 1991, Glasgow: Blackie & Son Ltd.

23. Kruk, M., et al., *Characterization of highly ordered MCM-41 silicas using X-ray diffraction and nitrogen adsorption.* Langmuir, 1999. **15**(16): p. 5279-5284.

24. Kloetstra, K.R., H.W. Zandbergen, and H. Vanbekkum, *Mcm-41 Type Materials with Low Si/Al Ratios.* Catalysis Letters, 1995. **33**(1-2): p. 157-163.

25. Cornu, A.M., R., *Compilation of mass spectral data*. 2nd ed. Vol. 1. 1975, London: Heyden.

26. De Hoffmann, E., J. Charette, and V. Stroobant, *Mass Spectrometry Principles and Applications.* 1996: John Wiley & Sons Ltd.

27. Morrison, R.T. and R.N. Boyd, *Organic Chemistry*. 6th ed. 1992: Prentice Hall International.

28. Lee, T., A., *A Beginner's Guide to Mass Spectral Interpretation*. 1st ed. 1998, Chichester: John Wiley & Sons.

29. McLafferty, F., W. and F. Turecek, *Interpretation of Mass Spectra*. 4th ed. 1993, Mill Valley: University Science Books.

30. Beynon, J.H., *Mass Spectrometry and its Application to Organic Chemistry*. 1st ed. 1960, Amsterdam: Elsevier.

7. Extension of the Work on the Aromatic/Silica Hybrid

7.1 Introduction

Of the organic-inorganic hybrid materials reported in chapter six the benzyl alcohol modified sample is described here in greater depth owing to its enhanced chemical interest.

This interest derives from a number of factors. Firstly; it has been shown, see chapter six, that it is possible to attach substantial quantities of benzyl alcohol to the siliceous host. Since it is the organic material which will confer any functionality achieved, this high loading may be advantageous. Additionally the greater thermal stability of this particular material, also discussed in the previous chapter, is helpful in terms of future possible applications.

Most importantly, however, is the susceptibility of the attached organic group to further reaction; this is required to attach a functional group. Since the chosen method of attachment results in a purely hydrocarbon attachment it is necessary that the hydrocarbon itself is susceptible to further reaction under fairly mild conditions because of the possible weakness of the Si-O-C bond.

The introduction of a functional group to the composite material was intended via the sulfonation of the organic component. It is necessary for this to be achieved by a direct means on the as-prepared material without forcing conditions. The aromatic ring, unlike straight chain hydrocarbons, is vulnerable to electrophilic attack[1].

7.2 Experimental

Additional Characterisation

The thermal stability of the attached group was tested by examining the material under temperature-programmed infrared spectroscopy; using the in-situ FTIR instrument, previously described in section 2.4. The sample was held at 303 K for two hours, then the temperature was raised to 423 K using a ramp rate of 5 K/minute, at which temperature there was another dwell period of 1 hour, followed by ramping (5 K/minute) to 823 K (dwell 1 hour) and then cooled to 303 K. The material was monitored every 10 K during heating, every 10 minutes during dwell periods and every 25 K during cooling. A pressure of 10^{-7} mbar was maintained throughout.
A full nitrogen adsorption/desorption isotherm was recorded on the benzyl alcohol modified sample using the vacuum frame apparatus previously described in section 2.1; the BET surface areas as well as the pore volumes reported are calculated from these measurements.

Water Stability Testing

The sample was stirred in water at room temperature for > 3 hours, filtered and dried in air at 375 K overnight. The water stirred sample was examined by infrared spectroscopy for evidence of remaining organic matter, as described in chapter 6. Additionally the full nitrogen adsorption isotherm and the powder x-ray diffraction were recorded and thermogravimetric analysis (TGA) was performed on the water stirred sample, as described in chapters 2 and 6.

Long-term Thermal Stability

A sample of this material was also stored open to the atmosphere at 375 K for a period of approximately 5 months and this was also subjected to infrared spectroscopy and thermogravimetic analysis.

Sulfonation of the Aromatic/Silica Hybrid

Direct sulfonation of the MCM-41/aromatic composite was carried out using the gas phase method adopted by Jones et al.[2].
The mechanism of the reaction is shown in figure 7.2.1, below.

Figure 7.2.1 Sulfonation of benzene

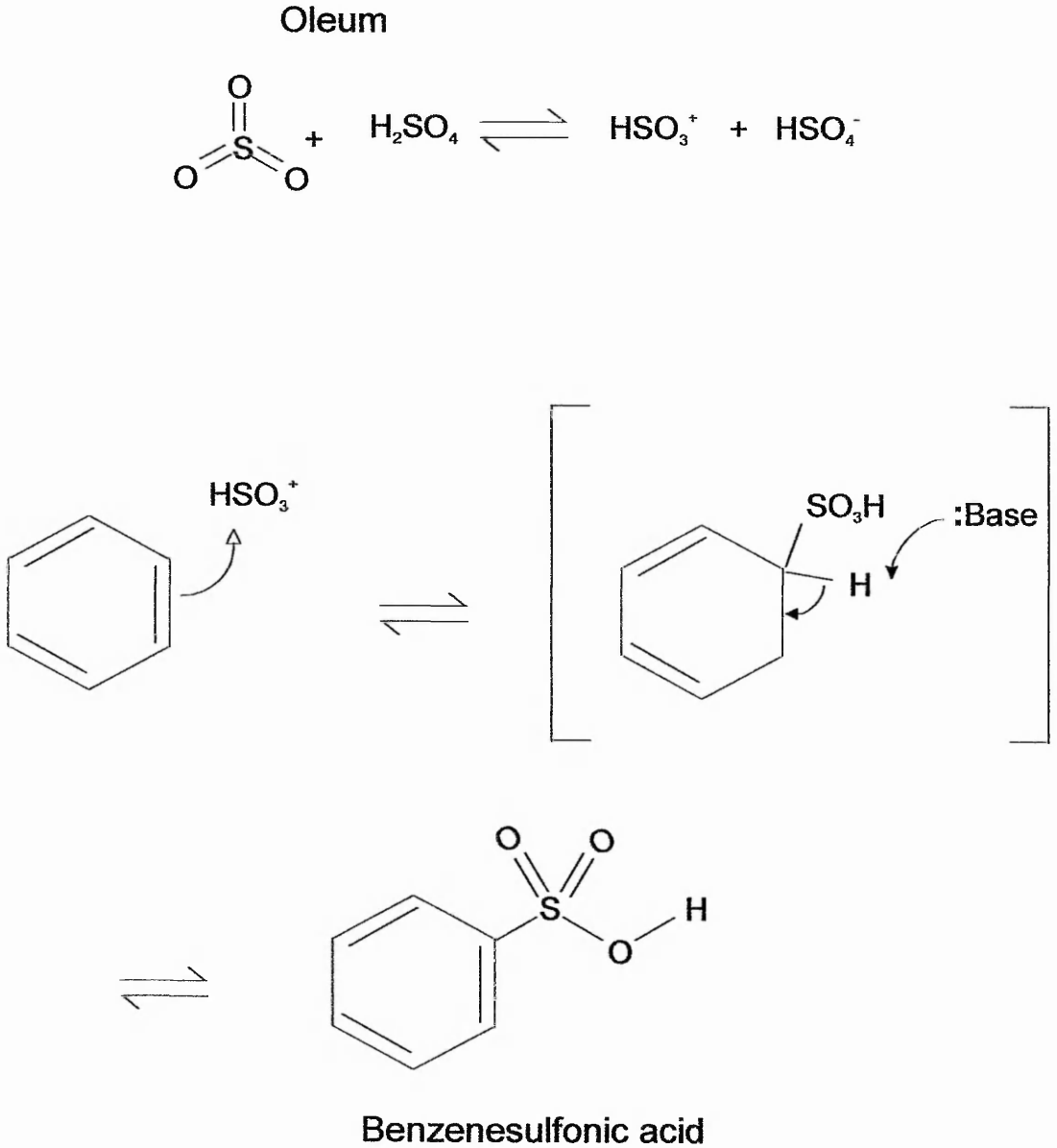

Benzenesulfonic acid

This was performed in a specially designed apparatus schematically shown in figure 7.2.2.

Figure 7.2.2 Apparatus for Sulfonation of the Aromatic/Silica Hybrid

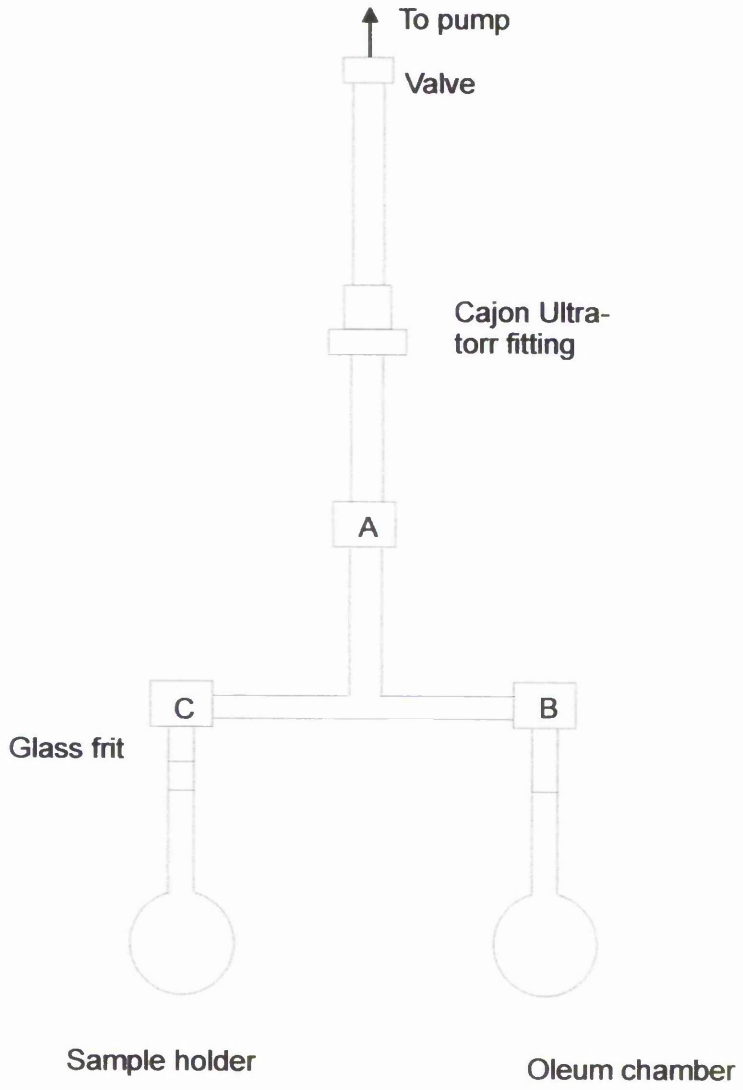

The sample (ca 50 mg) was placed in the sample holder with a small magnetic follower then the valve to the pump, stopcock A and stopcock C were opened. When the pressure had fallen, the sample was heated to approximately 425 K and held at this temperature overnight in order to outgas and dry the sample. The sample was then cooled to room temperature and stopcock C was closed. Oleum (ca 2 ml. Aldrich, 30%) was added to the oleum chamber.
The oleum was then degassed by immersing the oleum chamber in liquid nitrogen and, with the oleum frozen, opening stopcock B to pump out. After pumping out stopcock B was closed, the liquid nitrogen removed and the oleum allowed to thaw. The degassing procedure was repeated a further three times.

After degassing the oleum was frozen again using liquid nitrogen. While frozen both stopcocks B and C were opened and the whole apparatus pumped out for 15 – 30 minutes, after which time stopcock A was closed, the liquid nitrogen removed and the oleum allowed to thaw. The sample was left to react for 12 –24 hours and periodically stirred by means of a magnetic retriever, then the oleum was frozen, stopcock B closed and the sample holder brought up to atmospheric pressure by isolating the valve to the pump, loosening the Cajon fitting and opening stopcocks A and C. The sample was removed, washed with toluene (8 x 25 ml.) and dried overnight at 375 K.

Catalytic Reactor Screening Test

The sulfonated sample was screened for increased acidic activity by M. Van Den Berg, another member of the group, in a reaction already used in his work: the acid catalysed decomposition of iso-Propanol:

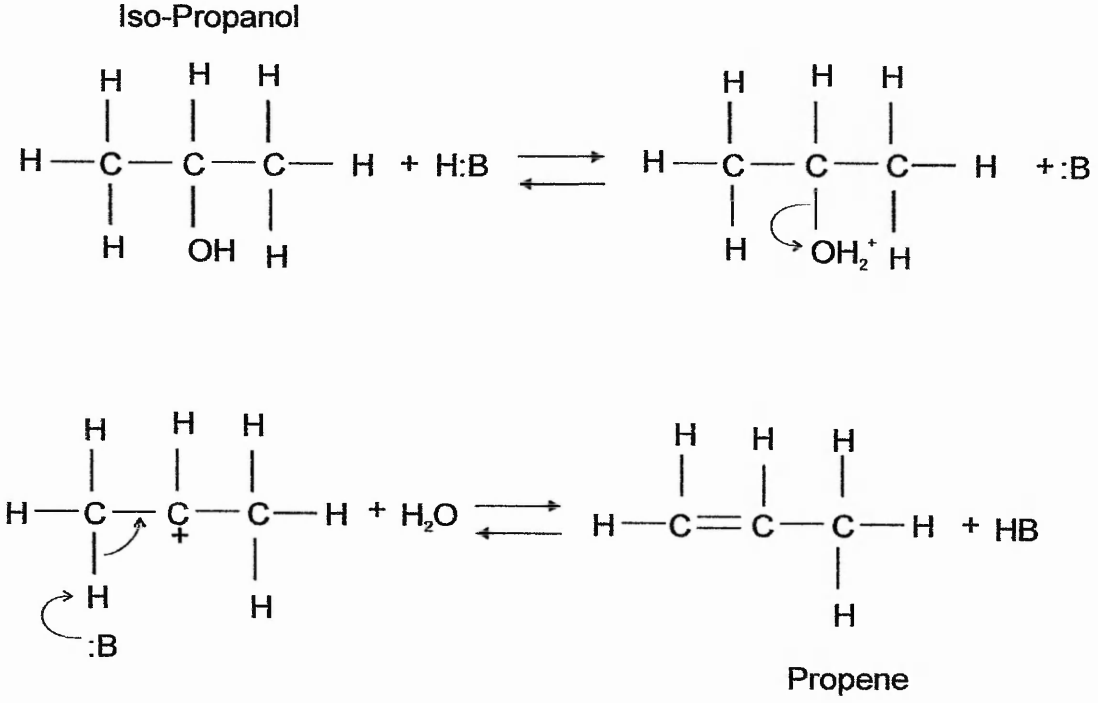

The sample was pressed and then granulated to provide pellets of 250 –425 μm diameter. Approximately 125 mg. of sample pellets were placed in a quartz glass

reactor tube in the reactor, shown below in diagram 7.2.3, held in place by quartz glass plugs.

Figure 7.2.3 Reactor for the Catalytic Decomposition of iso-Propanol

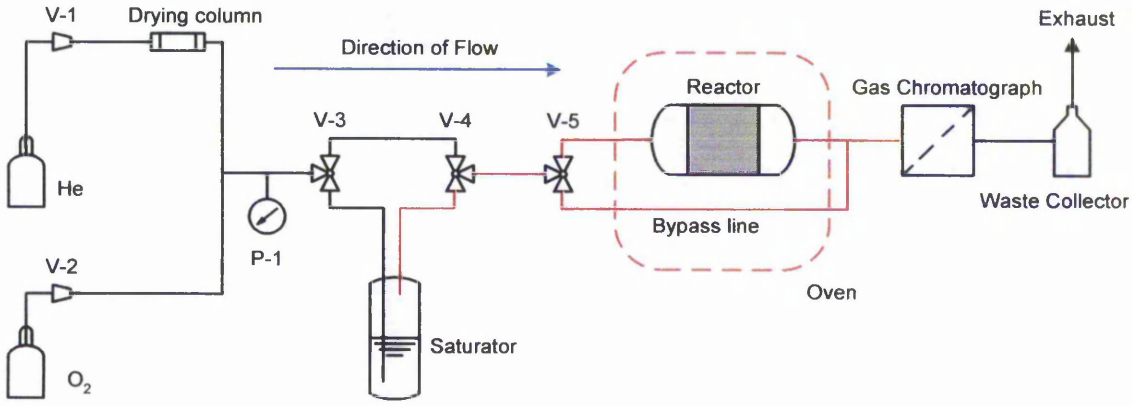

The sample was pretreated at 423 K for 1 hour (ramp 5 K/minute) in a flow of dried helium (BOC 99.996%, 177 ml./min) then cooled to 373 K. The Helium flow was then switched, by means of valves V3 and V4 to pass through the saturator of iso-Propanol (Aldrich, 99.5%, water content < 0.003%) and the reaction carried out to 623 K with a sampling interval of 50 K.

The products of the reaction were monitored by an ATI GC610 gas chromatograph fitted with a Porapak T column using a flame ioniser detector and recorded using a computer and the data treatment software provided by the manufacturer.

7.3 Results and Discussion

Figure 7.3.1 shows the infrared spectrum of the benzyl alcohol in *transmittance mode*[3]

Figure 7.3.1 Infrared spectrum of benzyl alcohol

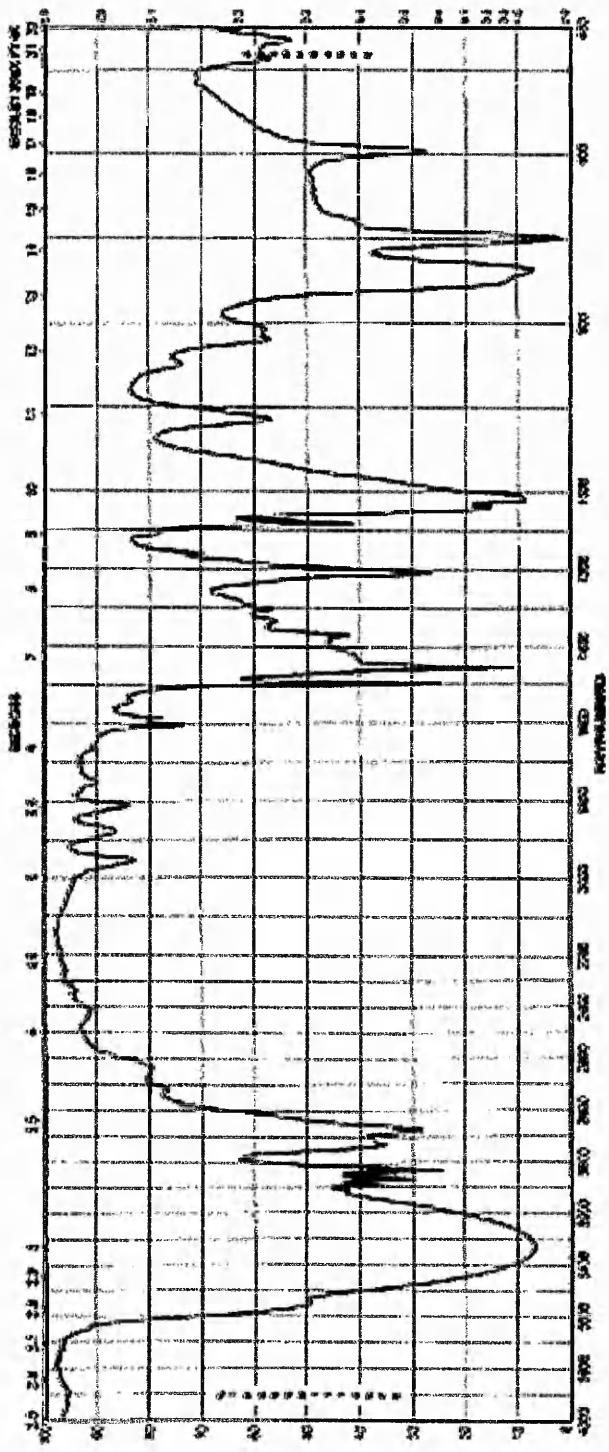

This shows the bands previously discussed in chapter 6 (detailed in table 6.3.2). Importantly it confirms our finding that the O-H stretching band in the spectrum of benzyl alcohol is a broad band centred around 3340 cm^{-1}. As reported in that chapter the MCM-41 material modified with benzyl alcohol showed a band in the O-H stretching region. However this band was a sharp one at 3630 cm^{-1}. Although this was tentatively assigned to O-H stretch the above spectrum shows that the band seen in the modified material is significantly different in both position and shape to that band in benzyl alcohol. This suggests that this band is not due to the O-H stretch of the benzyl alcohol, but is, in fact an additional band in the modified material.

Figure 7.3.2 shows the infrared spectrum of the benzyl alcohol modified MCM-41 before, during and after heating in vacuo.

Figure 7.3.2 Infrared spectra of benzyl alcohol-modified MCM-41 under various conditions

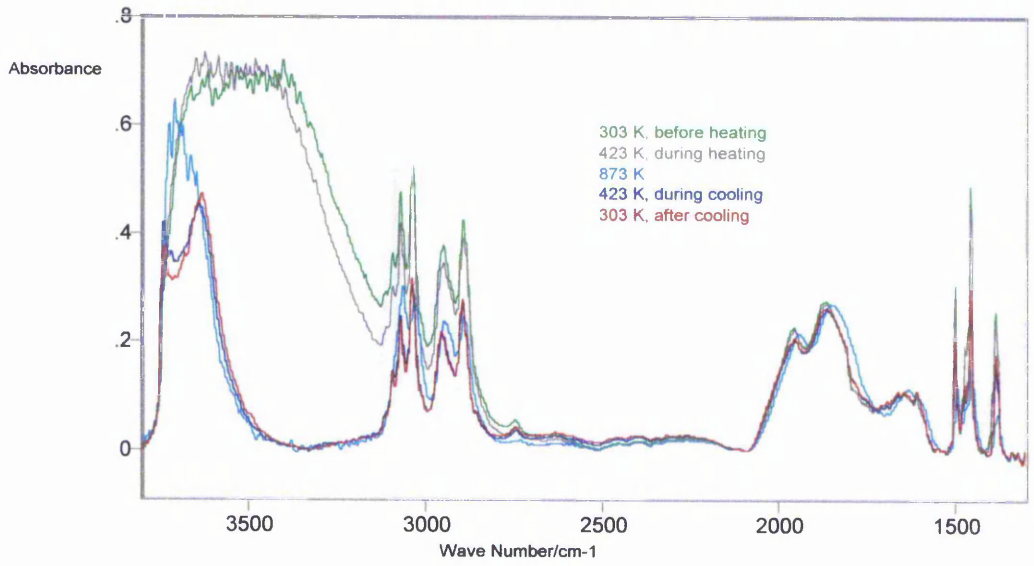

The spectrum recorded at 303 K, before heating, displays all the bands described in chapter six for this material (see table 6.3.2), with the exception of

the additional band at 3630 cm^{-1}. This has been attributed to free O-H stretching of the alcohol previously and is discussed above.

During heating some broadening of all the infrared bands can be observed; changes in frequency, band shape and intensity with temperature have been ascribed to thermal expansion and changes in population of energy levels[4]. As the sample is heated the broad band around 3550 cm^{-1} narrows, and on cooling a doublet is apparent; two bands at 3740 cm^{-1} 3635 cm^{-1}, the former being in a position consistent with terminal O-H groups of the silica host[5]. The broad band at 3550 cm^{-1} is normally attributed to Si-O-H groups with hydrogen bonding interactions (silanol nests) and adsorbed water[5, 6]. It is, therefore, evident that there is some loss of silanol nests as well as of water on heating.

However it should be noted that the observations here are not typical of unmodified MCM-41 heated under similar circumstances. Figure 7.3.3 shows the infrared spectra of a similar unmodified MCM-41 at room temperature and 423 K, before and after heating to 723 K (ramp 5 K/min, dwell 1 hour), in the same apparatus.

Figure 7.3.3 Infrared spectra of benzyl alcohol modified MCM-41 under various conditions

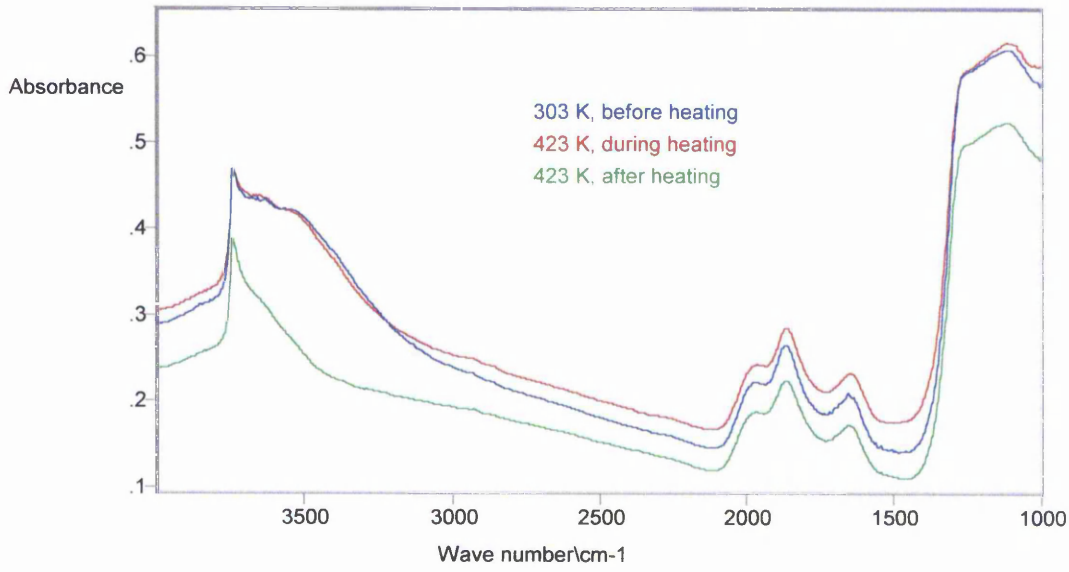

Here a narrowing of the broad band attributed to silanol nests can be seen, along with a loss of intensity of that band and the sharp band at 3740 cm^{-1} attributed to terminal Si-O-H groups. There is no evidence of the sharp band which exhibits itself in the case of the modified material.
For comparison figure 7.3.4 shows the spectra of the modified and unmodified materials at 423 K after heat treatment. These have been normalised to wafer thickness by integration of the bands between 2093 cm^{-1} and 1732 cm^{-1} attributable to the SiO_2 overtones of MCM-41.

Figure 7.3.4 Infrared spectra of modified and unmodified MCM-41 at 423 K after heat treatment.

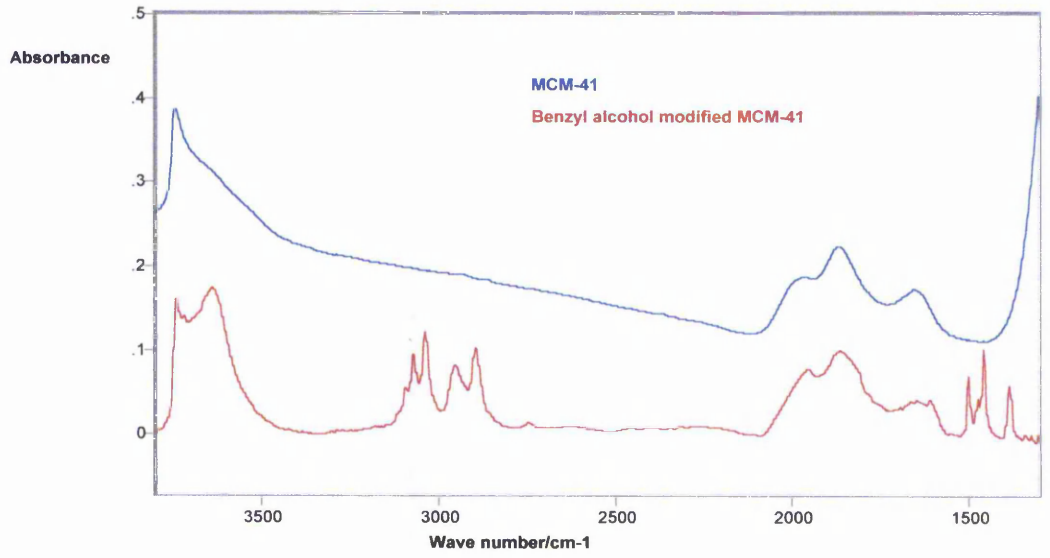

Figure 7.3.5 shows part of the difference spectrum at 423 K after heat treatment; the spectrum of the unmodified material has been subtracted from that of the modified MCM-41. The additional band can be seen, centred around 3635 cm^{-1}. From all of the above it is clear that this band is the same band that is reported in chapter 6 and that it arises from neither the parent MCM-41 nor from the alcohol *alone*. It is not, as previously considered, attributable to free O-H stretching of adsorbed alcohol as its position and appearance differ significantly. Furthermore the likelihood of *adsorbed* material remaining on a sample that has been heated to 873 K for an hour is remote. The band shows some characteristics of the band normally attributed to hydrogen bonded silanol

groups; it is broad and at high wave number. However, its position is more indicative of bridging –OH groups than silanol nests in MCM-41. It seems likely that this shift is the result of some influence by the bonded aromatic ring.

Figure 7.3.5 Difference spectrum (part, expanded) at 423 K after heat treatment.

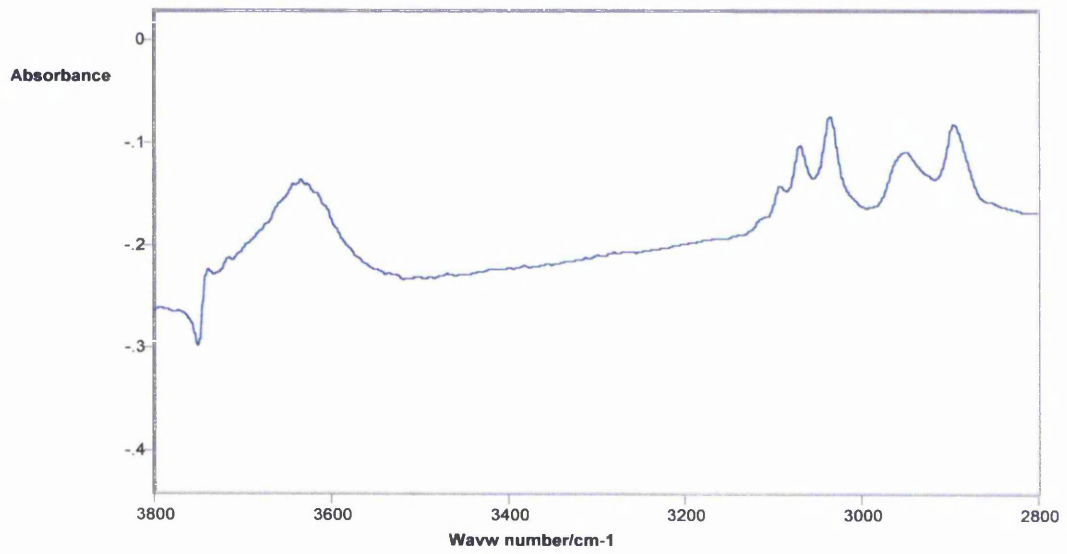

On cooling it is evident that the bands arising from the aromatic material are still present, but with a reduced intensity. Integration of the C=C ring stretching bands between 1500 cm^{-1} and 1380 cm^{-1} at room temperature before and after heating indicates ca. 3/5 of the organic material remains after heating.
From the nitrogen adsorption isotherm (shown later) the BET surface area falls from 950 m^2/g in the parent to 900 m^2/g on the attachment of the aromatic material. The total pore volume falls from 0.69 ml/g to 0.61 ml/g, a loss of ca 12%; this correlates with the results of the TGA (reported in chapter 6), and, viewed alongside the results of the x-ray diffraction (also shown later) and the fact that the area of the isotherm associated with surface coverage shows no change, supports the hypothesis that attachment is primarily within the pores of the material.
Attachment of the organic material leading to the formation of micropores would be expected to manifest itself by an apparent increase in the BET surface area as the region of the isotherm used for the BET calculation represents pore filling,

therefore pore volume, in a microporous solid. This would be accompanied by a decrease in total pore volume. Alternatively, attachment which did not result in microporosity but led to a roughening of the internal surface of the pores, for example sparse isolated attachment, would have the same effect. To date we have not been able to confirm or rule out the presence or absence of micropores in any of these materials.

However, if the pore diameter were reduced, but not to the micropore region, one would expect a decrease in both BET surface area and total pore volume. It is therefore evident that the latter process is occurring, whether or not either of the former two occurs alongside cannot be confirmed.

Water Stability Testing

The benzyl alcohol sample that had been stirred in water for three hours still exhibited the infrared bands described in section 6.3, but to a lesser extent, with the exception of the additional band at 3635 cm^{-1}. However, as previously mentioned, this falls within a region of the spectrum dominated by the broad band attributable to silanol nests and adsorbed water in the host material. Normalisation to wafer thickness as described in that section suggests that approximately one third of the organic material is retained, some of this loss may be due to adsorbed material, and the results of TGA also suggest that there is still a minimum of 5 wt% organic material present.

The full nitrogen adsorption isotherms of the parent MCM-41, the benzyl alcohol modified sample (designated B.A.MCM-41) and this material after water stability testing is shown in figure 7.3.6.

Figure 7.3.6 Nitrogen Isotherms of MCM-41 and Benzyl Alcohol-Modified MCM-41, Before and After, Water Stirring

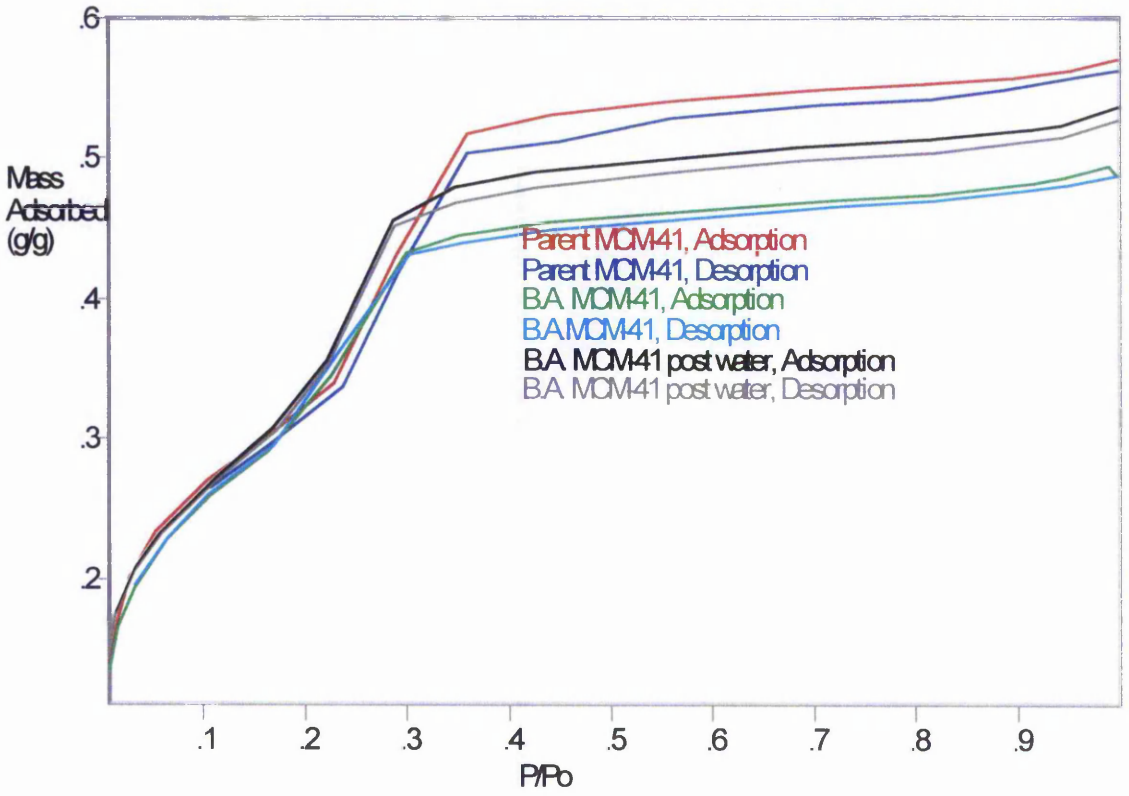

For the sample after water stability testing the BET surface area rises to 1030 m^2/g, an *increase* from the surface area of the original, unmodified, MCM-41 of ca. 8%. This may indicate disruption to the MCM-41 structure or that selective detachment creates a roughening of the internal surface of the pores. It does not indicate the collapse of the pore walls as this leads to a loss of surface area[7]. The total pore volume of the material lies midway between that of the parent and the benzyl alcohol modified material at 0.65 ml/g, a decrease of ca. 6% from the original, unmodified, material which again supports results from TGA which suggests around 5 wt% residual attachment.

Interestingly the x-ray diffraction pattern of the water stirred sample, shown below, did not show any disruption within the pores and almost totally returned to that of the original host material. This suggests that any blocking of the pores has been minimised by the subsequent removal of some of the material, and

also tends to indicate that no great structural damage has been done to the MCM-41 either by the organic attachment or by the subsequent contact with water.

Figure 7.3.7 X-Ray Diffraction Pattern of Parent MCM-41 and Benzyl Alcohol Modified Material, Before and After Water Stirring

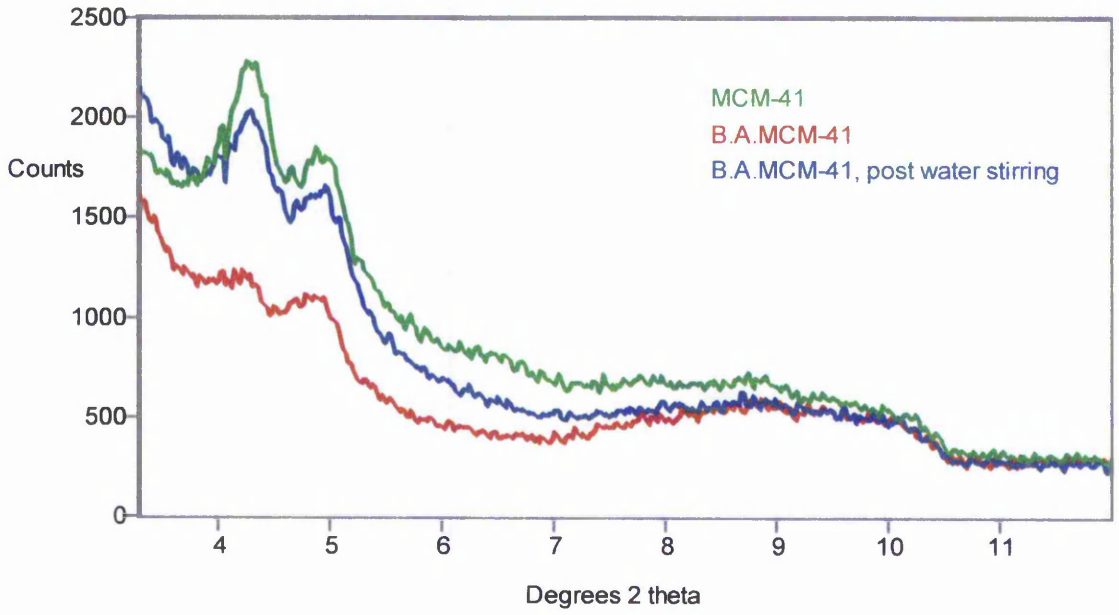

Long-term Thermal Stability

The portion of the benzyl alcohol sample that had been stored in the oven for ca. 20 weeks surprisingly underwent nearly 6% weight loss: equivalent to 3.7 mol%, (above 573 K, corrected for parent material weight loss) on being subjected to thermogravimetric analysis. Infrared spectroscopy confirmed that there was still attached material and quantitatively suggests ca. one third of the organic material is still present, with the additional band at 3635 cm^{-1} absent. The same material prior to oven storage showed a weight loss corresponding to 9.1 mol% (13.5 wt%) from TGA. The infrared spectroscopy also showed no evidence of disruption to the MCM-41 itself.

On being subjected to temperature-programmed removal as described in chapter six the low temperature removal peak (ca. 405 K, see figure 6.3.11) was completely absent suggesting there is no adsorbed organic material
The overall stability of this sample is remarkable considering the finding of other groups both in relation to MCM-41 and to attached organic groups. Edler and White and Zhao et al both reported the breakdown of MCM-41 pore structure under very mild conditions[8, 9]. Macquarrie et al attached organic species but reported the removal of alkyl groups around 753 K using TGA in nitrogen coupled with evolved gas FT-IR[10]

Catalytic Reactor Screening Tests

The sulfonated hybrid material did show some activity in the acid catalysed decomposition of iso-Propanol, but this was modest, reaching a peak of conversion of 6.8% at a temperature of 673 K. However the sample had been on line for several hours at raised temperatures and at temperatures as high as 673 K there is some visual evidence of the organic partially detaching; a sticky brown residue, soluble in acetone, seen here, and also in the temperature programmed removal experiments on the non-sulfonated materials. Furthermore this is nearly double the activity of an unmodified MCM-41 in the same reaction at that temperature. At lower temperatures, where conversion was lower, (< 573 K) the activity of the hybrid was an order of magnitude higher than the pure host material. With the hybrid material the selectivity to propene was high, ranging from 85% at 373 K to a figure in excess of 99% at 673 K; there was no product of the corresponding base catalysed reaction (acetone), but traces of an unidentified product. With the unmodified MCM-41, however the selectivity ranged from 3% (473 K) to 90% (673 K), at the lower temperatures this was again the unidentified product, but at 673 K there was 8% yield of acetone.
In order to establish that the organic attachment was necessary for this improvement in activity (for example to rule out the possibility that this was due to adsorbed acid) a further sample was prepared by subjecting an unmodified MCM-41 to the sulfonation procedure (precisely reproduced). This sample was also put through the catalytic screening reaction. This also showed a lower

activity in the reaction than the sulfonated hybrid, and at the higher temperatures (>523 K) showed a lower activity than the parent MCM. There was, with this sample, some evidence of adsorbed material with a fairly bright yellow deposit on the reactor tube after reaction, indicative of sulfur deposits. iso-Propanol conversion for these three samples is shown in figure 7.3.8.

Figure 7.3.8 iso-Propanol Conversion for MCM-41, Organically Modified "sulfonated" and Unmodified "sulfonated" MCM-41

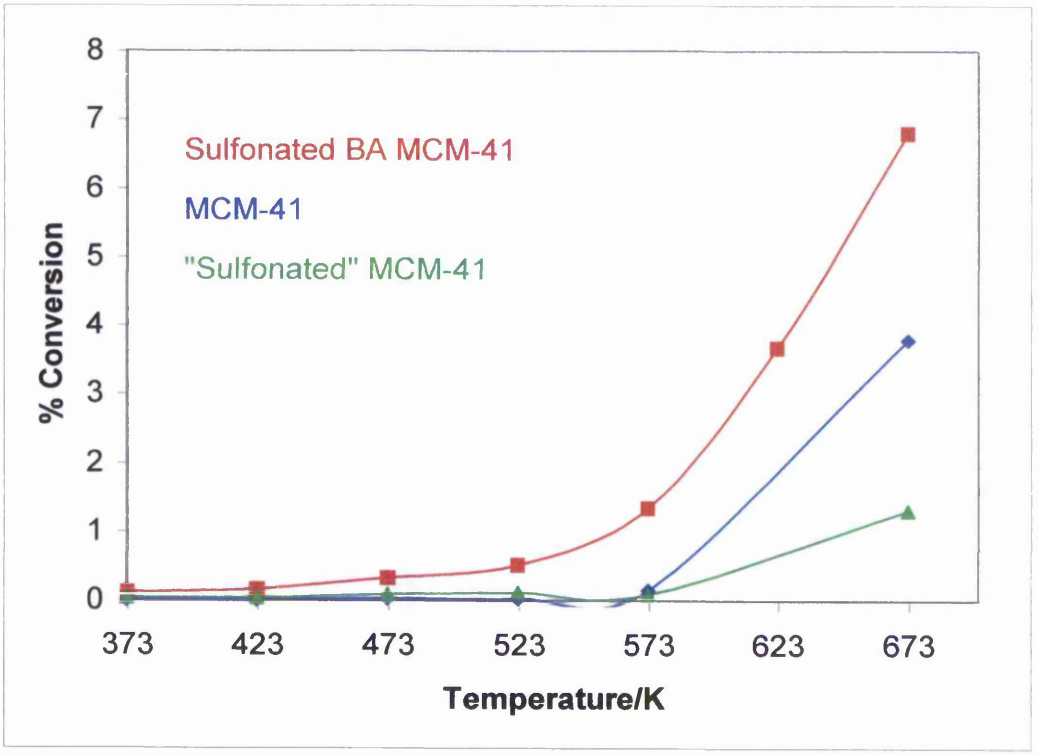

7.4 Conclusions

This attachment of an aromatic entity to MCM-41 occurs primarily within the pores of the material and does have significant effects on the pore void; this is explicable in terms of the bulk and rigidity of the aromatic ring as compared to the non-aromatic attachments discussed in the previous chapter. There is possibility that at the significant level of attachment that this method achieves, a degree of microporosity is created.

The hybrid material produced shows a good degree of thermal stability in vacuo as well as some amount of water stability. Although there is significant detachment of the organic material in water, this may even have advantages; as the partial removal appears to minimise the effects on the pore void. Its long-term stability at 375 K in air is remarkable.

On sulfonation of the material there is an increase in activity in acid catalysis, as judged by the chosen test reaction. Although this is modest the research on these materials is in its infancy and there has, as yet, been no attempt to optimise either the preparative technique or the reaction conditions. There is certainly an indication that the potential exists for the creation of an acidic catalyst through this route.

7.5 References

1. McMurray, J., *Organic Chemistry*. 4th Edition ed. 1996: Brooks/Cole Publishing Company.
2. Jones, C.W., K. Tsuji, and M.E. Davis, *Organic-functionalized molecular sieves (OFMSs). II. Synthesis, characterization and the transformation of OFMSs containing non-polar functional groups into solid acids.* Microporous and Mesoporous Materials, 1999. **33**(1-3): p. 223-240.
3. *www.sigma-aldrich.com.*
4. Clark, R.J.H. and H.R. E., *Advances in Infrared and Raman Spectroscopy*. Vol. 6: Heyden.
5. Stockenhuber, M., et al., *Transition metal containing mesoporous silicas - redox properties, structure and catalytic activity.* Microporous and Mesoporous Materials, 2001. **44**: p. 367-375.
6. Kosslick, H., H. Landmesser, and R. Fricke, *Acidity of substituted MCM-41-type mesoporous silicates probed by ammonia.* Journal of the Chemical Society-Faraday Transactions, 1997. **93**(9): p. 1849-1854.
7. Landau, M.V., et al., *Wetting stability of Si-MCM-41 mesoporous material in neutral and basic aqueous solutions.* Microporous and Mesoporous Materials, 1999. **33**: p. 149-163.
8. Edler, K.J. and J.W. White, *Preparation dependent stability of pure silica MCM-41.* Journal of Materials Chemistry, 1999. **9**: p. 2611-2615.
9. Zhao, X.S., F. Audsley, and G.Q. Lu, *Irrevesible Change of Pore Structure of MCM-41 upon Hydration at Room Temperature.* Journal of Physical Chemistry B, 1998. **102**: p. 4143-4146.
10. Wilson, K., et al., *Structure and reactivity of sol-gel sulphonic acid silicas.* Applied Catalysis a-General, 2002. **228**(1-2): p. 127-133.

8. Suggestions for Further Work

Perhaps the most interesting area for further study concerns the attachment of alcohols to MCM-41 reported in chapters six and seven. A number of questions raise themselves; as discussed in those chapters.

Firstly it has not been established whether there are trends in the attachment of straight chain alcohols, as outlined in chapter 6 because of differing experimental conditions. For this reason a controlled study of the attachment of the series of straight chain alcohols, and benzyl alcohol, would be illuminating. Such a study should involve using a single batch of parent MCM-41 and carefully controlling reaction conditions such as stirring speed, temperature and time of reaction. Subsequent characterisation of the resultant materials should establish whether there are systematic differences with chain length and whether the higher level of attachment of benzyl alcohol is consistent. Furthermore, since the long-term stability of the benzyl alcohol-modified sample discussed in chapter seven (in air, at elevated temperature) resulted from a chance discovery, it is not known whether the aliphatic materials share this property. It would be useful to study the effects on all the materials, under the same conditions, over a period of time.

Alternatively the materials could be studied by temperature-programmed oxidation using the apparatus for temperature-programmed reduction described in chapter five. This would probe thermal stability in air and would have an advantage in terms of time required. However it could not establish stability under variables such as moisture level, which are likely to exist under atmospheric conditions.

We believe that the high stability the benzyl alcohol-modified material may stem from the inability to form the α-unsaturated leaving group rather than from the presence of the aromatic ring itself. This should be confirmed by the preparation of a sample with benzeneethanol (Phenethyl alcohol) as the attaching species (see below).

Benzeneethanol:

This, while containing an aromatic ring, would be capable of leaving via the α-unsaturated product. This experiment could, therefore, confirm or refute the suggestion that thermal removal is driven by the reaction which produces that product.

The catalytic results for the sulfonated benzyl alcohol-modified sample showed modest improvements over the other materials, reaching a maximum conversion of ca. 7%. This does, however, indicate that acid sites exist in the material. A possible means of improving these results is to try to increase the number of sites. It is known that the benzyl alcohol/MCM-41 composite has a significant organic content. However the process of sulfonating the organic element may have not produced the optimum number of sulfonic acid groups. If this is the case there are a number of possible improvements. Experimentally the sulfonation apparatus could be improved by the repositioning of the glass frit to a position above stopcock A (diagram 7.2.2, chapter seven) and using a larger pored frit. This would not impair its function within the apparatus, but may improve the diffusion of the oleum, and so contact with the sample. Additionally the sulfonation process could be repeated with the water from the first reaction being removed between the two.

Chemically it may be helpful to attach a benzyl alcohol containing an activating group such as an alkyl group during the original grafting. A suggestion is 3-methylbenzyl alcohol:

Both this and benzeneethanol (mentioned previously) are, conveniently, liquid at room temperature and readily available[1, 2].

Additionally, a study of the attachment of bifunctional molecules, for example 1,4-benzenedimethanol and 1,4-cyclohexanediol may yield further information about the bonding and reactivity of the materials. If attachment is achieved through one functional group only with these molecules the resultant material, with an exposed functional group may have more potential for further modification of the organic species. Also, since it has been established that phenol does not attach to the MCM-41 material, it might be of interest to attempt to attach a molecule with both phenolic and non-phenolic alcohol functionality; such as 4-hydroxybenzyl alcohol. If this were to attach, and the nature of the phenolic group did not change, this would produce an acidic material in a one-step synthesis.

There may be problems finding a suitable solvent; these molecules, being more polar than alcohols, are generally insoluble in organic solvents such as toluene[2]. Suggestions for possible solvents are dimethylformamide (dielectric constant, $\varepsilon = 38.25$) and dimethyl sulfoxide ($\varepsilon = 47.24$). Preliminary work already undertaken suggests that the choice of solvent can inhibit attachment. For example benzyl alcohol will attach without solvent and from toluene but no attachment is seen when using acetone as solvent; so this must be borne in mind.

Alternatively, chemical vapour deposition could be employed; this is a technique widely used for the growth of aluminium oxide thin films on silica, and is the basis of the technique of atomic layer deposition[3-6].

References

1. Aldrich, *Aldrich Handbook of Fine Chemicals and Laboratory Equipment*. 2003: Sigma-Aldrich.
2. Lide, D.R.E., *CRC Handbook of Chemistry and Physics*. 75th ed. 1994: CRC Press.

3. Haanappel, V.A.C., et al., *Properties of alumina films prepared by metal-organic chemical vapour deposition at atmospheric pressure in the presence of small amounts of water.* Surface Coatings and Technology, 1995. **72**: p. 1-12.
4. Yoshikawa, N., et al., *MOCVD Kinetics and Morphologies of Al_2O_3 Deposits using Aluminium Tri-Isopropoxide(ATI) Precursor.* Transactions of the Materials Research Society of Japan, 1999. **24**(2): p. 151-156.
5. Koh, W., S.-J. Ku, and Y. Kim, *Chemical vapor deposition of Al_2O_3 films using highly volatile single sources.* Thin Solid Films, 1997. **304**: p. 222-224.
6. Cho, W., et al., *Atomic layer deposition of Al_2O_3 films using dimethylaluminium isopropoxide and water.* Journal of Vacuum Science and Technology A, 2003. **21**(4): p. 1366-1370.